UTILIZING MICRO-THERMAL NETWORKS FOR ENERGY DEMAND RESPONSE

UTILIZING MICRO-THERMAL NETWORKS FOR ENERGY DEMAND RESPONSE

By JESSICA VAN RYN, B.E.Sc.

A Thesis Submitted to the School of Graduate Studies

in Partial Fulfilment of the Requirements for

the Degree Master of Applied Science

MASTER OF APPLIED SCIENCE (2022) McMaster University

(Mechanical Engineering) Hamilton, Ontario, Canada

TITLE: Utilizing Micro-Thermal Networks for Energy Demand Response

AUTHOR: Jessica Van Ryn

B.E.Sc (Chemical Engineering)

University of Western Ontario, London, Ontario, Canada

SUPERVISOR: Dr. J. Cotton, Professor

Dr. M. Lightstone, Professor

NUMBER OF PAGES: xx, 177

Abstract

In recent years, the electrification of technology that is traditionally powered by fossil fuels has become a popular means to reduce greenhouse gases (GHG). Although the intentions are well founded, the strain on the electrical grid is seldom taken into consideration. When there is increased load on the grid, it is typically met by fossil fuel peaking power plants or additional fossil fuel infrastructure. Depending on the electrical generation technology deployed and the power plant efficiency, electrification can result in an increase in GHG emissions. To make better informed decisions for GHG reductions, policy makers and engineers are in need of smart energy systems, such as the Integrated Community Energy and Harvesting (ICE-Harvest) system. ICE-Harvest systems work with and can respond to changes on the electrical grid, providing demand response. The system creates electrical demand when renewable generation sources are available, reduces demand when fossil fuel generation is present, and can offset centralized generation using distributed combined heat and power resources.

In this thesis, steps to design a micro-thermal network (MTN) for the ICE-Harvest system are outlined and different operational strategies are explored that respond to grid behaviour in real time. How fast the thermal network reacts to grid level variations is defined as the response time. The physical response of the thermal network is a temperature set point change. A design map was developed presenting multiple parameters that contribute to the response time, the trade-offs between them, and the corresponding temperature difference achievable.

Through developing models in the equation-based object-oriented software Dymola, the viability for real time temperature set point changes in micro-thermal networks was explored. The MTN and the energy transfer stations (ETSs) that transfer energy between the thermal network and the

buildings have been modeled. Yearly system simulations were conducted to analyze the corresponding performance of the MTN in terms of electrical requirements and overall GHG emissions. An operational range of the system was presented demonstrating the flexibility of the ICE-Harvest system.

The simulation results have identified the ICE-Harvest system as a viable means to provide demand response to the grid and to reduce GHG emissions. Future work and recommendations will be made to improve the response of the system and further reduce electrical consumption and GHG emissions.

Acknowledgments

I would like to express my sincere gratitude to the Natural Sciences and Engineering Research Council of Canada and the Ontario Centre of Innovation for providing me the opportunity to undertake this thesis. I would also like to thank my supervisors, Dr. Cotton and Dr. Lightstone, for their thoughtful guidance, comments, and advice throughout my research work. I have learned valuable skills that I will take with me into future endeavors. It was a pleasure to be part of such a dedicated and innovative research group and I am fortunate for the friendships made along the way. And finally, I wish to thank my family for all the unconditional love and support that you have given me over these past years.

Table of Contents

List of Tables

List of Figures

List of Abbreviations, Symbols, and Notations

1GDH	1st Generation of District Heating
2GDH	2nd Generation of District Heating
3GDH	3rd Generation of District Heating
4GDH	4th Generation of District Heating
5GDHC	5th Generation of District Heating and Cooling
η	Effectiveness
α	Thermal Diffusivity
ρ	Density
AEF	Average Emission Factor
ASHP	Air Source Heat Pump
c_p	Specific Heat Capacity
c	Cold
C	Thermal Capacitance
CHP	Combined Heat and Power
COP	Coefficient of Performance
d	Depth
D	Diameter
DAE	Differential Algebraic Equation
DC	District Cooling
DE	District Energy
DH	District Heating
DHW	Domestic Hot Water
DLWC	Deep Lake Water Cooling
E	Energy
EMC	Energy Management Center

ETS	Energy Transfer Station
EWT	Entering Water Temperature
FAC	Flow Accelerated Corrosion
GA	Global Adjustment
GHG	Greenhouse Gas
GSHP	Ground Source Heat Pump
h	Hot
H	Enthalpy
HDPE	High Density PolyEthylene
HOEP	Hourly Ontario Energy Price
HP	Heat Pump
HT	High Temperature
ICE-Harvest	Integrated Community Energy and Harvesting
ICI	Industrial Conservation Initiative
IBPSA	International Building Performance Simulation Association
IESO	Independent Electricity System Operator
k	Thermal Conductivity
L	Length
LT	Low Temperature
$\dot{m}$	Mass Flowrate
M	Mass
MEF	Marginal Emission Factor
MSL	Modelica Standard Library
MTN	Micro-Thermal Network
NTU	Number of Transfer Units
N	Network
NOPH	No On-Peak Harvesting
ODE	Ordinary Differential Equation

P	Power
PDF	Peak Demand Factor
PE	PolyEthylene
PI	Proportional-Integral
Q	Heat Flowrate
R	Thermal Resistance
R^2	Coefficient of Determination
REI_{pump}	Relative Importance for Pumping Electrical Consumption
$RMSE$	Root Mean Square Error
RN	Reservoir Network
SH	Space Heating
t	Time
T	Temperature
ΔT	Temperature Difference
$TRNSYS$	Transient System Simulation Tool
$UDLTTN$	Unidirectional Low Temperature Thermal Network
V	Volume
$WSHP$	Water Source Heat Pump

Declaration of Academic Achievement

All of the work presented in this thesis is the original work of Jessica Van Ryn. Work was reviewed by academic supervisors Dr. J. Cotton and Dr. M. Lightstone. All published and/or presented work resulting from this thesis shall fully acknowledge contributing parties in accordance with the standard accrediting practices.

Chapter 1

1. Introduction and Problem Statement

The large quantity of greenhouse gas (GHG) emissions in the atmosphere necessitates the development and implementation of improved smart energy systems. Emission levels have already surpassed what was expected in this lifetime. GHGs are altering global temperature and causing adverse impacts across the globe at a rate faster than anticipated [1]. Many places around the world have launched GHG reduction efforts, including Ontario, which aims to reduce emissions by 30% below 2005 levels by the year 2030 [2]. To achieve this goal, Ontario has to decrease emissions by an additional 18 $MtCO_{2e}$ before 2030.

Table 1.1: Emissions in Ontario through the years [3]

	Emissions [$MtCO_{2e}$]						
	2005	2014	2015	2016	2017	2018	2019
Ontario	206	164	163	161	158	163	163

In Ontario, the emissions that comprise the values presented in Table 1.1 come from the buildings, oil and gas, electricity, transportation, heavy industry, and agricultural sectors. In 2018, the buildings sector was responsible for 21% of the provincial emissions and natural gas consumption made up 60% of the energy used by residential and commercial buildings [4]. Buildings sector emissions have been growing due to the rapid population increase in the province, and these trends are expected to continue [5].

Table 1.2: Ontario's transmission-connected electrical generation and supply for 2021 [6]

	Nuclear	Gas/Oil	Hydro	Wind	Biofuel	Solar
Installed Capacity [MW]	13,089	10,515	8,918	4,783	296	478
Installed Capacity [%]	34%	28%	23%	13%	<1%	1%

	Nuclear	Gas/Oil	Hydro	Wind	Biofuel	Solar
2021 Supply	58.2%	8.6%	24.0%	8.4%	<1%	<1%

Major decarbonization efforts have been made to the electrical grid, primarily the closure of coal-fired electrical generation plants, leading to a decrease in emissions in the electricity sector [3]. In Ontario, carbon free generation is 72% of the installed transmission-connected capacity as outlined in Table 1.2. Ontario also has contracts with independent generators, not connected to the main transmission system, that provide electricity to their local distribution network, called distribution-connected generation. Figure 1.1 indicates the additional generational capacity available. With the consideration of distribution-connected generation, carbon free generation capacity totals 74%. The electricity supply from wind and solar is a small percentage compared to their installed capacity of 19% due to the dependence on available sunlight and wind and the misalignment of supply and demand. Wind and solar are classified as variable generation due to the variable environmental factors that influence their output. A large installed capacity of gas generation is required to accommodate the intermittency of variable generation and to meet large peak demands.

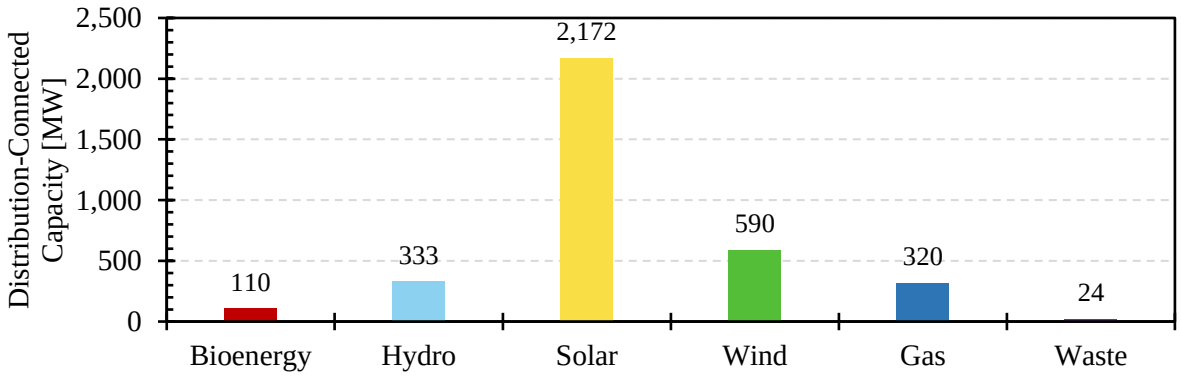

Figure 1.1: Distribution-connected capacity in Ontario [7]

To date, the electricity sector emissions in Ontario have decreased but the effect is not seen province wide. The overall Ontario emissions for the years 2014 to 2019 have remained fairly

constant according to the values presented in Table 1.1. This is due to the large buildings sector expansion and no significant change in how the buildings are receiving their energy. In the coming future, Ontario is set to retire a main nuclear generation facility and refurbishment projects are set for the remaining generation facilities. Proper renewable infrastructure is not in place in order to bridge the gap and meet the growing demand, therefore the large installed capacity of natural gas generation will be operated. With the use of natural gas generation, the grid level emissions are projected to increase 220% by 2030 [8]. Focus needs to be made on the buildings and electricity sectors to decrease emissions if Ontario is to meet the 2030 goal.

There is a push towards the electrification of traditional fossil fuel technologies to decrease buildings sector emissions. The primary focus of electrification for buildings is space heating. In Ontario, for the year 2018, the residential and commercial sectors consumed 509 PJ of natural gas for space heating, producing 24.8 $MtCO_{2e}$ [4]. Complete electrification of such demands would cause an unprecedented increase in electricity generation requirements on a grid level. The additional demand and strain on the electrical grid are generally not considered. It is thought that renewable generation will be able to meet these demands, when in reality wind generation is weakly correlated with heating demand and solar is anti-correlated with temperature and therefore with the space heating demand [9].

When baseload electrical generation in combination with renewable sources cannot meet the demand, natural gas peaking power plants are dispatched. If electricity is to become the power source for heating and peaking power plants are required to meet the demand, grid level natural gas generation is operating at a 42% efficiency [10]. Electricity produced on a grid level also encounters distribution system losses before reaching the end consumer. On average line losses in Ontario are 5.3% of the electricity produced [11]. In contrast, a natural gas furnace that is typically

used for building space heating, can range from 80 to 98% fuel efficiency [12]. Electrification of the heating demand does allow for flexibility, as the energy source of the electricity could come from many different technologies, if the demand is produced at the correct times. The need for smart energy systems that work with and balance the load of the electrical grid are critical for GHG reductions and the utilization of renewable electrical generation.

Additional ways to combat increasing GHG emissions is to utilize waste heat, which increases the efficiency of the energy system and reduces GHGs [13]. One such example is combined heat and power (CHP) installations, they generate electricity and make use the heat produced during electrical generation. The utilization of this residual heat, or waste heat, can cause the fuel efficiency of natural gas electricity generation to reach up to 80% [14]. Integrating CHP into an energy system, and only operating when natural gas is on the electrical grid, offsets the grid level generators and provides heat and electricity at an increased efficiency.

Waste heat can also be captured from industrial processes, refrigeration systems, and building space cooling. These waste heat sources are considered to produce low-grade waste heat, meaning the temperature of generated heat is at a low temperature. Additional energy input is then required to increase the temperature of the waste heat to the level needed for building space heating. The harvesting of this heat, that is traditionally expelled into the atmosphere, reduces the energy required from central generation sources.

District energy systems have been proven as an effective way to incorporate CHP resources. District energy systems generate energy at a central plant within the community and it is delivered to customers through a piping distribution network. In the most recent advancements in district energy, lower temperatures have been adopted in the distribution network. The lower network temperatures allow for the incorporation of carbon free resources, such as waste heat, that was

otherwise unsuitable for the traditional high temperature systems. Lowering the network temperature results in the distribution fluid to be lower than what is required to heat the buildings. Electricity is then used to increase the temperature of the fluid. Integrating the electricity, gas, and thermal grids creates flexibility in the energy system, leading to the creation of smart energy systems. Within smart energy systems, the electrification of heating plays a large role in the continued efforts towards decarbonization but needs the proper operational strategies to be effective.

1.1 Research Objectives

The Integrated Community Energy and Harvesting (ICE-Harvest) project is a smart energy solution utilizing grid connectivity, combined heat and power, energy storage, and district energy to provide community energy needs. Using the ICE-Harvest concept, this thesis aims to develop an operational range for the system. The operational strategies explored provide demand response to the electrical grid and reduce GHG emissions. The novel approach to demand response presented in this thesis is the change in distribution network temperature depending on the grid electrical generation source. Changing the distribution temperature controls the electrical consumption of the connected buildings. The operational strategy follows the behavior of the electrical grid in real time.

At the central plant or energy management center (EMC), a CHP is operated in tandem with the network temperature change based on the electrical grid generation source. At each building there is the opportunity to provide the heating demand through direct heat exchange or through electrification.

When there are natural gas peaking power plants generating electricity on the grid, it is considered an “on-peak” period, meaning that province wide demands are at a high and natural gas generators

have been dispatched. During this time, the on-site CHP is operated to offset the grid natural gas peaking power plants and run more efficiently. The heat from the CHP is used to produce a high temperature thermal network that can perform direct heat exchange with the buildings, therefore, no electricity for heating is consumed. When the grid natural gas generators are off, the assumption is that primarily carbon free generation sources are producing electricity. To avoid curtailment of these resources, the temperature of the network is lowered and electricity demand is created from the electrification of heating using heat pumps. The thermal network temperature is lowered over time with the removal of heat to meet the buildings' heating demand. Once the temperature has been reduced to the low temperature set point, energy is added back into the network from the EMC.

With current district energy systems, the networks are long in length and therefore have large volumes of fluid to control, or thermal mass. Lengths of traditional district energy networks can range from tens to hundreds of kilometers. The large amounts of thermal mass in these networks make it very difficult to change the distribution temperature in a reasonable time frame. In order to obtain controllability of the network temperature, it will be shown that the micro-thermal network (MTN) length needs to be less than 5 km.

The operational strategy presented that reacts based on electrical grid behavior creates an opportunity to levelize the grid, it utilizes natural gas generators more efficiently, and uses potentially curtailed renewable electricity when it is available. Along with providing demand response, this research also investigates the ability to harvest heat from building space cooling and refrigeration processes as a means to reduce GHG emissions.

1.2 Scope of Work

To meet the research objectives, a selection of component and system models were developed in the equation-based object-oriented software Dymola. The developed models were used to run yearly system simulations to outline the operational range of the system and highlight the behavior of different system elements.

A design strategy was developed that determines a reasonable thermal mass to ensure the successful temperature transition of the network. This allows the network to quickly respond to changes on the electrical grid in order to provide effective demand response.

Chapter 2

2. Literature Review

The following literature review will cover the main concepts explored in this thesis.

2.1 Electrification of Heating

The electrification of fossil fuel technologies has become a popular decarbonization strategy. When the local electrical grid is comprised of predominantly renewable generation, the electrification of heating can result in an overall decrease in emissions. Although, even with a large renewable generation capacity, the peaks associated with space heating do not align with the availability of renewables and result in the use of natural gas generation. Electrification of heating also results in a large increase in demand, causing additional generation infrastructure to be constructed. The challenge with the electrification of heating is the increase in required grid generation capacity and the incorporation of renewables with the new peak demand.

Tarroja et al. [15] conducted a simulation for the 100% electrification of heating for residential buildings and 80% for commercial buildings in the year 2050. The study used an electrical grid with the majority of generation coming from renewable sources and found that heating electrification provided a 30 to 40% reduction in GHG emissions. The large reduction in emissions comes from the near elimination of natural gas for heating and the increase in efficiency of a heat pump (defined in Section 2.1.1) versus natural gas heating on the building level. On a grid level, there was significant increase in capacity required from the electrical grid. The higher magnitude of loads and the lack of renewable generation that coincided with the load increase, caused dispatchable natural gas generation to support the grid when the heating loads occurred. Due to the use of natural gas generation, the emissions associated with electricity generation increased.

In the Netherlands, a study was conducted comparing the traditional system, a partial electrification, and full electrification of the buildings and transportation sector. The projected electrical demand and electrical generation sources were developed for 2050. An electrical grid of predominantly renewable resources, and their associated capacities, was predicted based on government targets. In the traditional scenario, where the majority of homes and vehicles operate on fossil fuels, predicted that renewable generation capacity was able to meet 70% of the total electrical demand. With the same installed renewable generation capacity, in the partial electrification scenario renewables met 50% of the demand. In the full electrification scenario, the level of electricity consumption increased greatly and renewable generation was only able to meet 40% of the demand while gas-fired plants were responsible for 50% [16]. Their findings echo the results of Tarroja et al. [15], as electrification increases the demand, the overall emissions decrease from the reduction in fossil fuel use, but the incorporation of renewable generation becomes increasingly difficult.

2.1.1 Heat Pumps

Heat pumps are a key technology and are expected to deliver up to 90% of heating energy in the future, especially in the residential sector [9]. Heat pumps take heat from low temperature sources, such as the ambient air, a body of water, the ground, or low quality waste heat, and utilize electricity to step it up to high temperature heat that can be utilized in space heating systems. The efficiency of a heat pump is denoted by the coefficient of performance (COP). The COP is a measure of the heat generated from the heat pump per unit of electricity. For example, with a COP of 5, for every 1 kW of electricity consumed, 5 kW of heat are generated. The COP equation is presented as Equation 2.1, where the heat produced by the heat pump (Q_h) is divided by the electricity/power input (P).

$$COP = \frac{Q_h}{P} \tag{2.1}$$

The issue at a national and international scale, is the effect of heat pumps on the electrical demand in countries with cold winters. Globally, a 100% heat pump adoption would require 11% of current world electricity and increase the peak demand by 65%, unless major, expensive, infrastructure is adopted this peak demand is unlikely to be met [9]. The air source heat pump (ASHP) is expected to be the most widely adopted on an individual scale, compared to ground source heat pumps (GSHP), as they do not require a large area of land [9]. Water source heat pumps (WSHP) are widely adopted in commercial operations to utilize heat from low temperature sources. When integrating large quantities of heat pumps into the power system without dedicated controls, negative effects could occur [17].

2.1.1.1 Ground Source Heat Pumps

GSHPs, along with various other HPs, are being widely adopted for the electrification of heating, but they provide additional challenges. When GSHPs are used for heating they are utilized for cooling as well. The heating and cooling loads need to be balanced to prevent the ground temperature from either increasing or decreasing drastically over time.

A study was conducted in China by Li et al. [18] exploring the use of GSHPs on multiple office buildings. In one scenario, the heating load was much higher than the cooling load. The large heating load removed heat from the ground that was not replenished, causing a decrease in ground temperature over the span of 10 years. Declining ground temperatures lead to a decrease in the COP/efficiency of the GSHP system. When the heating and cooling loads are balanced, the ground temperature trend year after year remains consistent and the GSHP efficiency remains stable at its

design value. Luo et al. [19] also prove that a thermal imbalance can lead to a temperature shift of the ground over time causing a change in system efficiency.

2.2 District Energy Systems

District energy systems have a long history of being a reliable and efficient way to distribute energy to a range of consumers. Over time the systems have taken on many forms with different applications, the systems will be outlined in this section.

2.2.1 District Heating

The central goal behind district heating is to recycle local fuel and heat resources that would otherwise be wasted and supply the heat demand to a network of consumers [20]. District heating (DH) systems as a source of heat distribution for buildings has been around for generations. The first known DH system was a medieval system located in Chaude-Aigues, France dating back to 1334, the system delivered hot water from a geothermal source through wooden pipes [20]. The first commercial DH system in the United States was implemented by Birdsill Holly in Lockport, New York in 1877 delivering steam to 14 customers [21]. In Europe they were commercially implemented in Germany in the 1920s [20]. It is approximated that the number of district heating systems today has reached 80,000 worldwide [20].

District heating encompasses a network of pipes that connect buildings within a certain area. The buildings receive their heat through a supply pipe carrying the hot temperature fluid. When the buildings have taken the heat they require, the fluid is sent to a return pipe which retreads back to the centralized plant to be heated again. The systems containing a supply and return pipe are labeled as 2-pipe systems. DH consumers can be served from one centralized plant or a number of distributed heat producing units [22].

Cogeneration, or combined heat and power (CHP), is the simultaneous use of electrical and thermal energy from a single source and is often used in DH centralized plants. Traditional fossil fuel fired electrical generation rarely exceeds 50% efficiency, the remaining fuel energy is wasted. When the "wasted" heat is captured and incorporated as a CHP system, the overall fuel efficiency can reach up to 80% [14]. CHP generation is often economic and reduces both GHG emissions and fuel consumption in a community [13].

As modernization and decarbonization efforts have taken place, DH has evolved and is classified into generations of district heating. The 1st to the 3rd generation of district heating (GDH) utilize the traditional approach with a supply dominated by fossil fuels and hot distribution temperatures [23], they are summarized in Table 2.1 and also in Figure 2.2.

Table 2.1: Summarization of the 1st to the 3GDH main characteristics [22]

	1GDH	2GDH	3GDH
Distribution Fluid	Steam	Pressurized hot water mostly over 100°C	Pressurized hot water often below 100°C
Heat Production	Coal steam boilers and some CHP plants	Coal and oil based CHP and some heat-only boilers	Large-scale CHP, distributed CHP, biomass and waste, or fossil fuel boilers
Circulation System	Steam pressure	Central pumps	Central pumps

2.2.2 District Cooling

District cooling (DC) systems employ the same concepts as DH. Cooling energy is supplied from a central distribution plant and is sent through an underground piping network to reach its consumers. The fluid is then sent via the return pipeline back to the plant where it is cooled again, demonstrating a 2-pipe system. Lund et al. [22] have defined a generational categorization for DC systems. The 1st generation was a pipeline refrigeration system consisting of centralized condensers and decentralized evaporators with refrigeration as the distribution fluid. The 1st

generation pipeline refrigeration systems were introduced in United States in the 1890s [20] and also seen in European cities. The 2nd generation district cooling systems are based on large mechanical chillers and utilize cold water as the distribution media. Early 2nd generation DC systems were established in Hartford, USA in 1962, Hamburg, Germany in 1967, and the La Defense district outside Paris in 1967 [20]. Lastly, the 3rd generation DC systems have integrated more diverse energy supply technologies such as absorption chillers, natural cooling from lakes, excess cold streams, and cold storages. The majority of 3rd generation systems were established in the 1990s. A large 3rd generation DC network exists in Toronto as a part of the Deep Lake Water Cooling (DLWC) project. The DLWC project uses Lake Ontario as a source to cool buildings in the downtown core, freeing up approximately 61 MW of electricity from Ontario's electricity grid during peak periods [24].

2.2.3 District Energy

Combined systems that provide both cooling and heating to a district of consumers take on the term district energy (DE) systems. Some DE systems provide electricity as well. With the incorporation of both heating and cooling, each system has their own set supply and return pipes, the traditional DE system therefore becomes a 4-pipe system. DE systems are flexible in terms of the sources they can accommodate for heating and cooling and can thus can be environmentally beneficial and cost effective in appropriate applications [13]. District energy is predominant in Europe and is making headway as an efficient energy distribution system in Canada. As of 2015, the distribution of main district energy systems across the country can be seen in Figure 2.1.

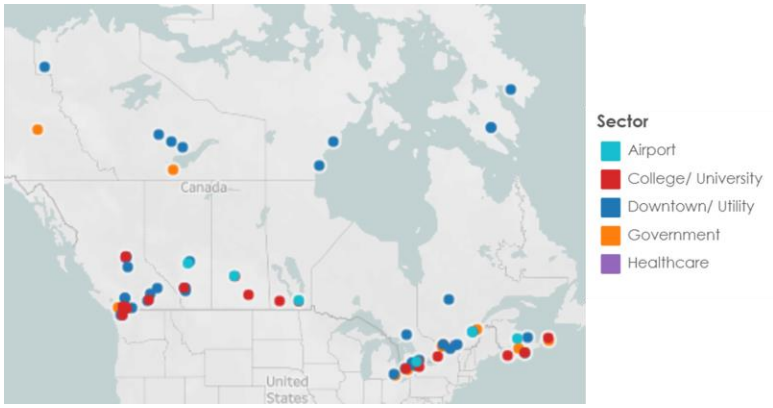

Figure 2.1: Canadian district energy systems map as of 2015 [25]

2.2.4 4th Generation District Heating

The 4th generation of district heating (4GDH) utilizes the structure of a traditional 2-pipe DH network, but with lower distribution temperatures (30 to 70°C). The drop in distribution temperature allows for the incorporation of heat from low temperature sources and the electrification of heating. An example of a low temperature heat source is the waste heat from industrial processes or cooling processes in buildings. The lower temperatures enable the linkage of the electrical, thermal, and gas grids. Integration of the various grids creates system flexibility, there can be numerous outcomes in terms of system energy usage and GHG emissions [26]. A summary of the aspects of a 4GDH network are outlined in Figure 2.2.

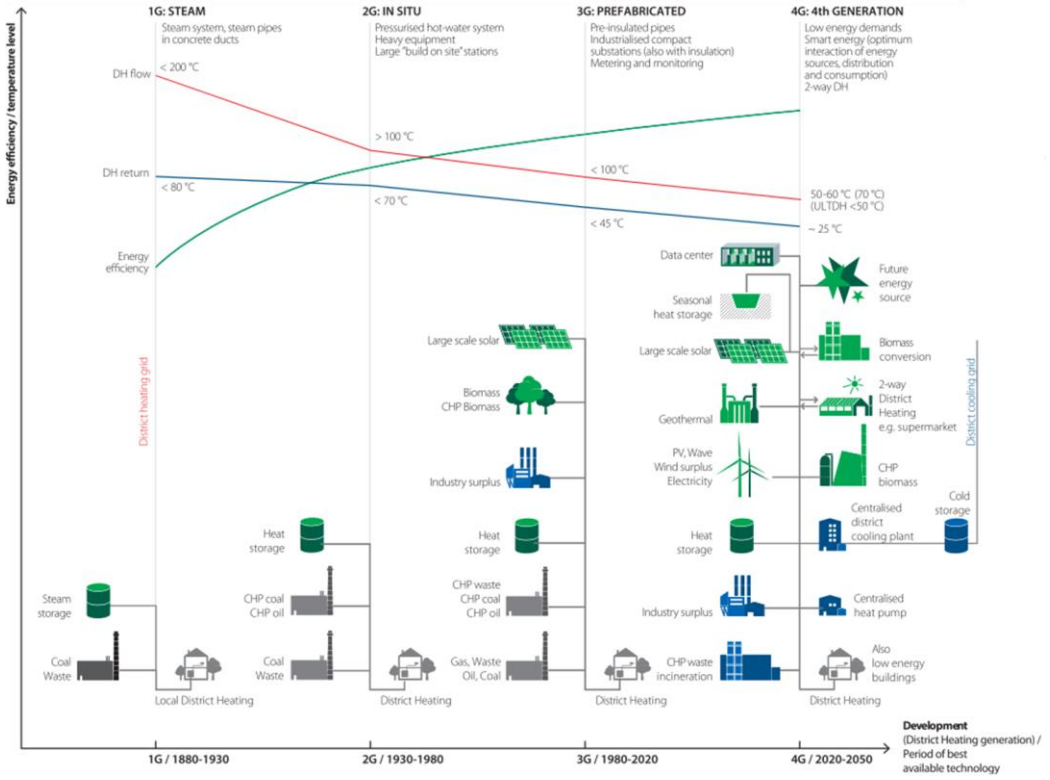

Figure 2.2: Summary of the evolution of district heating including 4GDH attributes [27]

Buildings attached to a 4GDH network can be thermal energy consumers and remove heat from the network to meet their heating demand. Additionally, in 4GDH there is the opportunity to provide heat to the network, introducing the "prosumer". A building containing cooling process heat, such as an arena, data center, or even traditional space cooling, can become a prosumer and add carbon free heat to the DH system. A district heating system that makes use of local waste heat from processes in commercial buildings is a much more complex type of district heating system that requires detailed dynamic performance investigation and planning [22].

Kauko et al. [28] performed simulations with the dynamic simulation software of Dymola, utilizing data centers and grocery stores as prosumers on the network. When the prosumers are active, water is taken from the return pipe, heated by the prosumer through direct heat exchange, and delivered to the supply pipe. Possible energy required for upgrading the heat provided by the prosumers was

not considered. A low temperature network at 65°C was simulated and compared to a network at the same temperature but including prosumers. The addition of prosumers decreased emissions by 29% because less heat was generated centrally by fossil fuel sources. It was recommended that thermal storage be investigated as the majority of heat from prosumers is available in the summer months when heating demand is low [28]. The use of thermal storage coupled with heat pumps in 4GDH has been seen as a feasible and fuel efficient option to incorporate carbon free sources of heat [29].

In 4GDH, there is also the ability to be a part of an integrated smart energy system, with the combination of the thermal, electric, and gas grids [28]. Smart energy systems veer away from single-sector thinking and allow for the design of systems that understand, benefit, and incorporate the needs of all sectors [29]. The transformation of thermal grids into smart energy systems, lends itself to the incorporation of heat pumps for the electrification of heating and the ability to utilize low temperature heat sources [22]. Implementation of heat pumps reduces the use of boilers, while at the same time enabling the use of renewable energy [27]. Merging the heating and electricity sector allows for DH systems to balance fluctuating renewables on the electrical grid with the implementation of CHP and power-to-heat technology [30]. The low temperature thermal network is crucial for the integration of renewable and innovative ideas into the DH network.

2.2.5 5th Generation District Heating and Cooling

The 5th generation of district heating and cooling (5GDHC) has a distribution temperature that operates in the range of 6 to 40°C. The ultra-low temperature thermal networks allow for the heating and cooling of buildings from a two pipe or one pipe system. 5GDHC networks are trigeneration systems, providing heating, cooling, and electrical energy to its prosumers.

Advances in 5GDHC are not meant to replace 4GDH, the 5th generation builds upon the ideas from 4GDH and is a complementary option suited for different system requirements [23].

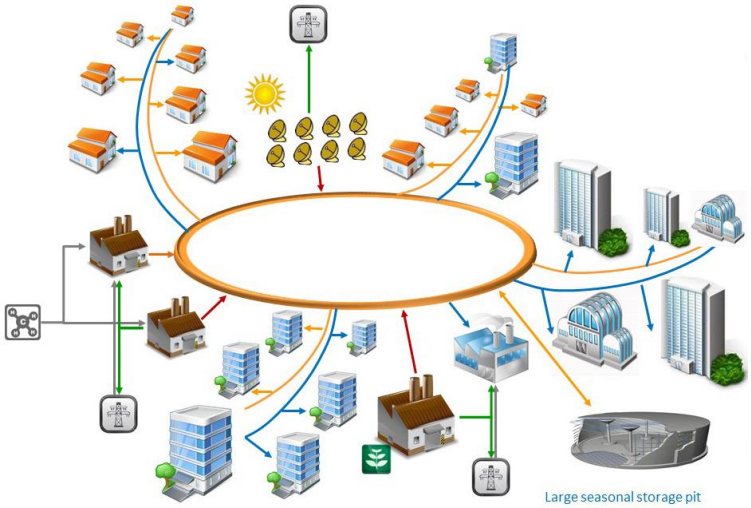

Figure 2.3: Visual representation of 5GDHC sources [31]

5GDHC has a foundation built on the incorporation of thermal and electrical renewable energy. The networks have a free-floating temperature and can exploit an infinite number of heat sources, visualization in Figure 2.3. The use of both short-term and seasonal energy storage is a key part of a 5GDHC system. Storage allows for bridging the temporal gap between supply and demand of heat and cold, as well as temporal gaps between availability of renewable electricity and operating moments for heat pumps [32].

The 5GDHC systems provide a high level of flexibility as a result of integrating heating, cooling, and electricity infrastructure and the availability of storage facilities at different temperatures and time scales [32]. Zarin Pass et al. [33] determined that the communities best suited for the implementation of 5GDHC systems are those with diverse loads. A community's diversity is represented by different types of buildings, such as residential, commercial, arenas, etc., each

building having a different load profile. Perfect density would mean the community has an equal heating and cooling load at any given time.

Buffa et al. [34], from their comprehensive review of 5GDHC systems, developed categories for 5GDHC systems based on the energy and fluid flow direction:

1. Bidirectional energy flow – unidirectional medium flow: typical for 5GDHC networks with a centralized pumping station where some users can be in heating and others in cooling mode. Systems commonly use a 1-pipe network where buildings are arranged in series, Figure 2.4 (b).
2. Bidirectional energy flow – bidirectional medium flow: typical for 5GDHC networks with decentralized pumping stations (one per substation) where simultaneously some users can be in heating and others in cooling mode. Systems commonly use a 2-pipe configuration with one warm pipe and one cool pipe, Figure 2.5 (b). Multiple types of hydraulic configurations can be considered for this case.

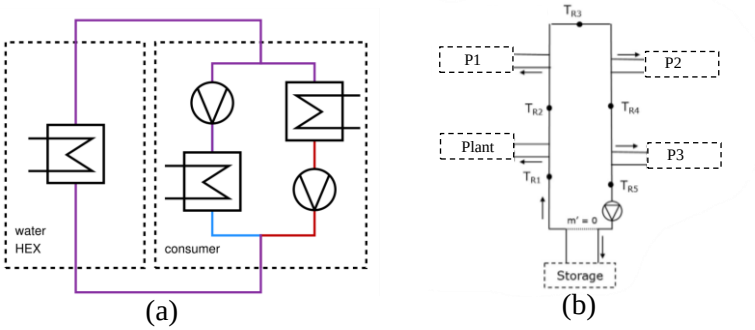

Figure 2.4: 5GDHC unidirectional medium flow schematics
(a) unidirectional substation at each building and the heat exchanger (HEX) at the plant [35] and (b) the unidirectional system schematic [36]

For category 1 bidirectional energy flow – unidirectional medium flow, Rogers [37] modeled a unidirectional low temperature thermal network (UDLTTN) as a retrofit on an existing district energy system and compared the performance to the traditional 4-pipe district system. The

UDLTTN is a one pipe system that operates between 15 and 25°C and the system on average reduced emissions by 46%. The emissions reduction was seen as a result of capturing cooling process waste heat, the lower distribution temperatures, and the integration of decentralized heat pumps to offset natural gas use. The model showed, however, the UDLTTN doubled the community's peak electrical demand. A carbon free electrical generation source is required to meet this increased demand to avoid an increase in GHG emissions.

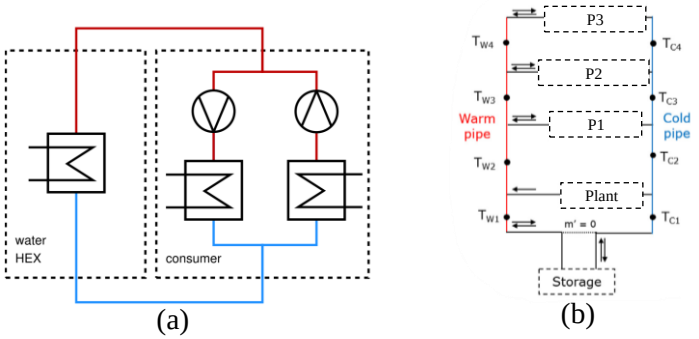

Figure 2.5: 5GDHC bidirectional medium flow schematics
(a) bidirectional substation at each building and the heat exchanger (HEX) at the plant [35] and (b) the bidirectional system schematic [36]

A wide range of 5GDHC systems were found in literature for category 2, bidirectional energy flow – bidirectional medium flow, such as [38], [39], [33], [40], [35], and [41]. For these systems, the buildings are typically arranged in a parallel configuration. Both Bunning et al. [35] and Schluck et al. [41] compare a bidirectional to a unidirectional medium flow system. Temperature ranges for the system are: for the bidirectional, the warm pipe is 12 to 20°C and the cold is 8 to 16°C, and the unidirectional was controlled to operate within the same limits. The authors concluded that the bidirectional system was more efficient than the unidirectional system. In a unidirectional system, the different temperature fluid returning from the heating and cooling systems is mixed into the same pipe, see Figure 2.4 (a), which decreases the usefulness of both the warm and cool fluid. Comparatively, in the bidirectional system, the returning fluid travels into the corresponding cool or warm pipe, Figure 2.5 (a), leading to the system having a greater efficiency.

Sommer et al. [36] modeled a one pipe, unidirectional thermal network, entitled the reservoir network (RN). The aim of this research was to eliminate the pumping complexities of a bidirectional fluid flow system. In the RN, the buildings take water from the network, that is operated between 6 and 17°C, to cover their heating or cooling demand and reinject the water into the same pipe, as demonstrated in [37] and Figure 2.4 (a). The RN electrical energy consumption is approximately equal to the bidirectional network when a variable mass flowrate was used. For RNs run with a constant mass flowrate, the electrical energy consumption increased by 48% compared to the bidirectional. The heat pump electrical consumption was on average 2% greater in the RN due to lower network temperatures, but overall, there was no notable difference in the efficiency of the heat pumps. Sommer et al. concluded that the bidirectional and RN with variable mass flow have comparable annual energy consumption. Advantages of the RN topology over bidirectional networks are its greater freedom in planning, its simplicity regarding further spatial extension of the network, and its robust operation as mass flowrates can be adjusted without affecting the hydraulics of other prosumers.

2.3 Pumping, Piping, Flow, and Heat Losses in District Energy

2.3.1 Thermal Losses

In traditional high temperature DH systems, thermal losses are on average 5 to 15% of the supplied heat. During the summer months, when the system is only operating to meet the domestic hot water (DHW) demand, the losses can reach 30% of the supplied heat [34]. The lower distribution temperature seen in 4th and 5GDH results in lower thermal distribution line losses. In modeling a 4GDH network, Kauko et al. [28] saw a 31% decrease in heat losses when comparing a constant supply temperature of 55°C to a reference case with 95°C. Köfinger et al. [42] saw a reduction in heat losses of 29% when comparing a supply temperature of 120°C to a LTDH scenario with a

constant supply temperature of 58°C. The relative heat losses, when evaluated as a percentage of the heat delivered to the system, in [28] was 2.9% and 4.2% for the 55°C and 95°C networks.

2.3.2 Pumping Power

The relative importance for pumping electrical consumption (REI_{pump}) of traditional high temperature district heating systems is measured as a ratio between the electricity consumption for pumping and the heat delivered to the substations. On average, this value is 0.5% for traditional DH systems and approximately one order of magnitude less than heating losses [34]. For the modeled 4GDH system in [28], the relative pump energy for the 95°C case was 0.20% and in the 55°C case 0.41% was observed, which is a 109% increase.

For their bidirectional 5GDHC network with a warm pipe at 18°C and a cool pipe at 14°C, Wirtz et al. [38] had a total rated electric power of the pumps of 22.82 kW. The total pumping energy for the year utilizing a variable mass flowrate was 22.4 MWh or 0.35% of the annual heating demand. Ruesch et al. [43], through modeling of a low temperature heating and cooling network in Zürich, predicted pumping energy consumptions to be 0.6 to 3.4% of the delivered energy to the buildings. From the implementation of the system, the pump electricity consumptions result in 125 MWh per year corresponding to a relative pumping energy of 2.7% [34].

Overall, little information has been reported for the pumping power in 5GDHC networks. But, in 5GDHC systems, the relative importance ratio for pumping power is expected to increase compared to traditional networks due to the low temperature difference between the supply and return flows [34].

2.3.3 Flowrate and Velocities

To determine the flow parameters through DH distribution piping, it was commonly seen that a desired pressure drop was chosen within a permissible range to reduce system pumping requirements. The velocity, mass flowrate, and pipe dimensions were calculated accordingly.

Kauko et al. [28] state that 150 Pa/m is a typical design criteria used by DH suppliers. Wirtz et al. [38] use a maximum pressure drop of 200 Pa/m. Ommen et al. [44] use a pressure drop of 50 Pa/m as they mention that a pressure drop in the range of 50 to 100 Pa/m is typical for DH networks. Yildirim et al. [45] found that designing for a pressure loss between 50 to 200 Pa/m was common practice.

Martin-du Pan et al. [46] summarized the typical design velocities for steel pipes from the Chartered Institution of Building Services Engineers (CIBSE) and the Swedish District Heating Association (SDHA) and corresponding pressure drop. For pipe sizes ranging from 50 to 300 mm, the velocities and pressure drop range from 1 to 2.5 m/s and 100 to 180 Pa/m. Stevanovic et al. [47] states that the range for the velocity in the main district heating pipe can reach up to 3 m/s. Olsen et al. [48] states that the recommended maximum velocity through the pipes is 2 m/s for their low temperature district heating network with a supply and return temperature of 55 and 30°C. Yildirim et al. [45] state the acceptable velocity range for water in a district heating system is 1 to 3 m/s. Smaller velocities in DH piping not only result in lower pressure losses but also reduce the affects of flow accelerated corrosion.

In the reservoir network (RN) by Sommer et al. [36], three scenarios are explored. The mass flowrates utilized for the pipe design are equal to the 95th percentile of the hourly mass flowrate required by the buildings. For RN3 the mass flowrate is variable and controlled based on the network temperature. The corresponding pipe diameters were then chosen based on the desired

pressure drop. Values are summarized in Table 2.3. In the constant mass flowrate scenarios, RN1 and RN2, a large pumping requirement is seen, whereas in the variable flowrate scenario, RN3, the pumping requirement significantly decreases. During periods when the thermal demand is low, in RN3, only a small mass flowrate is required to maintain the network temperature. Whereas with a constant flowrate, the larger design mass flowrate is consistently pumped through the network. The dips in flowrate in the variable flow case prevent the yearly power requirements from reaching large levels.

Table 2.3: Network piping and fluid flow parameter summary [36]

	Circulation Pump Design Mass Flowrate [kg/s]	Pipe Design Mass Flowrate [kg/s]	Pressure Drop [Pa/m]	Resulting Pipe Diameter [m]	Velocity [m/s]	REI_{pump} [%]
RN1	95	95	250	0.21	2.7	14%
RN2	95	95	125	0.23	2.3	8.5%
RN3	97.3	69.5	250	0.18	2.7	2%

2.3.4 Pipe Material in District Heating Networks

The traditional material for district piping is steel. Pre-insulated rigid steel pipes have the largest share in DH systems [49]. In traditional steel piping flow accelerated corrosion (FAC) is a large issue. The FAC rate peaks at temperatures in the range of 140 to 160°C and a pH of 7 [50]. The FAC rate also increases with an increase in flow velocity due to the effect that velocity has on mass transfer [51]. The corrosion rate vs velocity was experimentally analyzed and plotted by [51], it was concluded that the corrosion rate increases exponentially with an increase in velocity.

New developments in the DH field have introduced pre-insulated rigid polymer pipes and pre-insulated flexible PolyEthylene (PE) pipes with a life span of more than 30 years [49]. Flexible pipes made of polymer material, such as PE, are corrosion resistant. Nevertheless, they are sensitive to the high temperatures used in DH systems [49]. As district heating systems head

towards the 4th and 5th generations, the high temperatures of traditional systems are no longer a concern for the polymer piping. Lund et al. [22] identify 4GDH networks and future to have flexible piping networks.

Installation time and costs of High-density polyethylene (HDPE) are reduced with respect to traditional DH systems. Flexible pipes can be rolled-out during installation and adapted to different geometries while pipe joints can be performed with fittings. Thus, welding processes, exhaustive inspection, and local insulation of joints, that required skilled manual work in traditional DH systems with steel piping, can be avoided with HDPE piping [34]. The plastic piping also has a very smooth surface, resulting in lower pumping power requirements and smaller pipe sizes [52].

2.4 Demand Response

With the introduction of fluctuating renewable energy sources like wind and solar, electricity generation is changing in time depending on the weather conditions. This brings additional challenges to the existing power system. Changing the electricity demand to compensate for fluctuating renewable electricity generation can help to reduce the negative aspects of renewable energy sources on the power system [17].

Demand response involves changing the time when electricity is consumed to avoid burdening the electrical generation systems. Demand response actions are non-permanent, as opposed to demand side management, which involves altering a building's energy efficiency to reduce the overall electricity consumption at the source [53].

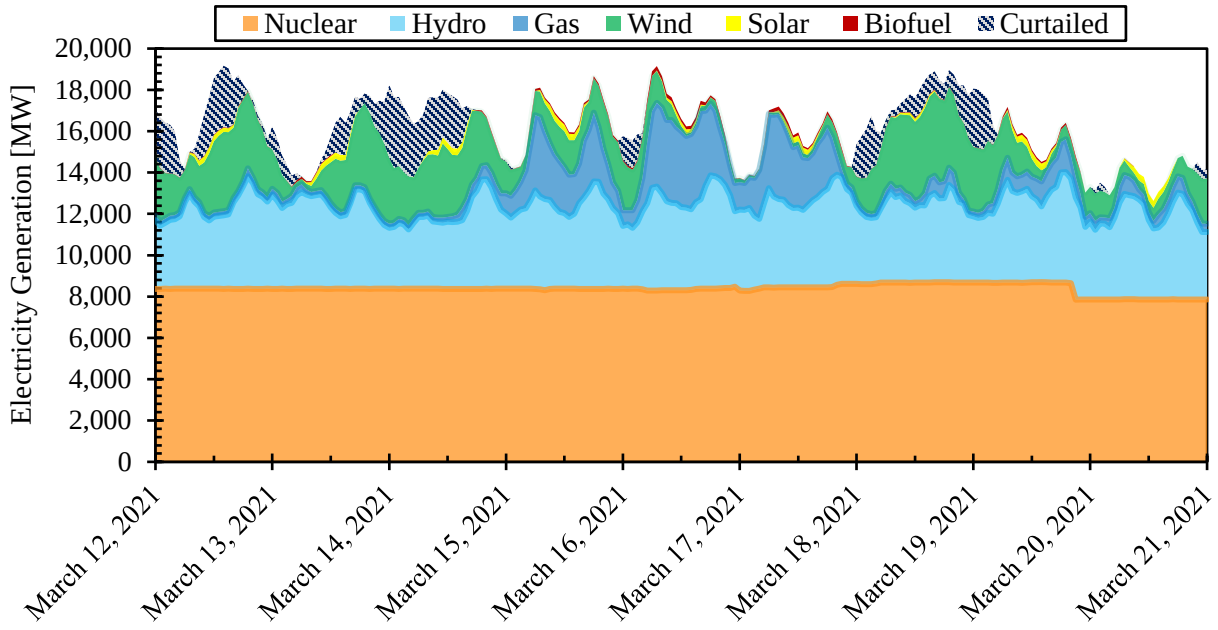

Figure 2.7: Ontario electrical grid generation for a week in March, 2021 [54]

Figure 2.7 displays the supply of electricity on the Ontario electrical grid based on the generation source. Data was collected for a week in March, 2021 from the IESO [54]. The week of data collection had especially windy days, March 13th and 14th, and the demand was not great enough when there was wind generation available, therefore, that electricity was curtailed. A total of 1,289 GWh of variable generation was curtailed in 2021, representing 12% of total variable generation [6]. Later in the week, March 16th and 17th, natural gas peaking power plants are dispatched at a peak of approximately 4 MW to meet the peak demand. With demand response strategies, electrical demand can be increased during periods where there are renewable generation sources available, avoid curtailment, and reduce the use of natural gas electrical generation.

2.4.1 Incentive to Alleviate Demand

In Ontario, there is financial incentive to reduce the peak demand. The Industrial Conservation Initiative (ICI) program reduces the cost of electricity for large consumers when they reduce their electrical consumption during hours of peak demand.

In Ontario, the electricity price is typically determined by the Hourly Ontario Energy Price (HOEP) and the Global Adjustment (GA) factor. The HOEP is the wholesale price of electricity, it is dynamic in nature and changes hourly. The wholesale price of electricity is based on demand, the availability of supply, and the operational cost of the electricity generator. The GA is the electricity bill component that covers the cost of building new electricity infrastructure in the province to ensure electricity supply into the future [54].

Under the ICI program, the GA component of the electricity bill, for the eligible customer, is based on their contribution to the peak demand. As the customer reduces their electricity consumption during peak periods, less electrical infrastructure is required by the grid, therefore, their GA rate decreases. Through the ICI program, the GA rate paid is based on the Peak Demand Factor (PDF). The PDF is the customer's contribution percentage to the 5 peak demands of the year, a sample calculation is displayed in Table 2.4.

Table 2.4: Sample calculation of the PDF [54]

Peak	Day	Hour	Customer Consumption [MWh/h]	Peak System Consumption [MWh/h]
1	July 19th, 2019	HE 12	4.1	22,367.8
2	July 5th, 2019	HE 17	3.1	22,294.1
3	July 29th, 2019	HE 17	3.9	22,129.1
4	July 20th, 2019	HE 17	4.4	22,103.4
5	July 4th, 2019	HE 18	4.3	21,683.9
Total			19.8	110,578.3
PDF = 19.8/110,578.3 = 0.000179				

In Table 2.4, the customer consumed 19.8 MW during the top 5 peaks, contributing to 0.018% of the peak load. The calculated PDF is multiplied by the GA rate, resulting in the GA cost billed to the customer. The less demand generated by the customer the greater financial savings. Customer

consumption can be reduced by on-site generation, such as CHP, or with demand response strategies that shift the customer load to an off-peak period.

2.4.2 Demand Response Strategies in Literature

With traditional district heating networks, there was no connectivity to the electricity grid, therefore, the focus was on shifting thermal demand to avoid straining the central heat generation source. The shifting of thermal peaks also avoids the use of a peak boiler and the increase in pumping costs due to the increase in flow needed during peak periods. Guelpa et al. [53] summarize the thermal demand response strategies. The majority of concepts from shifting the thermal peak can be applied to electrical peaks as well.

Guelpa et al. [55] accomplish thermal peak shaving by rescheduling building heating demands. The peak heating demands of buildings attached to the network are staggered by a 20 to 90 minute delay time so buildings no not reach their peak demand simultaneously, therefore reducing the overall peak thermal demand by 35%.

Cai et al. [56] conduct building heating demand optimization in DH networks for demand response. Thermal power for each building is analyzed cumulatively and the amount of power each building receives is optimized as to prevent peaks at the central plant. A building could receive less power than their heating demand, leading to the decrease in the temperature of the building. Thermal comfort of the occupants was included in the optimization and was maintained at a reasonable level. Minor temperature variations were demonstrated to have minimal impact on thermal comfort, demonstrating the flexibility of buildings.

Leśko and Bujalski [57] demonstrate the potential of controlling the heat delivered to buildings based on when heat is available. The basis of the paper is the variable nature of a CHP plant, the

operation is based heavily on the price of electricity and therefore the operation of the CHP may not always coincide with heat demand. The heating power of the DH network is reduced when heat resources are not abundant. During this time, the building's thermal mass is required to sustain the heat load until periods where heat is available. When the CHP is operational, the network can re-heat and the building's full demand can be met.

Lesko and Bujalski [58] build upon their previous paper [57] and explore thermal energy storage in the network pipes by changing the temperature of water. Utilizing the concept of the unstable nature of CHP plants, instead of shifting the heating load, the network is "over heated" when the CHP is on to store energy in the pipes for times when the CHP is not operating. Thermal energy storage in the pipeline requires no additional investment. The temperature in the pipeline was changed from 93 to 97°C. The transportation time of the temperature propagation through the network was also analyzed.

Basciotti et al. [59] also used the DH piping network as thermal storage to reduce the heating peaks. The network was heated before a peak load to reduce the peak heating requirements. During regular operation, the DH network supply temperature is 95°C. Pre-heating the fluid in the DH piping to 115°C when heating demand is low, reduced heat production required from the plant during the peak heating demand. The proposed strategy reduced heating peaks by 15%, enabled a fuel costs reduction by 2%, and CO_2 emissions reduction by 20%. The constraint is the storage capacity of the network piping.

To achieve electrical demand response, the coupling of HPs with thermal storage has been explored. Researchers in [60], [61], and [17] have implemented the electrical demand response strategy on an individual building scale to mitigate electrical peaks. Fischer et al. [17] conclude that this is an effective way to shift peak loads. Miara et al. [61] found that although the peak load

was shifted to off-peak times, the overall electricity consumption increased by 9 to 19% due to thermal losses of the storage and efficiency differences between large and small sized heat pumps.

As mentioned in Section 2.2.4 and 2.2.5, the 4GDH and 5GDHC networks are better suited for the application of electrical demand response due to the incorporation of the electrification of heating. Edtmayer et al. [62] couples thermal storage and heat pumps connected to a 5GDHC network, where the thermal storage is charged and discharged based on the electricity price. Their system led to savings in electricity cost for the operation of the heat pumps. It was demonstrated that 5GDHC networks show significant potential to couple the heat and power sectors. This is beneficial for the balance the energy market, and systems with larger quantities of thermal mass (including storage) offer greater impact.

2.5 Relationship to the ICE-Harvest System

The modeled ICE-Harvest system is a hybrid between the 4GDH and 5GDHC. The proposed network only provides the heating demand to the building and utilizes the existing building cooling infrastructure. An operational temperature range between 20 and 70°C was explored, which is typical of a 4GDH system. A one pipe network is utilized as seen in 5GDHC; bidirectional energy flow – unidirectional medium flow. There were contradictory conclusions regarding a bidirectional versus a unidirectional system. Since the research conducted utilizes the existing building chiller for space cooling and only harvests the rejected heat into the thermal network, the inefficiencies regarding the unidirectional network do not apply. The implementation of prosumers, electrification of heating, and merging of the electrical, gas, and heating networks are seen in both new generations of DH.

The ICE Harvest system provides demand response to the electrical grid through changing the temperature of the thermal network The network temperature changes from a low temperature to

a hot temperature depending on grid level natural gas peaking power plant generation. During periods when the network temperature is low, electricity is used to meet the heating demand. When the network temperature is hot, direct heat exchange is used at the building to reduce the electricity consumed. Such demand response strategies are not seen in the literature.

In order to achieve large temperature differences in relatively short periods of time, a design strategy is proposed for the thermal network. For the implementation of a large temperature set point change, a smaller distribution network design is required to reduce thermal mass and total travelling time in the network. Hence, the system will be classified as a micro-thermal network.

Chapter 3

3. System Modeling

3.1 Modeling Methodology

The object-oriented, equation-based software of Dymola was used for the modeling of the ICE-Harvest system. Dymola uses the programming language Modelica [63]. The Modelica language supports the dynamics and complexity of energy system modeling and its use is growing within academia and industry [64].

Rogers [37] compares different software for district heating system modeling. The researcher indicated that Dymola is better suited for larger network simulations vs. programs traditionally used for detailed modeling, such as TRNSYS. The difference is Dymola uses acausal modeling and TRNSYS uses causal modeling. In causal modeling, the modeled system is, directly or indirectly, described by a system of ordinary differential equations (ODE) in explicit form. The equations are directed, making it clear how the unknown quantities are derived from the known ones. In acausal modeling, the modeled system is, directly or indirectly, expressed as a system of differential algebraic equations (DAE) in implicit form. There is no longer a directed interpretation of the equations. Instead, given the known quantities, the priori of the equations is inferred when the models are used. The DAE formulation means that the modeler can focus more on what to model, rather than on how to model it. Acausal modeling is also known as declarative, mathematical, physical, or equation-based modeling in the literature. Further, the fact that the knowns and unknowns are not given a priori makes the models more reusable; allowing them to be more suitable for large scale system modeling. The most widely used language for acausal modeling is Modelica [65].

Giraud et al. [66] compared the use of TRNSYS and Dymola for the modeling of a DH network. The author noted that solving hydraulics is a requirement for any simulation program intending to address a DH network with a looped architecture. This issue can be naturally addressed by the Modelica language since it encompasses native multi-physics simulation capabilities. Extending the TRNSYS simulation capabilities to include hydraulics would be a very time-consuming task. Moreover, the acausal, equation-based, object-oriented nature of the Modelica language helps the programmer to significantly decrease development time. Dymola/Modelica was also used in [28], [36], and [67] due to its flexibility and efficiency as a dynamic modeling tool of DH systems. Validation studies of Dymola/Modelica have been completed by performing tests on an individual component basis and system level modeling. Examples can be found in studies [42], [59], [68], and [69].

An additional benefit to Dymola is the repository of established component models to implement into a large system model. Libraries used in this research include:

- Modelica Standard Library [70]
- Buildings Library [71]
- AixLib [72]

A Dymola library was created to model the ICE-Harvest system, which contains the models described in the following sections. The developed models contain a combination of logic and PI controllers. Tuning of the PI controllers was done on a trial and error basis. The integration constant and gain of the controller was varied until the output signal displayed the desired set point.

3.2 Network Pipe Model

3.2.1 Pipe Model

Two pipe models from existing Dymola libraries were explored: the district pipe from the Modelica Standard Library and the plug flow pipe from the IBPSA Buildings Library.

Multiple articles have been published using the IBPSA library's plug flow pipe model, such as [73] and [74], as an alternative to the Modelica Standard Library's (MSL) dynamic pipe. The dynamic pipe uses the element method and the plug flow pipe uses the node method. In the element method the pipes are discretized, they are divided into 'n' equally spaced volumes, or elements, in order to compute the temperature and heat losses [75]. To solve the partial differential equations within the mass, energy, and momentum balances, the finite volume method and staggered grid scheme are used [76]. The node method only considers the inlet and outlet of the pipe and calculates an outlet temperature based on the propagation delay, or residence time of the water in the pipe, the inlet temperature, and the boundary conditions [68]. Van der Heijde et al. [68] in their development of the plug flow pipe model compared it's performance to the dynamic pipe model. A district heating system was modeled and the simulated pipe outlet temperature was compared to measured data. It was concluded that both pipe models had similar accuracy in the prediction of the fluid temperature, but the plug flow pipe simulation speed was 68 times faster than the dynamic pipe using 1 node per meter.

To compare the behaviour between the pug flow and dynamic pipe model, a validation study was conducted based on the experimental work completed by Van der Heijde at al. In the experiment, a straight pipe length of 39 m was fed by water at an initial temperature of 18°C that was then heated to a temperature of 52°C. The pipe was located in a room where the heat transfer to the surrounding air was assumed to be 4 W/m^2K. Throughout the experiment, the mass flowrate, inlet

pipe temperature, and outlet pipe temperature were monitored. The input temperature profile from the experiment was used as a simulation input to the created Dymola model. In the Dymola simulation, the plug flow pipe using the node method was compared to the dynamic pipe varying the number of elements.

The plug flow and dynamic pipe simulated outlet temperature was analyzed and compared to the Van der Heijde at al. experimental data, presented in Figure 3.1. When 2 elements were used in the dynamic pipe, the experimental outlet behaviour of the fluid was not matched. Although using 2 elements in the dynamic pipe is computationally similar to the plug flow pipe, the temperature profile of the outlet fluid begins to change temperature before the residence time of the pipe is reached and the final temperature of 52°C is not met until after the experimental value. As the number of nodes is increased, the temperature profile of the delayed input is matched, not the experimental/measured output. With 1,000 nodes, the outlet temperature profile of the dynamic pipe matches with the delayed input signal, representing the theoretical output, and had a computation speed 275 times greater than the dynamic pipe. The plug flow pipe outlet temperature prediction shows good agreement with the experimental values, displaying its ability to determine the realistic behaviour of the fluid.

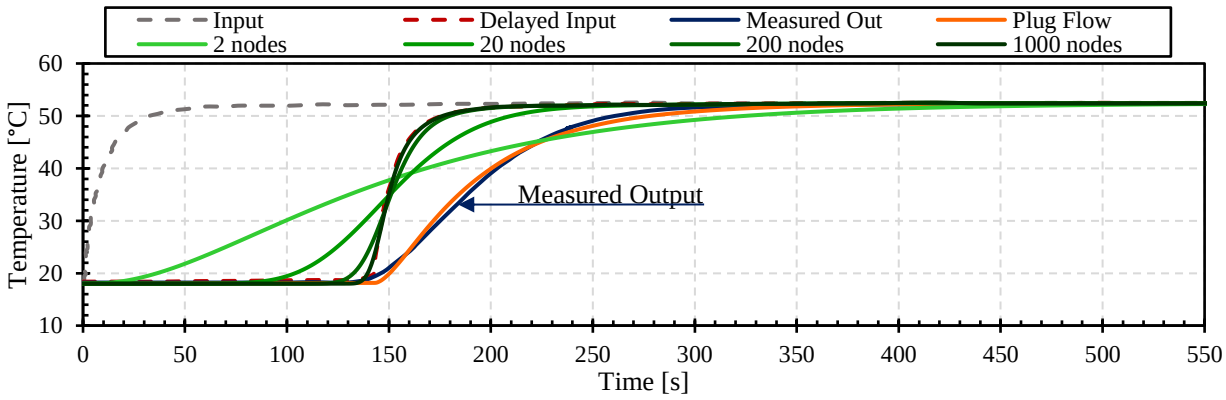

Figure 3.1: Recreation of Van der Heijde's experiment including the dynamic pipe

The MSL district pipe displayed large amounts of numerical diffusion at a low number of control volumes and required a large number of control volumes in order to obtain the theoretical output temperature of the fluid travelling through the pipe. This resulted in high computation times, which is not ideal for large system simulations. The main difference in the models, besides the methods used to solve for the fluid behaviour, is the incorporation of the thermal inertia of the pipe wall. The plug flow pipe uses the pipe material properties and wall thickness to calculate the thermal capacity of the pipe, the only material property in the dynamic pipe is the surface roughness. Including the thermal inertia allowed the simulated outlet temperature to match the experimental outlet temperature. Additional advantages of the plug flow pipe over the dynamic pipe are the fact that the grid size and time step do not have to be adapted to the flow velocity, and that there is no numerical diffusion [68]. Ultimately, the plug flow pipe was chosen for its computational efficiency and behavior that was experimentally validated through Van der Heijde et al.'s test.

3.2.2 Pipe Thermal Losses

The temperature of the ground is needed in order to determine accurate pipe losses from the thermal network. In Dymola, a model was developed, entitled *GroundTempDepth*, to determine the ground temperature at a specified depth from the ambient air temperature. Firstly, a correlation is used to convert the ambient air temperature to the ground surface temperature. The model then determines the ground temperature as a function of time and is dependant on the ground surface temperature, buried depth of the pipe, and soil properties. The model connects to the micro-thermal network piping as demonstrated in Figure 3.2. Equations and methodology for the ground temperature model are detailed in Appendix A.

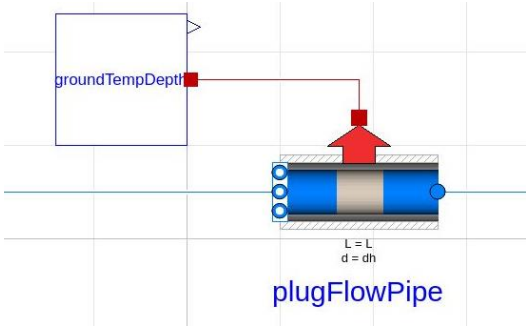

Figure 3.2: Developed ground temperature model in Dymola
and how it connects to the micro-thermal network piping

Once the ground temperature is calculated, it is converted into a heat flowrate for connection to the thermal network piping. The plug flow pipe, discussed in Section 3.2.1, uses the ground temperature as the boundary condition and the time delay of the fluid travelling through the pipe to calculate the outlet temperature of the fluid. Equation 3.1 outlines the method used in the plug flow pipe.

$$T_{outlet} = T_{boundary} - (T_{inlet} - T_{boundary})e^{\left(-\frac{t_{outlet}-t_{inlet}}{RC}\right)} \quad (3.1)$$

Table 3.1: Parameters for the plug flow pipe outlet temperature equation

Variable	Description
T_{outlet}	Outlet temperature of the fluid [K]
$T_{boundry}$	Boundary temperature (ground temperature) [K]
T_{inlet}	Inlet temperature of the fluid [K]
$t_{outlet} - t_{inlet}$	Time delay of the fluid in the pipe [seconds]
R	Thermal resistance per unit length from the fluid to the boundary temperature [mK/W]
C	Thermal capacity per unit length of fluid in the pipe [J/mK]

3.3 Heat Pump Model

3.3.1 Background

With the electrification of heating in the ICE-Harvest system, the heat pump COP plays a large role in the determination of site electrical consumption. Due to the extremely transient and unique

modelling requirements for the ICE-Harvest system, existing heat pump models were not able to provide adequate results/behaviour. The existing heat pump (HP) models and the motivation for developing a new model will be discussed.

3.3.2 The Carnot Model

The Carnot heat pump retrieved from the Buildings Library [71], is briefly discussed in this section. For more details, the model is described in [77].

The Carnot model determines the Carnot efficiency (COP_{Carnot}) based on the fluid inlet temperature to the evaporator and the outlet temperature of the condenser. The Carnot efficiency is then multiplied by a Carnot effectiveness (η_{Carnot}) and a compressor part load effectiveness (η_{PL}). The user specified effectiveness values normalize the Carnot efficiency in order to create a more realistic COP value.

$$COP = \eta_{Carnot}\,\eta_{PL} COP_{Carnot} = \eta_{Carnot}\,\eta_{PL}\,\frac{T_{con}}{T_{con} - T_{eva}} \tag{3.2}$$

The Carnot effectiveness is constant throughout the simulation. As shown in [78], the effectiveness of commercially available heat pumps does not remain constant with variations in the source inlet temperature. Therefore, Sullivan [78] developed an additional dynamic effectiveness scaling factor ($\varepsilon_{scaling}$) to add to the existing Carnot model. Resulting in Equation 3.3.

$$COP = \varepsilon_{scaling}\eta_{Carnot}\,\eta_{PL} COP_{Carnot} \tag{3.3}$$

The scaling factor is determined from the nominal operating conditions of the unit. Due to the changing thermal network temperature explored in this thesis, a nominal operating point cannot be identified. The scaling factor also uses the source inlet temperature to adjust the COP value, but with additional transient factors involved that have an influence on the COP, such as mass flowrate

and condenser temperature, the COP needs to be determined by more than the source inlet temperature.

Additionally, with the Carnot model, with and without the scaling factor, the COP would increase beyond feasible values as the temperature entering the evaporator increases. In reality, the COP would plateau and the HP would stop operating as the inlet temperature exceeds the maximum value allowed by the unit. For the reasons listed above, the Carnot model was not used to determine the COP of the heat pumps in the ICE-Harvest system.

3.3.3 The Scroll Compressor Model

From the Buildings Library [71], the scroll compressor heat pump model was analyzed. The scroll water to water heat pump model was constructed based off of the Ph.D. thesis by Jin [79].

The scroll compressor model is a deterministic model based on manufacturer performance data. Each equation describing the system components may have one or more parameters that are estimated simultaneously based on the manufacturer catalog data [79]. The evaporator and condenser are modeled as effectiveness-NTU heat exchangers with phase change on one side. The scroll compressor along with the refrigeration loop is also modeled.

The available model provides the complexity and accuracy needed for the ICE-Harvest system modeling. The main issues with the model, however, are the computation time (due to the need for interpolation between manufacturer data points) and the temperature limitations available from the built-in manufacturer data (maximum of 29°C entering the evaporator). The evaporator temperature limits would restrict the thermal network temperature ranges that can be tested. Therefore, due to the temperature limitations and high computation time, the scroll compressor was not chosen for implementation in system models.

3.3.4 Developed Heat Pump Model

A new heat pump model was constructed that uses a COP correlation from real manufacturer data. The heat pump component modeling was primarily based on the Carnot model, where just the condenser and evaporator were modeled and the heat flowrate was calculated as a function of the power consumption and COP. The evaporator and condenser are modeled by the Buildings Library *MixingVolume* [71] to represent the fluid mass in the components, the volumes were determined from HP manufacturer data sheets. The calculated heat flow is applied to the fluid in the mixing volumes. The remaining components in the model were retrieved from the Modelica Standard Library [70].

The power consumption is calculated from the part load of the "compressor" which is an input to the model determined from an outside control system. The expansion valve and compressor have been faded in Figure 3.3 (a) to signify that the components are not being modeled, only components outlined in black were modeled. The input signal "y" signifies the part load of the compressor. The compressor is assumed to be variable speed operating at the specified part load. Temperatures and mass flowrates of the heat pump are restricted by the operating limitations of the unit.

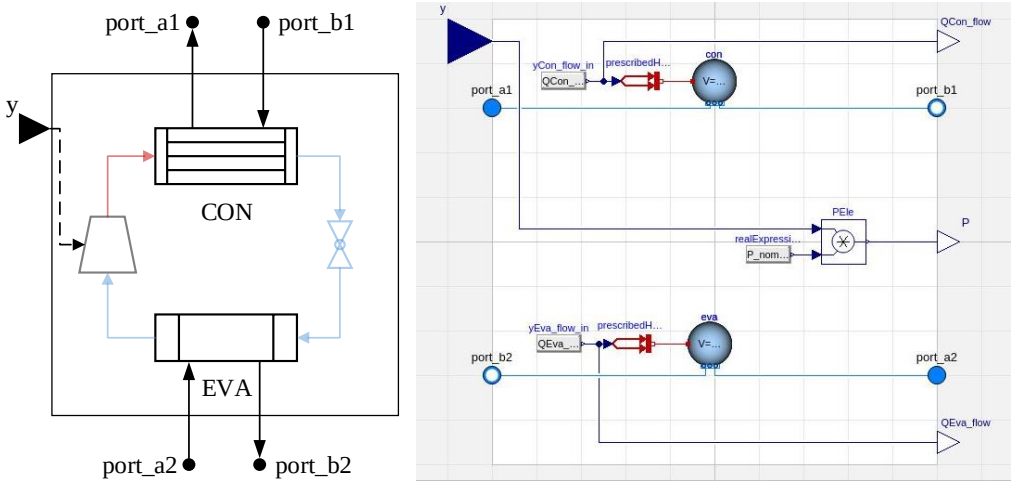

Figure 3.3: HP model diagram
(a) is a simplified schematic of the HP and (b) is the HP model in Dymola

To abide by the flowrate restrictions of the unit, the developed heat pump model simulates the heat pump as if there were multiple units in parallel, see Figure 3.4. The units are assumed to operate at the same part load capacity and have the same flowrate, and therefore the same COP. Each one outputs the same heating or cooling load, which totals to the desired load from the building. This way the COP calculation does not receive mass flowrate values that exceed the unit capacity and give unrealistic COP values.

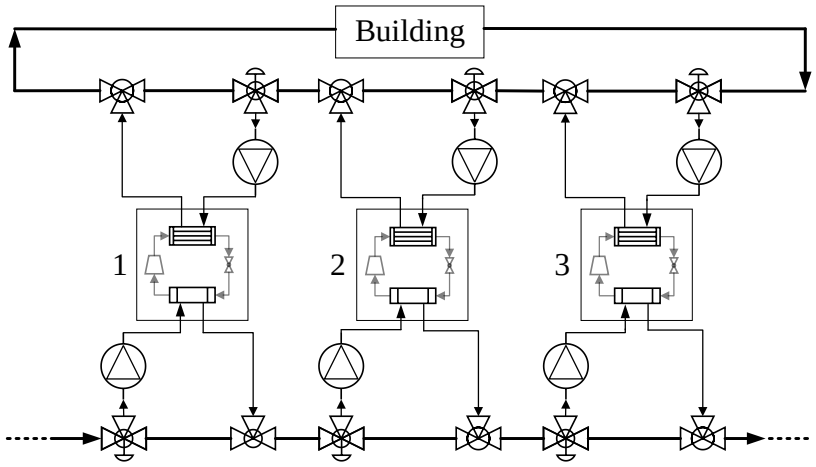

Figure 3.4: HP model methodology of multiple units in parallel

Three different heat pump models were constructed. Each HP has the same core methodology but contains a different COP correlation depending on if the heat pump is used for heating, cooling, or refrigeration.

3.3.4.1 Heating Heat Pump

The heating heat pump model is based on performance data retrieved from a confidential manufacturer. From the 630 data points provided, two training sets and test sets were established. Each training set was randomly selected and consists of 80% of the full data set, the test sets are the remaining 20% of the data. A regression analysis was performed with both training sets to

construct a COP equation. The regression analysis was performed in Minitab, with each equation having the form of Equation 3.4. The temperatures in the equation are in degrees Celsius.

$$COP = A + B\,T_{eva_{in}} + C\,\dot{m}_{eva} + D\,T_{con_{out}} + E\,T_{eva_{in}}^2 + F\,T_{con_{out}}^2 + GT_{eva_{in}} \cdot T_{con_{out}} \quad (3.4)$$

Table 3.2: Parameter description and units for the heating HP COP correlation

Parameter	Description
$T_{eva_{in}}$	Evaporator inlet temperature [°C]
$T_{con_{out}}$	Condenser outlet temperature [°C]
$\dot{m}_{eva}$	Mass flowrate through the evaporator [kg/s]

Analysis in MiniTab concluded that the mass flowrate through the condenser had a negligible influence on the HP COP and was not included in the equation. The variable with the largest influence on the COP is the condenser outlet temperature.

Table 3.3: Heating HP equation performance results

	Training Set #1	Training Set #2
R^2	98.90%	98.90%
RMSE	0.12979	0.13277

The equation results from Minitab resulted in the same R^2 value, observed in Table 3.3. Therefore, the test sets were used to analyze their corresponding training sets. When the calculated COP was compared to the manufacturer data, both equations showed the ability to predict the COP accurately, results displayed in Figure 3.5. Ultimately, the RMSE for training set #1 was the lowest and therefore, the corresponding correlation was used in the model.

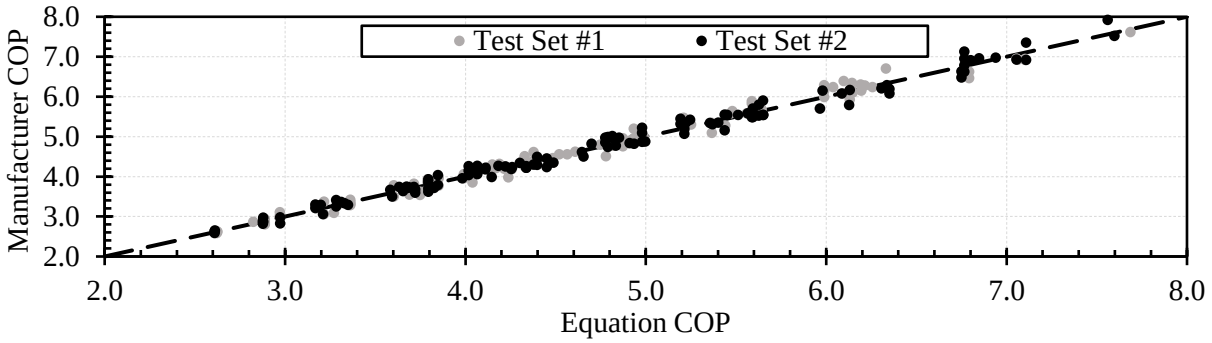

Figure 3.5: Ability of the Heating HP COP equation to calculate COP values

The ICE-Harvest system being modeled in this thesis has large fluctuations in thermal network temperature, therefore, the evaporator temperature occasionally exceeds the HP limitations. To ensure the heating HP remains within its specified operating constraints, restrictions have been placed on the temperatures used in the COP equation. For example, if the evaporator inlet temperature measured by port_a2 (Figure 3.3) is greater than the unit maximum evaporator outlet temperature plus the temperature difference across the evaporator, the temperature used in the COP equation is forced to be the maximum evaporator outlet temperature plus the temperature difference. In a real implementation of the system, a mixing valve would be used to ensure the proper temperature enters the heat pump. But for modeling purposes and control simplicity, the temperatures were altered in the equation. The heat flow was then applied on the correct temperature fluid. The temperature limitations are outlined in Figure 3.6.

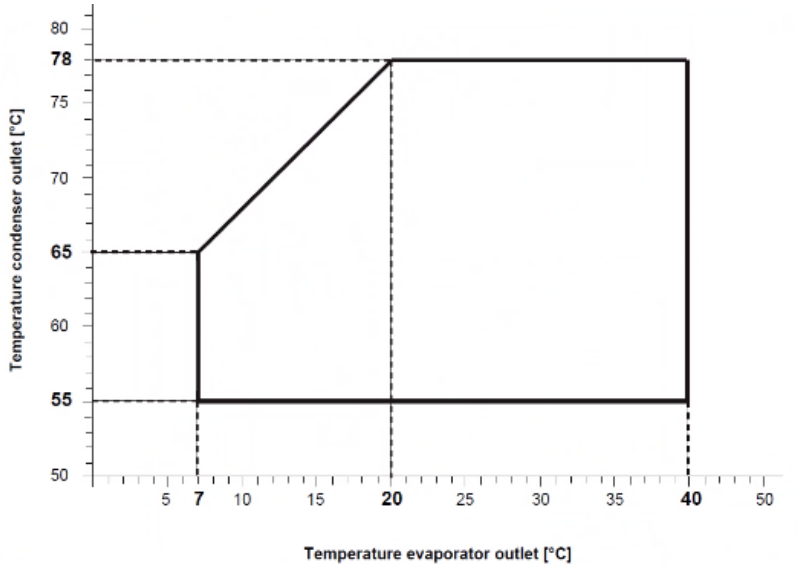

Figure 3.6: Temperature constraints for the heating HP

As mentioned in Section 3.3.4, the heat pump is modeled to represent multiple heat pumps in parallel, to determine the number of parallel heat pumps required, x, the mass flowrate is used.

$$x = \frac{\dot{m}_{actual}}{\dot{m}_{max}} \tag{3.5}$$

Within the equation for x, the value is rounded up to the nearest whole number. The flow coming through the fluid port port_a2, $\dot{m}_{actual}$, is divided by x to get the flowrate for an individual unit.

$$\dot{m}_{unit} = \frac{\dot{m}_{actual}}{x} \tag{3.6}$$

If value of $\dot{m}_{unit}$ is less than the minimum flowrate of the individual heat pump unit, like the temperature constraints, the flowrate used in the COP equation is forced to be the minimum flowrate.

With the COP and compressor power determined, they are used as inputs for the condenser and evaporator heat flow. The Equations utilized are 3.7 and 3.8.

$$Q_{eva} = (1 - COP) * P \tag{3.7}$$

$$Q_{con} = P - Q_{eva} \tag{3.8}$$

3.3.4.2 Cooling Heat Pump

The cooling heat pump is based on the Daikin WCA 420 cooling heat pump. The Daikin WCA 420 water to water cooling heat pump at a nominal capacity of 123 kW was chosen due to its temperature range and in depth publicly available data sheet [80]. The form of the equation takes a similar form to the heating HP, seen in Equation 3.9. The Minitab analysis identified different key parameters that influence the COP, similarly the source side flowrate was chosen, in this case the source is the condenser, and the condenser inlet temperature had the largest influence on COP.

$$COP = A + B\,T_{con,in} + C\,T_{eva,out} + D\,\dot{m}_{con} + E\,T_{con,in}^2 + F\,T_{con,in} \cdot T_{eva,out} \tag{3.9}$$

Table 3.4: Cooling HP equation performance results

	Training Set #1	Training Set #2
R^2	99.43%	99.41%
RMSE	0.131365	0.129998

Two training and test sets were made for the data set of 291 data points. From Table 3.4, the R^2 and RMSE for both training sets are very close in value. In Figure 3.8, both equations show the ability to accurately determine the COP from the temperatures and mass flowrate. Both equations would be sufficient for use in the model, therefore, training set #1 was chosen and the resulting equation coefficients are displayed in Equation 3.10. The temperatures in the equation are in degrees Celsius.

$$\begin{aligned} COP = {} & 6.59 - 0.158T_{con_{in}} + 0.244T_{eva_{out}} + 0.136\dot{m}_{con} + 0.00101T_{con_{in}}^2 \\ & - 0.00136T_{con_{in}} \cdot T_{eva_{out}} \end{aligned} \tag{3.10}$$

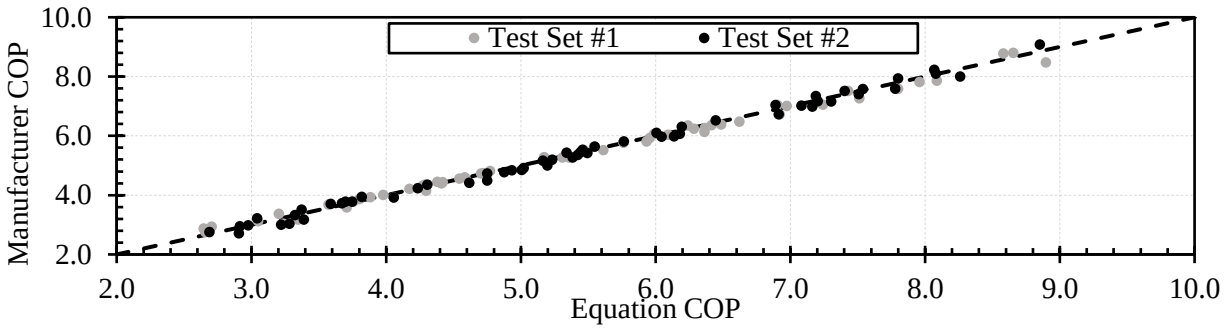

Figure 3.7: Ability of the cooling HP COP equation to calculate the COP values

When the cooling HP is implemented in the system, there is no risk of the surrounding temperatures exceeding the unit limitations. To ensure the HP is operating within its operating limits, restrictions have been placed on the COP based on the maximum power and cooling load of the unit. Throughout the simulation the power input is monitored, if it reaches the maximum power of the unit the COP is forced to equal the maximum cooling load divided by the maximum power. Therefore, at the maximum power the unit cannot exceed the maximum cooling capacity. Such constraints are computationally expensive when the unit is consistently reaching the limits of its capacity, which is why it was not implemented on the heating HP. The environment surrounding the cooling HP is much more stable.

The mass flowrate and power are determined following the same methodology as in Section 3.3.4.1, the difference is in the condenser and evaporator heat flowrate equations, as observed in Equations 3.11 and 3.12. The evaporator flowrate is negative to represent that heat is being removed from the fluid.

$$Q_{eva} = -COP * P \tag{3.11}$$

$$Q_{con} = P - Q_{eva} \tag{3.12}$$

3.3.4.3 Refrigeration Heat Pump

For the refrigeration HP, data was retrieved from an industrial partner's building refrigeration system and a COP correlation was constructed based on the condenser inlet temperature, see Equation 3.13. A refrigeration model is required for buildings, such as a grocery store or an ice rink, where temperatures around -12°C are needed for their systems. Due to the large decrease in temperature requirements compared to a building requiring space cooling, heat pump system components change, like the refrigerant used, which changes the performance of the unit.

$$COP_{refrigeration} = -0.0798\, T_{con_{in}} + 5.8666 \tag{3.13}$$

For the refrigeration model, no sizing information for the unit was given, therefore, there are no mass flowrate, power, or temperature constraints. The input signal for the part load of the compressor is multiplied by an arbitrarily large nominal power and the heat flowrate equations are the same as the cooling heat pump.

3.3.4.4 Model Testing

To ensure the HPs behave as intended and per the manufacturer limitations, the heating HP was tested to ensure the proper performance of the temperature constraints and for the unit overall. Since the equation developed for the heating HP is confidential, testing of the control strategy was conducted with a low temperature (LT) HP equation; equation development and temperature boundaries are outlined in Appendix B.

The testing model for the heating HP in Dymola is outlined in Figure 3.8. The HP evaporator side is connected to an infinite source and sink model, while the condenser is attached to the Buildings Library *HeaterCooler_u* to simulate a building heating load.

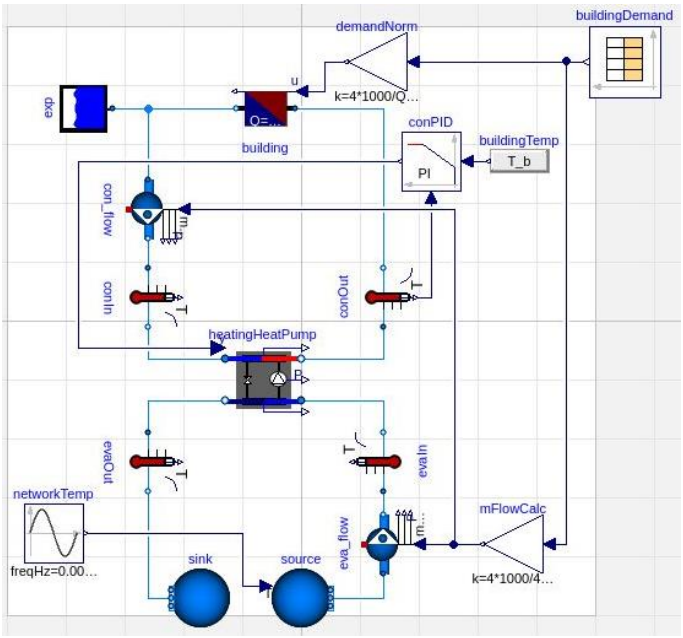

Figure 3.8: Heat pump testing model in Dymola

To test the heating HP performance, on the evaporator side a sinusoidal temperature profile was simulated ranging between 20 and 40°C. On the condenser side a PI contoller adjusted the power consumption of the heat pump to deliver a constant temperature of 45°C to the building. The temperature profile used in the COP equation is represented by the black line in Figure 3.9. The evaporator temperature does not exceed it's maximum value of 26.7°C. Therefore, the COP does not increase to an unrealistic value and the equation is not extrapolating data points. The heat flowrate calculated with the COP is applied to the fluid at the correct temperature to achieve the desired temperature difference, observed by the dark and light blue temperature profiles.

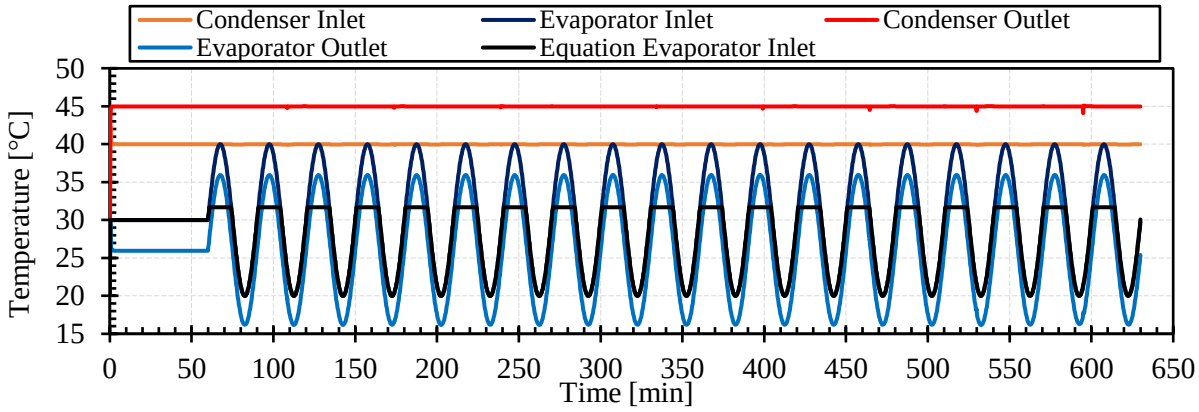

Figure 3.9: Temperature profile of heating HP, testing model constraints

The flowrate for the condenser and the evaporator is calculated based on the building heating load assuming a temperature difference of 5°C and a specific heat capacity of 4.187 kJ/kg°C. Based on the flowrate entering the evaporator, the model will determine the required number of units to meet the heating load and the flowrate will be divided evenly among the units. The number of units needed to meet the load of the building determines the maximum power requirement for the group of HPs and sets the upper limit on the PI controller. Figure 3.10 shows the mass flowrates throughout the simulation. The unit flowrate is used to calculate the COP.

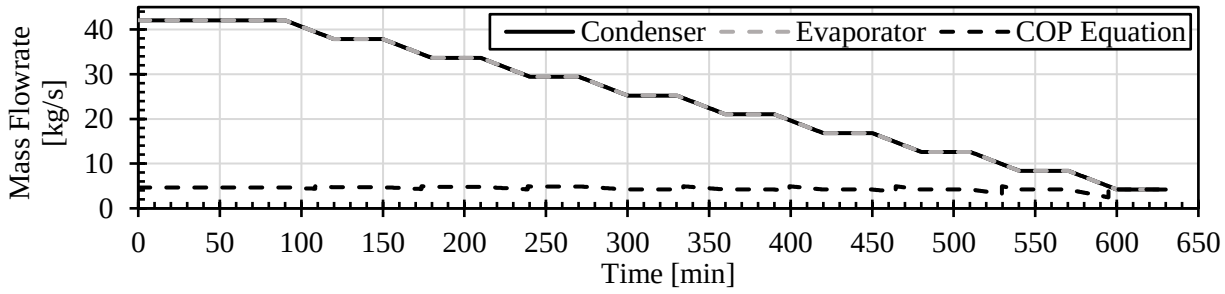

Figure 3.10: Mass flowrate values throughout the test simulation for the cooling HP

Resulting thermal and electrical power for the unit is seen in Figure 3.11. The operation is as expected and within the unit limitations. The COP follows the opposite trend of the power consumption, when the power consumption increases the COP decreases and vice versa. The COP

fluctuates between 5.3, when the evaporator temperature is higher, and 4.2 with the lower evaporator temperatures.

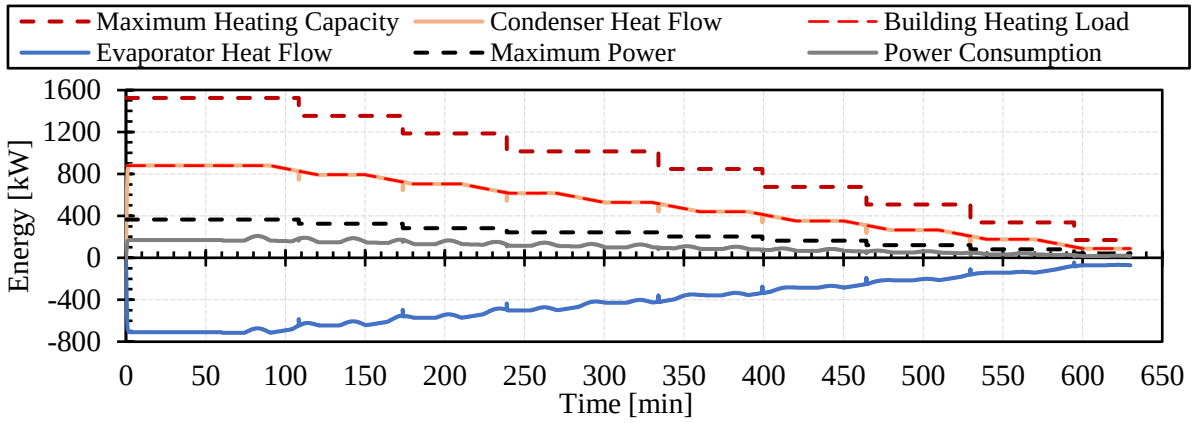

Figure 3.11: Building demand and resulting HP performance

3.4 Energy Transfer Station Model

At each building attached to the micro-thermal network there is an energy transfer station (ETS). The ETS contains two components, the heating ETS and the harvesting ETS, shown in Figure 3.12. In the heating ETS, heat is removed from the thermal network to meet the building's heating demands. Heat is removed from the network through either a heat pump or heat exchanger. For the harvesting ETS, the heat rejected from the existing building chiller, refrigeration or space cooling, is harvested and added to the thermal network. Like the heating ETS, the heat is harvested through a heat pump or heat exchanger dependent on the temperature of the thermal network.

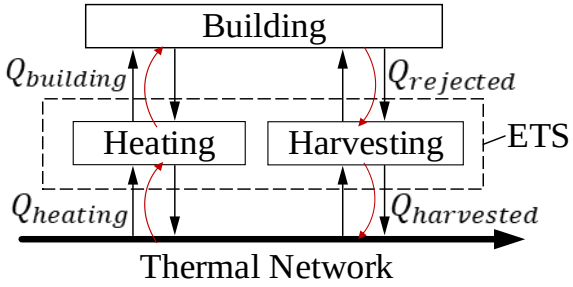

Figure 3.12: Energy transfer station schematic.
The black arrows represent the fluid flow direction and the red arrows represent the heat flow direction.

For modeling the ETS in Dymola, components were taken from the Buildings Library, the Modelica Standard Library, and Sullivan's thesis [78]. The developed ETSs with the inputs and outputs to the model can be seen in Figures 3.13 and 3.14. The figures also contain how the ports are connected amongst each other and the view of the model from a system level perspective. Each model differentiates in the way heat is harvested. Figure 3.13 displays the model where all available rejected heat is harvested according to the Boolean signal *harvestHeat*. In Figure 3.14, the network temperature is used to determine when to harvest heat.

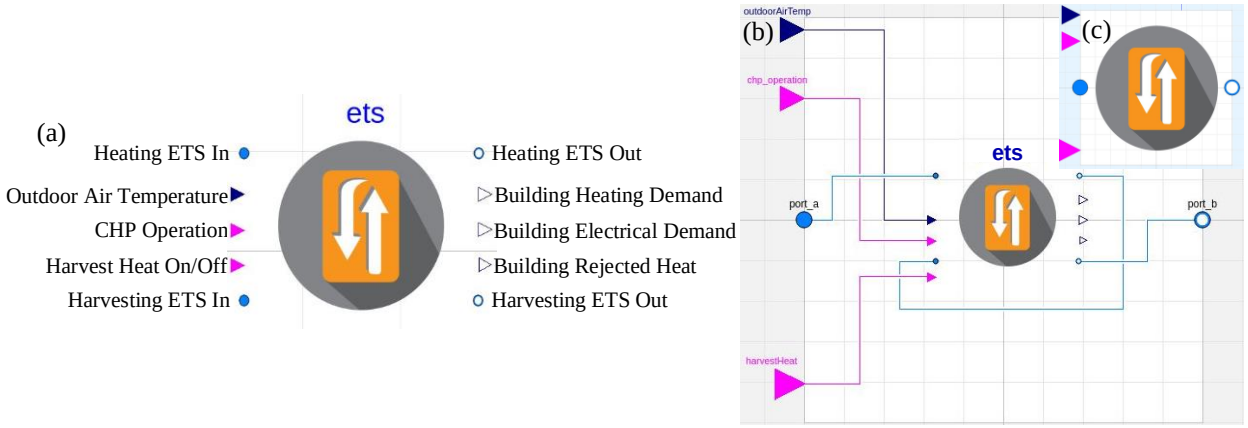

Figure 3.13: ETS model where harvested heat is controlled by an on/off signal
containing (a) the ETS icon in Dymola with labelled inputs and outputs, (b) how the fluid ports are connected, and the (c) model interface from the system level perspective

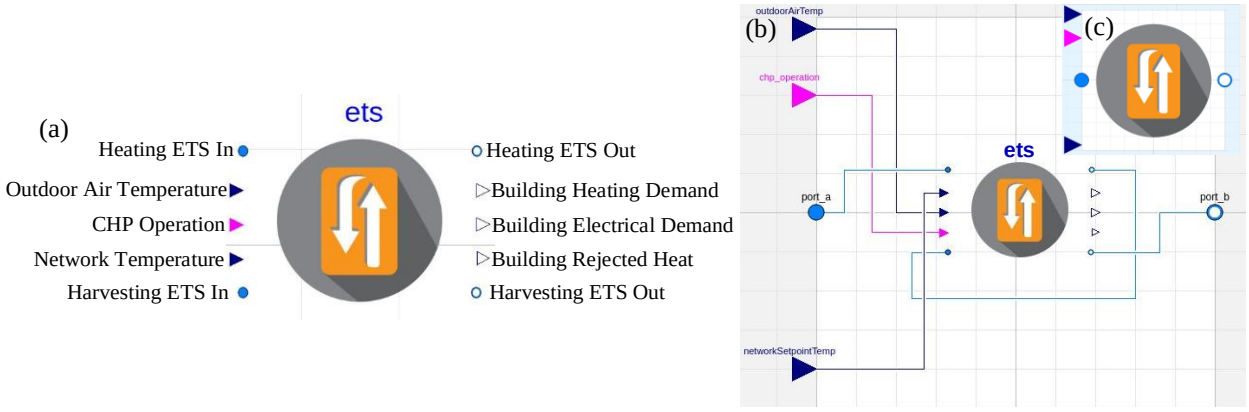

Figure 3.14: ETS model where harvested heat is based on the thermal network temperature
containing (a) the ETS icon in Dymola with labelled inputs and outputs, (b) how the fluid ports are connected, and the (c) model interface from the system level perspective

There was a total of 6 ETS models developed, they are listed in Table 3.5. Each model utilizes different combinations of harvesting control strategies and heating and harvesting ETSs. The models will be discussed in detail in the following sections.

Table 3.5: Different ETS models used throughout system simulations

	ETS Model					
	1	2	3	4	5	6
Heating ETS	✓	✓	✓	✓		
Heating ETS with thermal storage					✓	✓
Harvesting ETS with space cooling chiller	✓		✓		✓	
Harvesting ETS with refrigeration chiller		✓		✓		✓
Harvesting based on network temperature	✓	✓			✓	✓
Harvesting according to on/off control			✓	✓		

3.4.1 Heating Energy Transfer Station

The heating ETS removes heat from the micro-thermal network in order to meet the buildings heating demand. Heat is removed from the thermal network by either a heat pump or heat exchanger, all dependent on the thermal network temperature entering the heating ETS in real time. The important variables in the heating ETS are described in Table 3.6.

Table 3.6: Hating ETS main variable list and descriptions

Variable	Name	Description
$T_{Network}$	Thermal network temperature [°C]	Temperature of the thermal network upstream of the heating ETS
$T^{heat}_{building_{setpoint}}$	Building set point temperature [°C]	Temperature required to provide heating to the building
$T^{heat}_{building_{return}}$	Building return temperature [°C]	Temperature of the fluid exiting the building, will return colder than the building set point temperature
$T^{heat}_{building_{supply}}$	Building supply temperature [°C]	Temperature of fluid entering the building, should equal the building set point temperature
$\Delta T_{heating}$	Heating temperature difference [°C]	Temperature difference across the heat pump and heat exchanger, used to calculate the mass flowrate of the building heating loop
$\Delta T_{threshold}$	Temperature difference for direct heat exchange [°C]	Temperature difference to ensure the network will able to provide the heating demand through direct heat exchange

Variable	Name	Description
$Q_{building}^{heat}$	Building heating demand [kW]	Amount of heat required by the building to meet their heating demands, to meet heating demands fluid enters the building at the building set point temperature
$Q_{heating}$	Heat removed from the thermal network [kW]	Heat removed from the thermal network, either through the heat exchanger or heat pump evaporator, to meet the heating demand of the building

Figure 3.15 details the interior of the heating ETS. The fluid from the MTN can branch off and enter the heat pump evaporator. The flowrate of fluid entering the evaporator (pump P1) is calculated with the heating temperature difference, the building heating demand, and the specific heat capacity for the fluid. Or the thermal network can branch off into the network side of the heat exchanger. Flow into the heat exchanger is determined by a PI controller to maintain the building supply temperature at the building set point temperature. The mass flowrate through the building loop (pump P3) is determined by the building heating load, following the same methodology as P1. The strategy controlling if/when the thermal network branches off is outlined in Table 3.7.

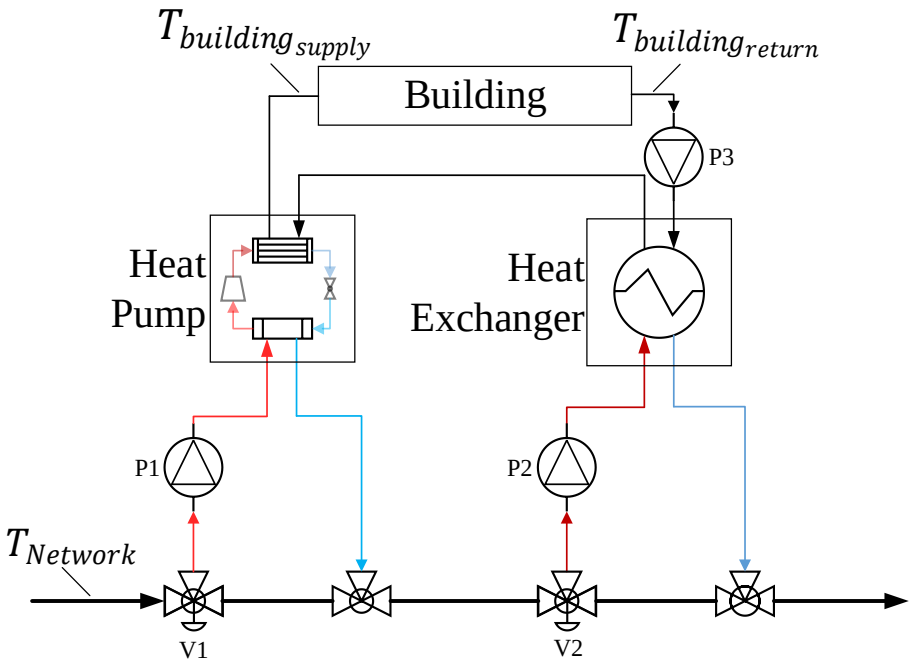

Figure 3.15: Components of the heating ETS with temperature locations

Table 3.7: Heating ETS control strategy

Scenario		Heat Pump		Heat Exchanger		Heating Loop
$T_{Network}$	$Q_{building}^{heat}$	P1	V1	P2	V2	P3
$\geq T_{building_{setpoint}} + \Delta T_{threshold}$	YES	OFF	CLOSED	ON	OPEN	ON
$< T_{building_{setpoint}} + \Delta T_{threshold}$	YES	ON	OPEN	OFF	CLOSED	ON
$\geq T_{building_{setpoint}} + \Delta T_{threshold}$	NO	OFF	CLOSED	OFF	CLOSED	OFF
$< T_{building_{setpoint}} + \Delta T_{threshold}$	NO	OFF	CLOSED	OFF	CLOSED	OFF

3.4.2 Heating Energy Transfer Station with Thermal Storage

The decentralized short-term thermal storage at the heating ETS is to be used while the micro-thermal network temperature transitions from the cool to hot temperature. A period of network temperature transition would take place when the CHP turns on after a period of non-use and begins to increase the temperature of the network. The ETS storage tank provides the heating load to the building for the duration of the temperature change, or response time (discussed in Chapter 4), it will alleviate the building heating demand from the MTN so that the temperature can transition as quickly as possible. To charge the ETS storage, the heating HP is used. During charging, the heating HP removes heat from the MTN during off-peak periods with carbon free electricity and provides heat to the ETS storage at the storage set point temperature. The heating ETS model with thermal storage contains all of the same variables listed in Table 3.6 and the additional variables defined in Table 3.8.

Table 3.8: Heating ETS with thermal storage variables

Variable	Name	Description
$T_{storage_{setpoint}}$	Storage set point temperature [°C]	Temperature required to charge the thermal storage tank
$T_{storage}$	Temperature after storage [°C]	Temperature of the fluid in the building loop after the thermal storage tank
$T_{charging}$	Storage charging temperature [°C]	Temperature of the fluid used to charge the storage tank, should be equal to the storage set point temperature

Variable	Name	Description
$T_{discharging}$	Storage discharging temperature [°C]	Temperature of the fluid used to discharge the storage tank, equal to the building return temperature
$\Delta T_{storage}$	Storage temperature difference [°C]	Difference between the storage charging and discharging temperature that is used for sizing the storage tank
T_{top}	Top of storage temperature [°C]	Temperature of the fluid at the top of the thermal storage tank
T_{bottom}	Bottom of storage temperature [°C]	Temperature of the fluid at the bottom of the thermal storage tank
$T_{HP_{setpoint}}$	Heat pump temperature set point [°C]	Temperature used to determine the temperature exiting the condenser of the heat pump, depends on if the storage is charging or fully charged
$T_{con_{out}}$	Temperature after the heat pump [°C]	Temperature of the fluid in the heating loop after the heat pump condenser, should equal the heat pump temperature set point

The thermal storage tank at the heating ETS will be sized based on the peak heating demand of the building, the storage temperature difference ($\Delta T_{storage}$), and the decided response time of the MTN. The two dotted black lines in Figure 3.16 represent the volume of a 6 and 12 m long shipping container. The ICE-Harvest system is to be a modular containerized installation, therefore, the benchmark for designing the thermal storage is the size of a shipping container that can fit into one or two average sized parking spaces.

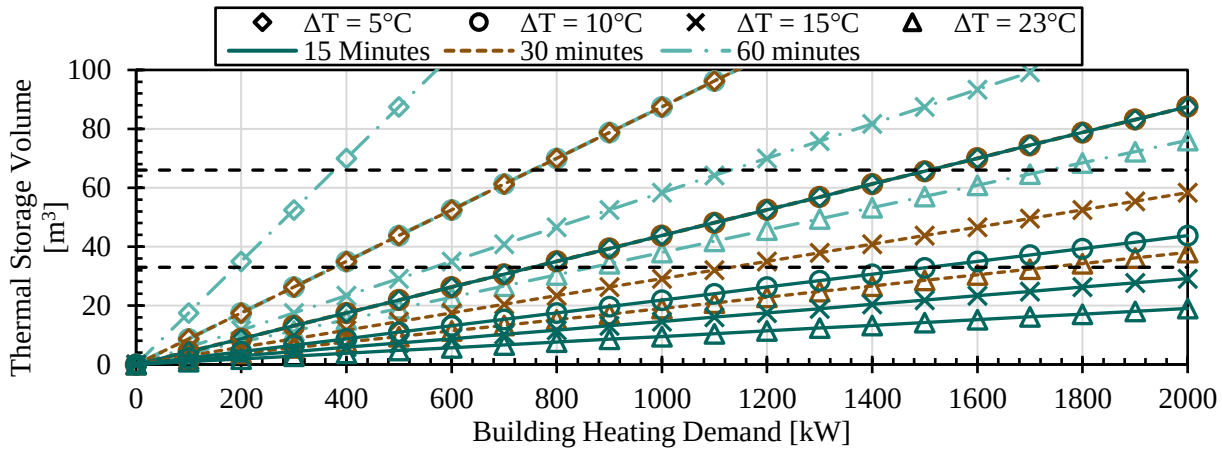

Figure 3.16: Sizing the ETS short-term thermal storage tank

For modeling the ETS thermal storage in Dymola, the *StratifiedEnhanced* model from the Buildings Library is used. The basis of the thermal storage tank control strategy is retrieved from [78]. Incorporation of the thermal storage in the heating ETS can be seen in Figure 3.17.

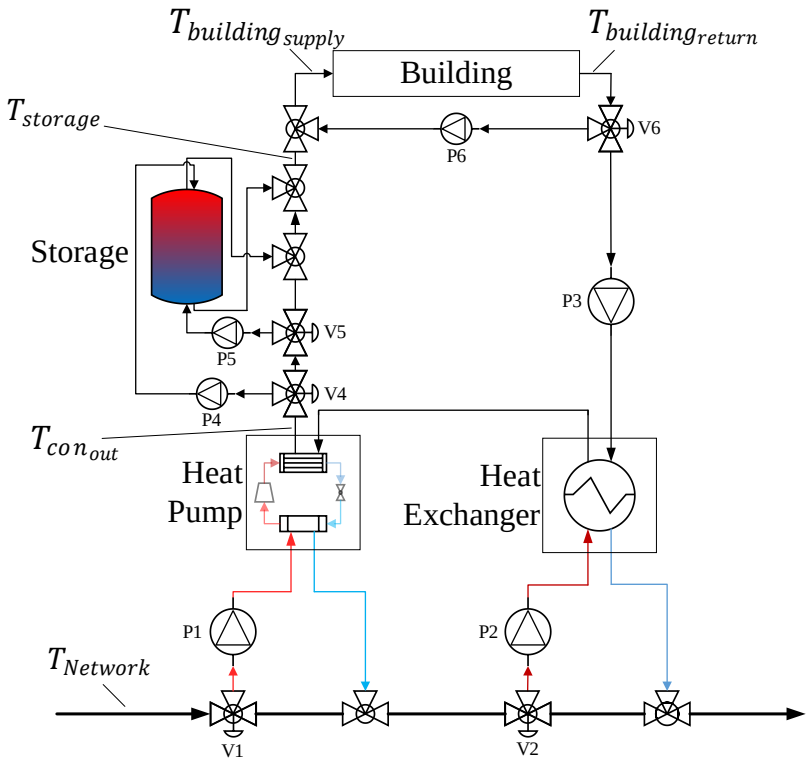

Figure 3.17: Components of the heating ETS with thermal storage and temperature locations

The mass flowrates are all the same as previously outlined in the heating ETS (Section 3.4.1). There is also the addition of the mass flowrate through the storage (pumps P4 and P5) and the supply and return mixing (pump P6). Flow through the storage depends on if the tank is in charging or discharging mode. When the tank is charging, fluid flows through P4, and if the tank is discharging, the fluid flows through P5. The flowrate through each pump is determined by a PI controller that aims to make the temperature after the storage tank, $T_{storage}$, equal to the building temperature set point.

When the storage is in charging mode and the bottom of the storage tank reaches a temperature where $T_{storage}$ can no longer be maintained at the building set point temperature, the supply and return mixing is used. If $T_{storage} > T_{building_{setpoint}}$, P6 and V6 are operational and the mass flowrate through P6 is determined by a PI controller to ensure the building supply temperature is equal to the building set point temperature for heating. If $T_{storage} \leq T_{building_{setpoint}}$ then P6 and V6 are off.

Adding the thermal storage in the heating ETS requires additional layers of control. Different control strategy scenarios are listed in Table 3.9 and the response of the equipment to each scenario is listed in Table 3.10. Starting the simulation, the initial state for the thermal storage is discharged. When the storage is charging, the condenser outlet temperature increases to the storage set point temperature and the temperature difference across the HP increases. Once the storage is charged, the condenser outlet temperature decreases back to the building set point temperature.

Table 3.9: Heating ETS thermal storage charging scenarios

Case	CHP	State of Storage	$T_{Network}$	$Q_{building}^{heat}$
1	OFF	Charging	Cool	> 0
2	OFF	Charged	Cool	> 0
3	ON	Discharging	Transitioning	> 0
4	ON	Discharged	Hot	> 0
5	-	-	-	0

Table 3.10: Control strategies for the heating ETS with thermal storage

Case	Heat Pump			Heat Exchanger		Heating Loop	Charging Storage		Discharging Storage	
	P1	V1	$T_{con_{out}}$	P2	V2	P3	P5	V5	P4	V4
1	ON	OPEN	$T_{storage_{setpoint}}$	OFF	CLSD	ON	ON	OPEN	OFF	CLSD
2	ON	OPEN	$T_{building_{setpoint}}$	OFF	CLSD	ON	OFF	CLSD	OFF	CLSD
3	OFF	CLSD	-	OFF	CLSD	ON	OFF	CLSD	ON	OPEN
4	OFF	CLSD	-	ON	OPEN	ON	OFF	CLSD	OFF	CLSD
5	OFF	CLSD	-	OFF	CLSD	OFF	OFF	CLSD	OFF	CLSD

3.4.3 Harvesting Energy Transfer Station

The harvesting ETS is used to capture, or harvest, the heat that is rejected by the existing chiller at each of the buildings attached to the MTN. Harvested heat is added to the MTN and is used to meet the heating demands of neighbouring buildings. Important variables for the harvesting ETS are listed in Table 3.11.

Table 3.11 Harvesting ETS important variables

Variable	Name	Description
$T_{Network}$	Thermal network temperature [°C]	Temperature of the thermal network before the harvesting ETS
$T^{cool}_{building_{setpoint}}$	Building set point temperature [°C]	Temperature required to provide space cooling or refrigeration to the building
$T^{cool}_{building_{return}}$	Building return temperature [°C]	Temperature of the fluid exiting the building, will return warmer than the building set point temperature
$T^{cool}_{building_{supply}}$	Building supply temperature [°C]	Temperature of fluid entering the building, should equal the building set point temperature
$T_{rejection}$	Temperature of rejected heat [°C]	Temperature of the fluid exiting the building chiller condenser
$T_{ambient}$	Ambient temperature [°C]	Temperature of the outdoor air
$T_{chiller_{setpoint}}$	Chiller set point temperature [°C]	The temperature set point used by the heat pump, heat exchanger, and cooling tower to cool the fluid
$T_{chiller_{supply}}$	Chiller supply temperature [°C]	Temperature of the fluid entering the building chiller condenser, should equal the chiller set point temperature
$\Delta T_{chiller}$	Chiller temperature difference [°C]	Temperature difference across the building chiller evaporator, used to calculate the mass flowrate of the building loop
$\Delta T_{harvest}$	Temperature difference for direct heat exchange [°C]	Temperature difference to ensure the network will be able to provide the cool the rejected heat through direct heat exchange
$Q^{cool}_{building}$	Building cooling demand [kW]	Amount of cooling required by the building to meet the demand, fluid enters the building at the building set point temperature
$Q_{rejected}$	Rejected heat [kW]	Heat rejected by the building chiller condenser
$Q_{harvested}$	Harvested heat [kW]	Heat that was added to the thermal network through a heat pump or direct heat exchange from the heat rejected

Figure 3.18 contains two main loops, the building loop that connects the building and the chiller evaporator, and the rejection loop that connects the chiller condenser, the harvesting equipment, and cooling tower. The harvesting ETS contains only the harvesting equipment and cooling tower, the building chiller is a part of the existing building system, both are modeled to receive accurate amounts of rejected heat.

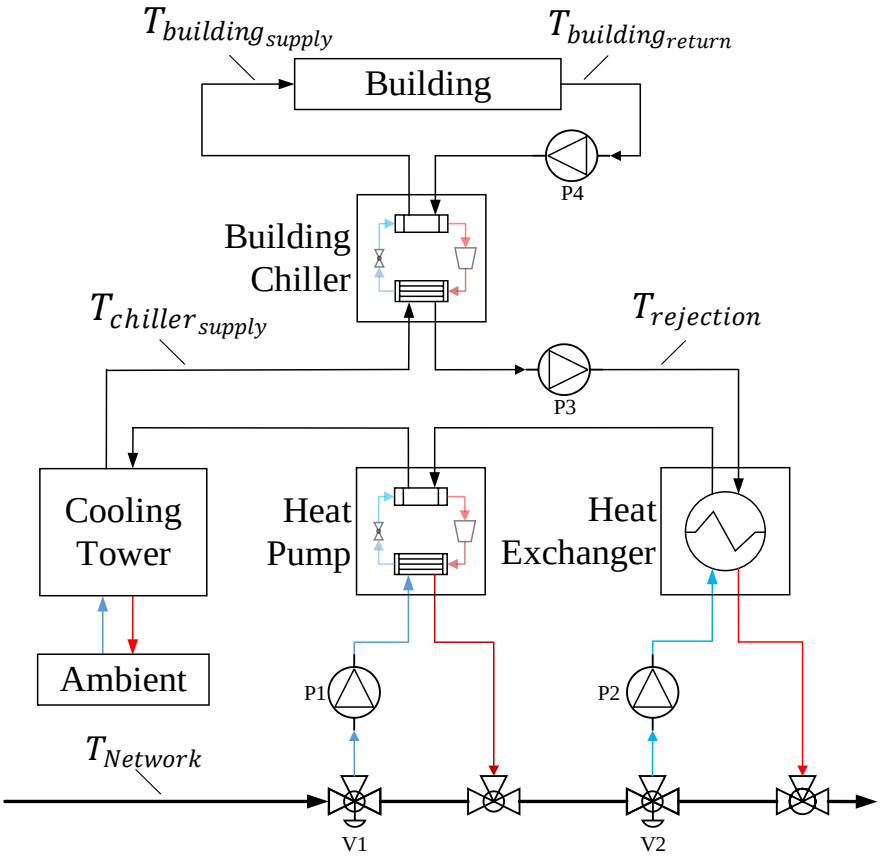

Figure 3.18: Components of the harvesting ETS with temperature locations

The mass flowrate through the building loop is constant and based on the peak building cooling demand and the chiller temperature difference. The flowrate through the rejection loop is also constant and is 1.25 times greater than the building loop mass flowrate. An increase of 1.25 was chosen in order to maintain the 5°C temperature difference across the condenser with the increase in heat flowrate. The value of 1.25 is the average increase in condenser heat flowrate compared to

the evaporator, calculated from the Daikin WCA 420 data. When the harvesting heat pump is in operation, pump P1 will circulate water at a constant mass flowrate equal to the rejection loop mass flowrate. When the harvesting heat exchanger is in use, the flowrate through P2 is determined by a PI controller that ensures the rejection loop temperature is being cooled to the chiller set point temperature.

The cooling tower ensures the chiller supply temperature is kept at the chiller set point in case the heat pump or heat exchanger were not able to harvest all of the rejected heat. The cooling tower is modeled as a simple cooler, specifically the *SensibleCooler_T* from the Buildings Library, and the heat exchanger is the *PlateHeatExchangerEffectivenessNTU* model.

There are two control strategies for the harvesting ETS. The first control strategy depends on the operation of the CHP; when the CHP is on, to avoid electrical consumption on-peak, the harvesting heat pump will not operate. The second control strategy is always harvesting energy regardless of CHP operation. Table 3.12 outlines the first control strategy and Table 3.13 outlines the second strategy.

Table 3.12: Harvesting ETS control strategy following CHP operation

Scenario			Heat Pump		Heat Exchanger		Rejection Loop	Building Loop
$T_{Network}$	$Q_{building}^{cool}$	CHP	P1	V1	P2	V2	P3	P4
$\geq T_{rejection} + \Delta T_{cooling}$	YES	OFF	ON	OPEN	OFF	CLOSED	ON	ON
$< T_{rejection} + \Delta T_{cooling}$	YES	OFF	OFF	CLOSED	ON	OPEN	ON	ON
$\geq T_{rejection} + \Delta T_{cooling}$	YES	ON	OFF	CLOSED	OFF	CLOSED	ON	ON
$< T_{rejection} + \Delta T_{cooling}$	YES	ON	OFF	CLOSED	ON	OPEN	ON	ON

Table 3.13: Harvesting ETS control strategy always harvesting energy

Scenario			Heat Pump		Heat Exchanger		Rejection Loop	Cooling Loop
$T_{Network}$	$Q_{building}^{cool}$	CHP	P1	V1	P2	V2	P3	P4
$\geq T_{rejection} + \Delta T_{cooling}$	YES	OFF	ON	OPEN	OFF	CLOSED	ON	ON
$< T_{rejection} + \Delta T_{cooling}$	YES	OFF	OFF	CLOSED	ON	OPEN	ON	ON
$\geq T_{rejection} + \Delta T_{cooling}$	YES	ON	ON	CLOSED	OFF	CLOSED	ON	ON
$< T_{rejection} + \Delta T_{cooling}$	YES	ON	OFF	CLOSED	ON	OPEN	ON	ON

Within the two control strategies, there is the option to harvest all rejected energy or to only harvest when the thermal network temperature is below the desired set point. When harvesting all rejected energy available, the heat pump or heat exchanger will harvest all rejected energy into the thermal network based on the control signal input *Harvest Heat On/Off* from Figure 3.13. In the case where the harvesting ETS is only harvesting what is required, the thermal network temperature entering the harvesting ETS is measured and if it is below the network set point then energy is harvested, and if the temperature is greater than or equal to the set point heat will not be harvested.

3.4.4 ETS Model Testing

The performance of the designed energy transfer stations was tested in Dymola with a simple fluid source and sink, along with source blocks to replicate real system behavior. A trapezoidal input signal with a 15 minute ramp up and down was used to simulate the micro-thermal network temperature and replicate the response time of the network. The CHP operation was given by a pulse signal that coincides with the temperature signal and the outdoor air temperature was constant at 10°C.

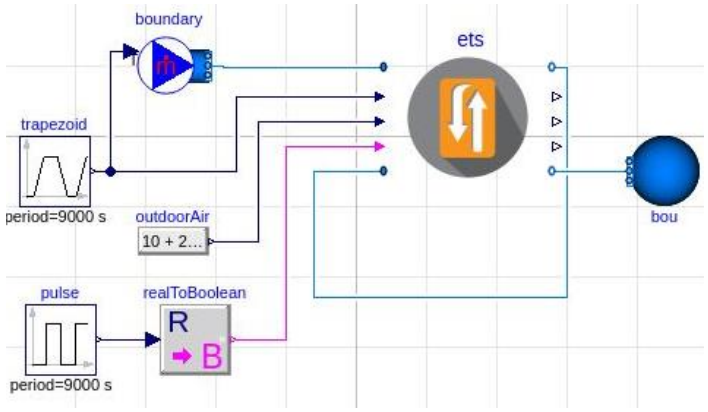

Figure 3.19: Dymola simulation schematic for testing the ETS

Real building data was used to test the ETS, the building demand was taken for a period of 10 hours in the winter time. The time step for the simulation was 5 minutes. The heating and cooling demand profiles used are in Figure 3.20.

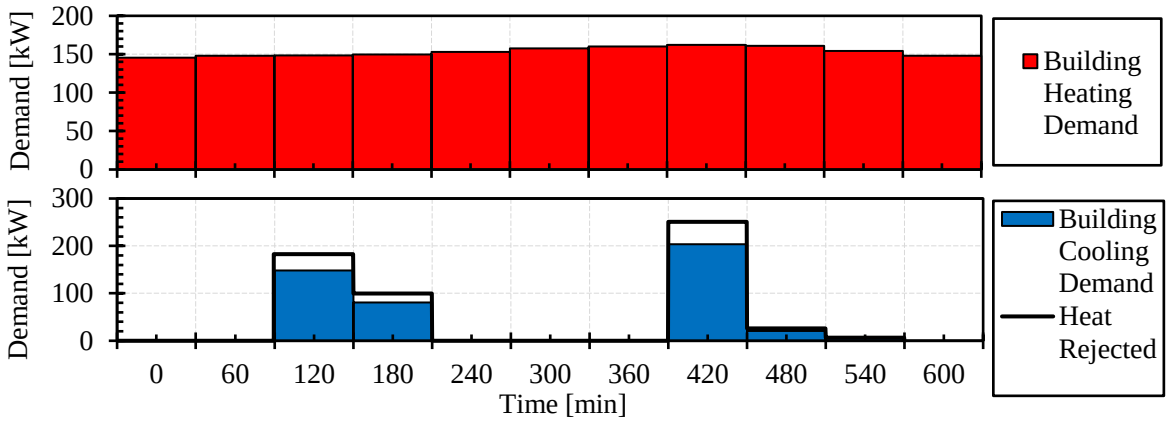

Figure 3.20: Building heating and cooling demands along with the heat rejected

3.4.4.1 Heating ETS Performance

The heating ETS control strategy was tested to ensure that the heat pump and heat exchanger were operating correctly. In Figure 3.21 the network temperature profiles are shown. When the network temperature is hot, at 70°C, there is no change in temperature after the heat pump but there is a temperature drop after the heat exchanger, indicating that direct heat exchange was being used to

deliver the heating load to the building. The opposite occurs when the network temperature is cool, at 20°C, the heat pump is in operation and is suppling the building heating demand.

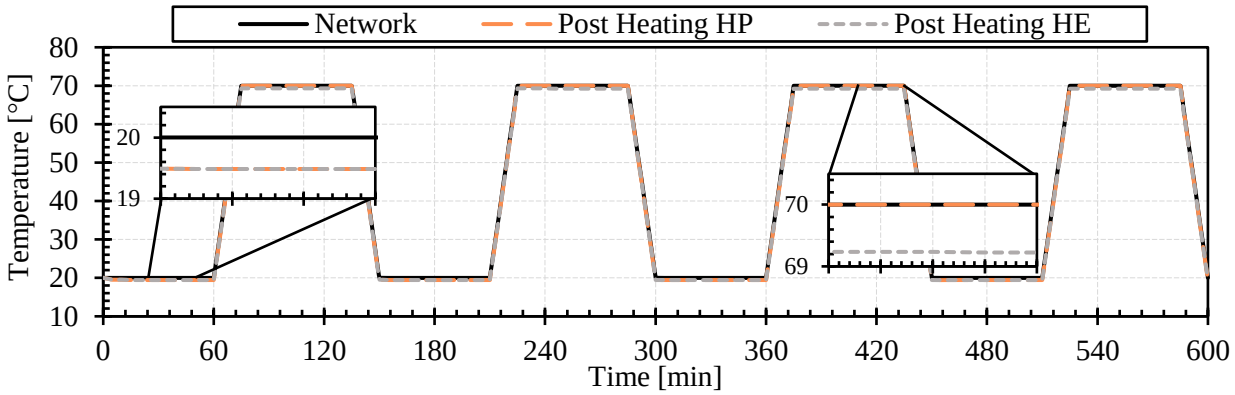

Figure 3.21: Thermal network temperature profiles within the heating ETS

The operation of the heat pump and heat exchanger can also be visualized in Figure 3.22 with the heat flow diagram. The operation of the heat pump and heat exchanger alternates while still meeting the building heating demand. The same trend can be seen in Figure 3.23 with the mass flowrates of each component.

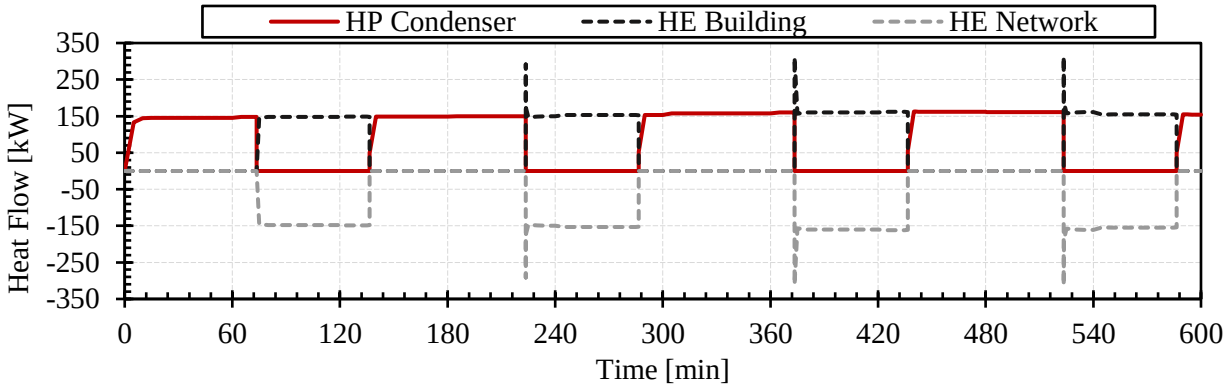

Figure 3.22: Heat flowrates of the HP and heat exchanger in the heating ETS

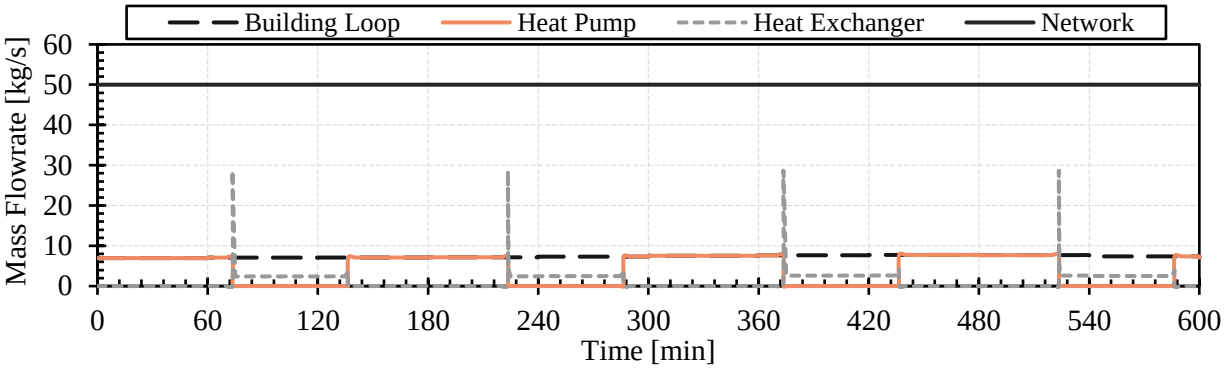

Figure 3.23: Mass flowrates for each component in the heating ETS

3.4.4.2 Harvesting ETS Performance

The harvesting ETS is after the heating ETS on the thermal network, therefore the harvesting ETS receives the cooler fluid leaving the heating ETS. The control strategy for the harvesting ETS in the simulation is to always harvest the rejected heat. From Figure 3.24, the heat pump is utilized to harvest heat when the thermal network temperature is hot and the heat exchanger is in operation when the thermal network temperature is cool. Harvesting energy increases the temperature of the micro-thermal network and assists in meeting the heating demands of the neighbouring buildings.

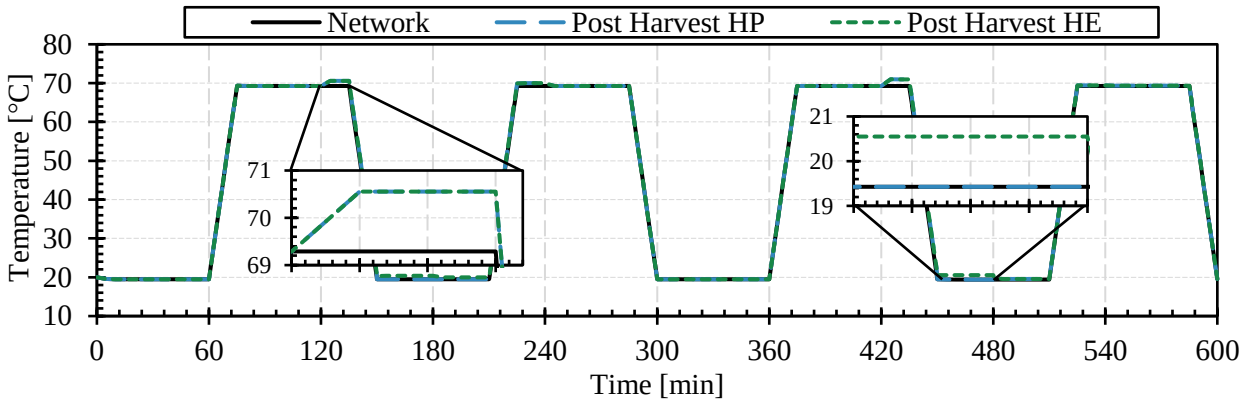

Figure 3.24: Thermal network temperature profiles within the harvesting ETS

The heat flowrates for the harvesting ETS can be seen in Figure 3.25, the heat exchanger and heat pump alternate to harvest the rejected heat and add it to the thermal network. In a few scenarios, where the heat exchanger could not harvest all of the rejected heat, the cooling tower works to cool

the rejection loop further to ensure that the chiller supply is always at the chiller set point temperature.

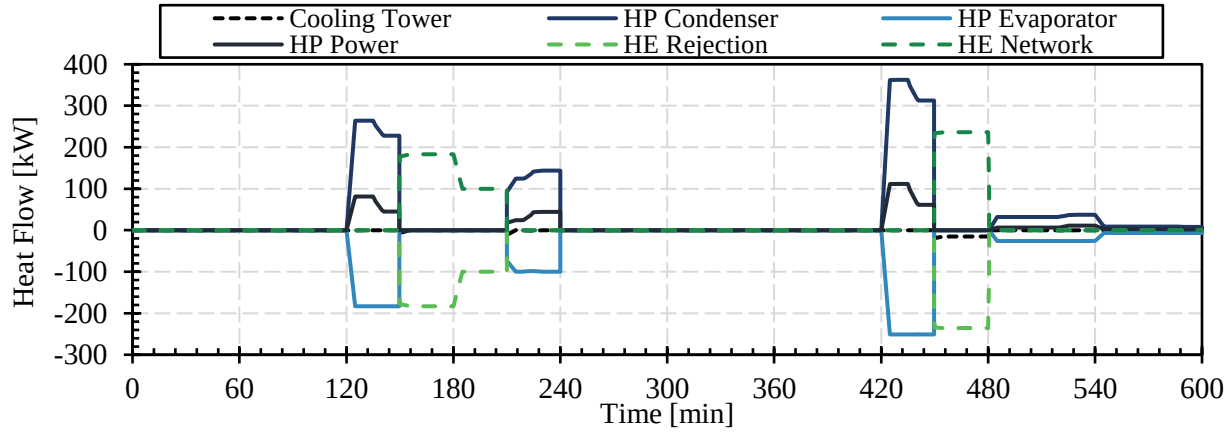

Figure 3.25: Heat flowrates of the components in the harvesting ETS

Figure 3.26 displays the mass flowrates for each component. When the harvesting HP is operational, the flowrate is constant and equal to the rejection loop mass flow. The mass flowrate entering the network side of the heat exchanger is determined by the PI controller in order to reduce the rejection loop temperature to the chiller set point.

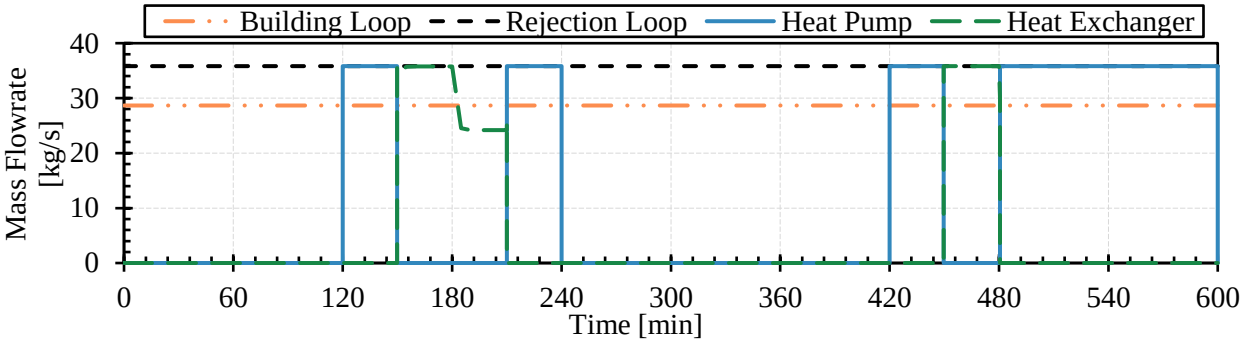

Figure 3.26: Mass flowrates for each component in the harvesting ETS

3.4.4.3 Heating ETS with Thermal Storage Performance

With the incorporation of thermal storage at the heating ETS, the thermal network temperature profile after the heat pump has changed compared to Figure 3.21. The temperature of the network

decreases more because additional heat is needed from the network to charge the storage tank. In Figure 3.27, the CHP operation can be seen relative to the temperature of the network.

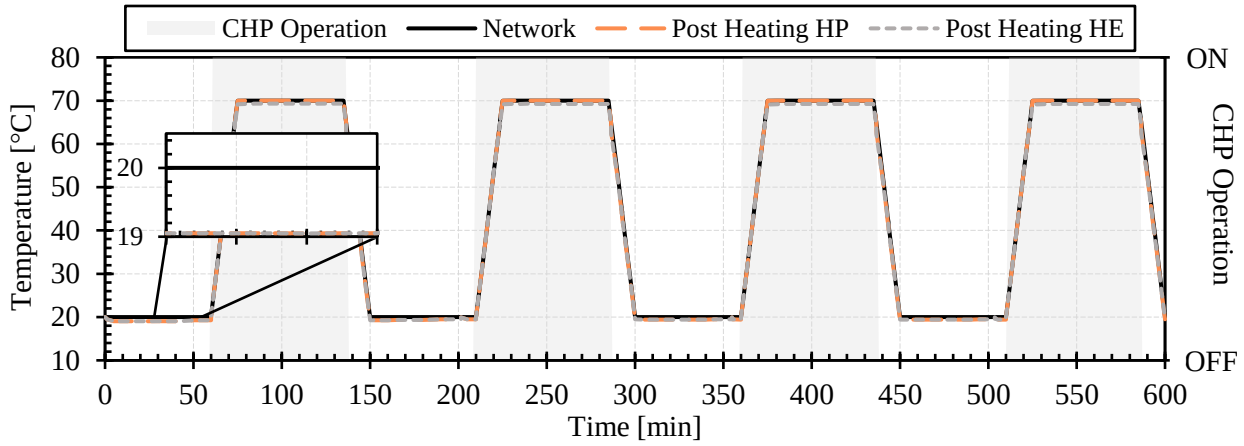

Figure 3.27: Thermal network temperature profiles within the heating ETS with storage

In the heat flow plot, Figure 3.28, the times of charging and discharging the ETS storage can be seen. The charging of the ETS storage is a negative heat flow because heat is being removed from the building loop, and when the storage is discharging the heat flow is positive. The storage is being charged with the heat pump while the CHP is off, creating a larger load for the heat pump. The time it takes to charge the storage varies and is dependant on the state of charge and the available capacity of the heat pump. Initially, when charging the storage from a fully discharged state of 55°C, the storage receives 130 kW of heat for approximately the whole hour, which is the maximum capacity of the heat pump at that time subtract the heating load. When the CHP turns on and the network temperature is increasing, the storage is discharging for that 15 minute period, and when the thermal network temperature reaches its hot temperature the heat exchanger then provides heat to the building. After the CHP turns off, the amount of heat required to re-charge the storage reduces as the storage was not fully discharged during the temperature transition.

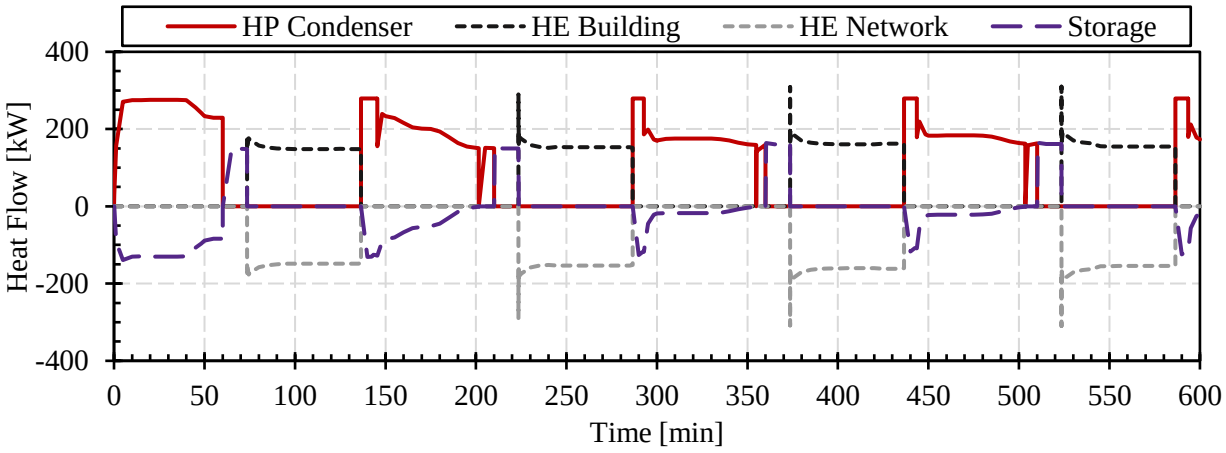

Figure 3.28: Heat flowrates of the components in the heating ETS with storage

An additional component not in the original heating ETS, is the mixing of building return and supply. The mixing pump, seen in Figure 3.29, is only required to operate during the period where the storage tank is almost charged and no longer has any cool fluid at the bottom of the tank to mix with the warmer water leaving the heat pump. When the temperature at the bottom of the storage tank has reached the storage set point, the heat pump will stop charging the storage and only provide heat to the building.

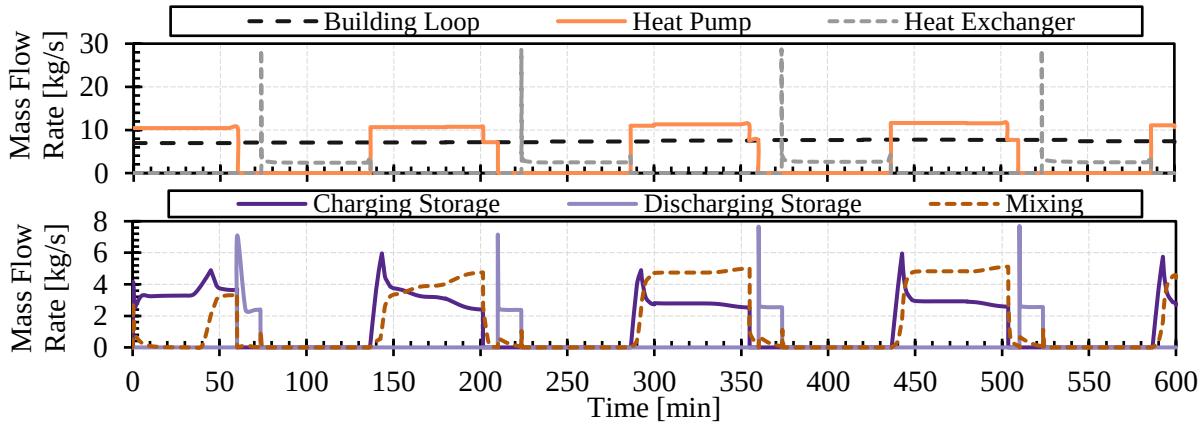

Figure 3.29: Mass flowrates for each component in the harvesting ETS

The heat pump electricity consumption was compared for the heating ETS with and without thermal storage, outlined in Figure 3.30. In the thermal storage case, the electricity consumption

increases due to the larger condenser load from charging the thermal storage. With no storage there is 185 kWh used and with storage it increases to 270 kWh. This is an example of a demand management tool to increase electrical consumption during off-peak times and eliminate the use of the heating HP during on-peak periods.

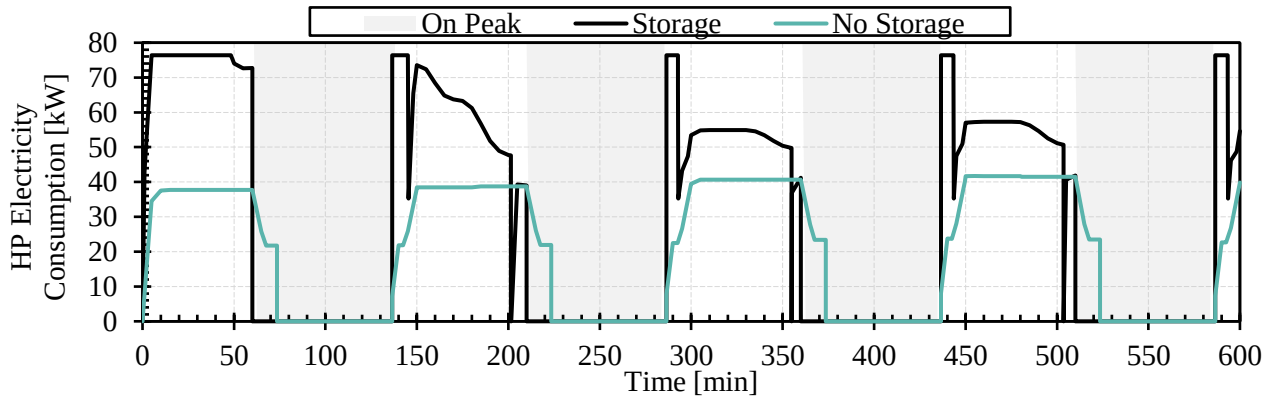

Figure 3.30: HP electrical consumption for the heating ETS with and without thermal storage

3.5 Energy Management Center Model

The energy management center (EMC) provides heat to the micro-thermal network through various heat sources. The original model created by Sullivan [78] was adjusted to better suit the nature of the simulations conducted in this thesis. The current work utilizes the adjusted EMC model from [78] for running thermal network simulations with a constant temperature, and there were four additional models created for changing temperature network simulations.

3.5.1 Constant Temperature Network EMC Model

The EMC for a constant temperature network contains: the heat exchanger that interfaces with the thermal network, a pump for fluid circulation, piping to represent the thermal mass of the EMC, a short-term thermal storage tank, cooler to represent the cooling tower, the CHP, and boiler. The EMC also contains temperature sensors to be able to monitor the performance of the components. Table 3.14 lists the components of the EMC and their corresponding source library.

Table 3.14: EMC components and their source libraries

Component	Library	Component Name
Equation/Variable Blocks	Modelica Standard	-
PI Controller	Buildings	*LimPID*
Boiler	Buildings	*BoilerPolynomial*
EMC Storage	Buildings	*StratifiedEnhanced*
Cooler	Buildings	*SensibleCooler_T*
CHP	AixLib – Modified by Sullivan	*CHP*
Piping	Buildings	*PlugFlowPipe*
Pump	Buildings	*FlowControlled_m_flow*
Temperature Sensors	Buildings	*TemperatureTwoPort*
Heat Exchanger	Buildings	*PlateHeatExchangerEffectivenessNTU*

The CHP's operation is determined by a user inputted schedule. The schedule consists of the on/off operation for the CHP on an hourly basis. To change the operating hours of the CHP, the schedule can be adjusted to reflect the desired operation and the remainder of the system would run accordingly. CHP operation dictates whether it is an on-peak or an off-peak period. If the CHP is operating, the implication is that natural gas peaking power plants are producing electricity on a grid level and the on-site CHP offsets that generation. When the CHP is off, is it assumed to be an off-peak period and primarily carbon free generation sources are producing electricity. The EMC storage tank is used to store excess CHP heat that is not used by the MTN instantaneously. The EMC storage is discharged during off-peak periods when the CHP is not operating. If the EMC storage is fully charged and there is excess CHP heat, the heat is expelled through the cooler. The heat removed by the cooler provides a measure of the heat that would charge a potential long-term thermal storage, which is not modeled in this thesis.

The piping at the EMC is modeled after the experimental facility at McMaster university. At McMaster, the piping throughout the site is approximately 43 m with a diameter of 0.0508 m. The resulting mass of the fluid within the piping is 87.15 kg. For simplification, in the modeled EMC

the piping was split into two 21.5 m segments. The EMC model in Dymola is displayed in Figure 3.31.

The *HeatingHeatExchanger* component in Figure 3.31 (a) contains the heat exchanger model displayed in Figure 3.31 (b). On the outside of the *HeatingHeatExchanger* component, the temperature set point of the thermal network and the temperature of the thermal network after the heat exchanger are connected. Within the component, there is a PI controller that uses the input temperatures to adjust the flowrate that will branch off of the EMC loop. The flowrate will provide the thermal network fluid with enough heat to exit at the desired set point. A nominal heat exchanger effectiveness value of 0.7 was used in the model.

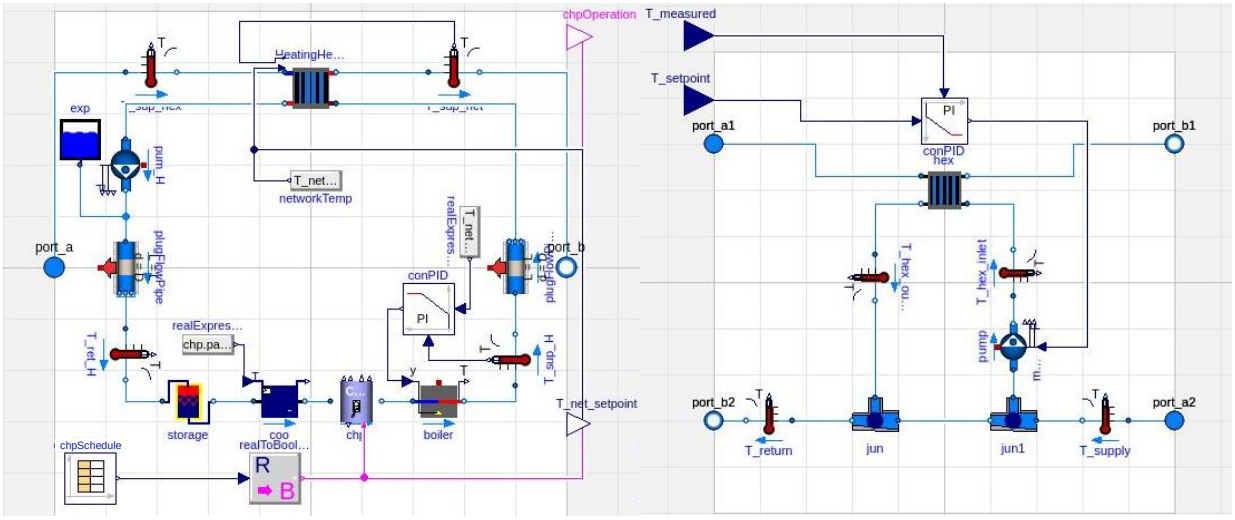

(a) (b)

Figure 3.31: EMC model for a constant temperature network in Dymola
(a) is the EMC model for a constant temperature network and (b) the heat exchanger model and control strategy

All junctions (or *jun*) are set to have a very low thermal mass as not to alter the temperature of the fluid leaving the component, but not too small as to cause instability with the component. The time constant, *tau*, used to determine the volume of fluid in the junctions, valves, and pumps was set to 0.0001 seconds. This practice was also followed in the ETSs.

Operation of the equipment in the EMC follows a sequential order. The fluid from the heat exchanger, that has transferred heat to the thermal network, travels to the thermal storage. If the fluid is greater than or equal to the storage set point, the storage tank will charge, and vice versa, if the fluid is less than the set point and if the storage has enough energy stored, it will discharge. If the fluid from the heat exchanger is at a temperature greater than the storage set point and was not able to charge the storage, the cooler will then reduce the temperature of the fluid to the desired set point in order to guarantee that the fluid maintains the CHP at its operating temperature. After the CHP, if the fluid has not reached a temperature suitable to heat the thermal network (5°C above the thermal network temperature set point) then the boiler will turn on to increase the temperature. A flow chart of the EMC sequence is seen in Figure 3.32.

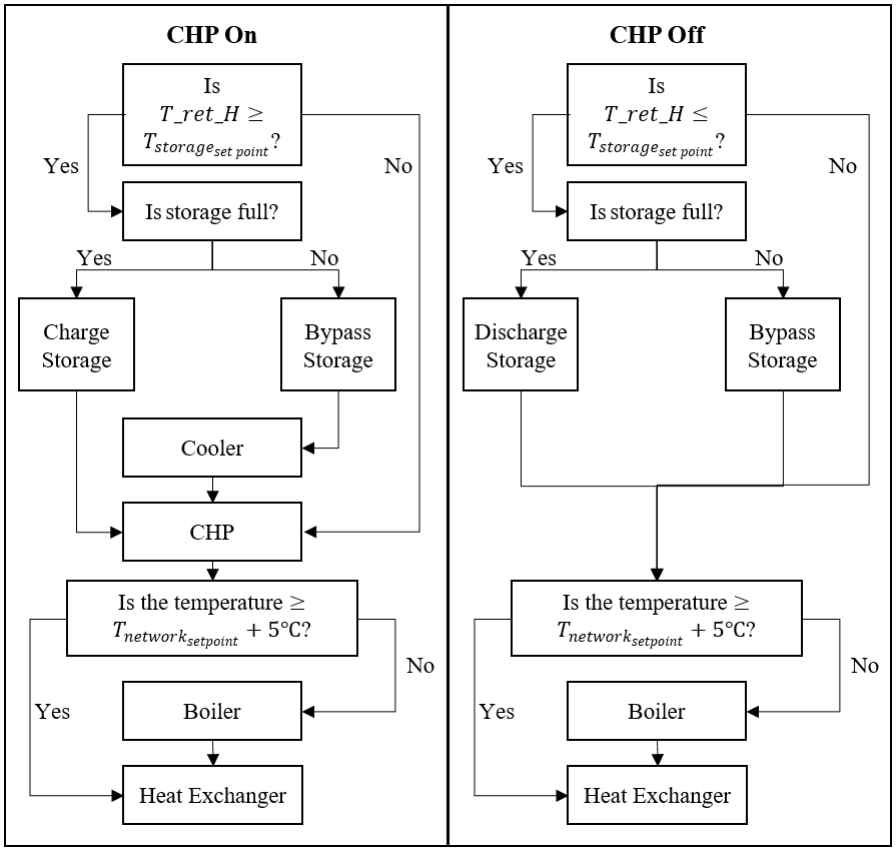

Figure 3.32: EMC control sequence flow chart

3.5.2 Changing Temperature Network EMC Models

The changing temperature EMC models utilize the constant temperature EMC model as a basis. For each changing temperature model, a new component or control strategy is added.

3.5.2.1 Fundamental Changing Temperature Model

For a changing temperature network, the additional component in the EMC is the switch that will change the thermal network temperature set point signal entering the heat exchanger (see the highlighted components in Figure 3.33). The network temperature set point is based on the CHP operation. When the CHP is on, the network temperature set point will be the hot temperature and when the CHP is off the set point will be the cool temperature. The remaining components follow the same operation as outlined in Section 3.5.1.

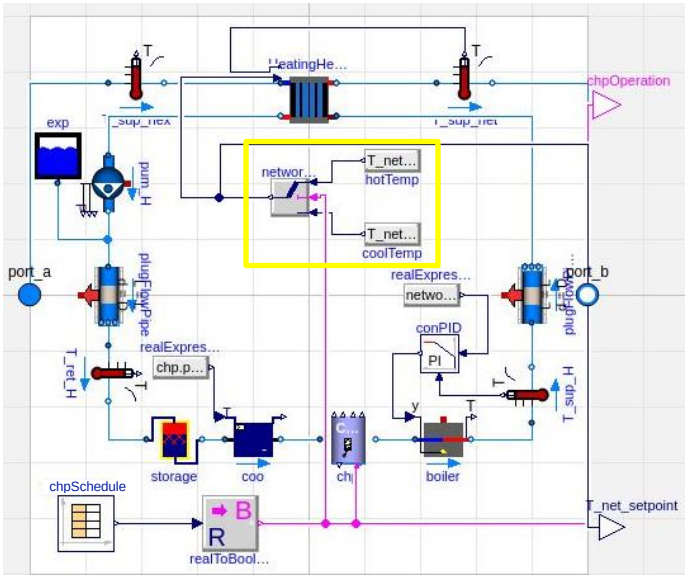

Figure 3.33: EMC model for a changing temperature network

3.5.2.2 Boiler Delay Model

Building on the fundamental changing temperature model, when decentralized thermal storage is used at the ETSs, the boiler should not be utilized during the network temperature transition. Therefore, the temperature set point used by the PI controller for the boiler has been delayed by

the response time (Chapter 4). This delay will allow only the CHP heat to increase the temperature of the network. The boiler will return to regular operation once the thermal network temperature has reached its hot set point to assist the CHP in meeting the building heating demands, if required. The signal is only delayed when the CHP is first turned on, the boiler is used when the CHP turns off so there is always a reliable heat source for the thermal network.

3.5.2.3 Network Pre-Heating Model

To incorporate a pre-heating aspect into the EMC, the fundamental changing temperature model described above is extended. Pre-heating the thermal network will allow harvested heat to increase the temperature of the micro-thermal network, to a maximum of the hot temperature set point, using off-peak electricity. The pre-heat of the network utilizes a carbon free heat source to reduce the heat required from the EMC during the temperature transition. The network will start pre-heating, if rejected heat is available, one hour before the CHP turns on. In order for the building ETSs to begin harvesting more energy, the value of *T_net_setpoint* is determined by reading the CHP schedule an hour in advance. If the CHP is on, the hot temperature set point is applied to *T_net_setpoint* and received by the ETSs. The ETSs will then harvest as much heat as possible within the hour to attempt to raise the network temperature to the hot set point.

3.5.2.4 Network Pre-Heating and Boiler Delay Model

This EMC model combines the network pre-heating with the boiler delay control strategies. Utilizing the network pre-heating and boiler delay ensures that the boiler is not being used when the ETS decentralized storage is available. The pre-heat of the network allows for the use of carbon free electricity to increase the temperature of the network as much as possible. Occasionally, when enough rejected heat is available, the temperature of the network is increased to its hot temperature

with harvested heat alone. This eliminates the need to discharge the ETS storage, allowing the heat to be used at a different time.

3.6 Micro-Thermal Network Model and Verification

3.6.1 Micro-Thermal Network Model

Three micro-thermal network models were developed. Each network model combines the previously outlined pipe model with different variations of the ETS and EMC models. The network models differ in the way that rejected cooling process heat is harvested. Previously outlined EMC and ETS models can be combined within each network model following the corresponding energy harvesting strategy.

3.6.1.1 Network Cooling Tower

In the network cooling tower model, all rejected heat is harvested. The harvesting ETSs at the buildings have the *HarvestHeat* signal always set to on. Figure 3.34 displays the location of the centralized network cooling tower. The heat that is harvested, but not utilized by the building heating system, is removed with the network cooling tower. If the temperature of the thermal network before the cooling tower is greater than the network set point, the cooling tower will remove the heat from the fluid and return the network to its set point.

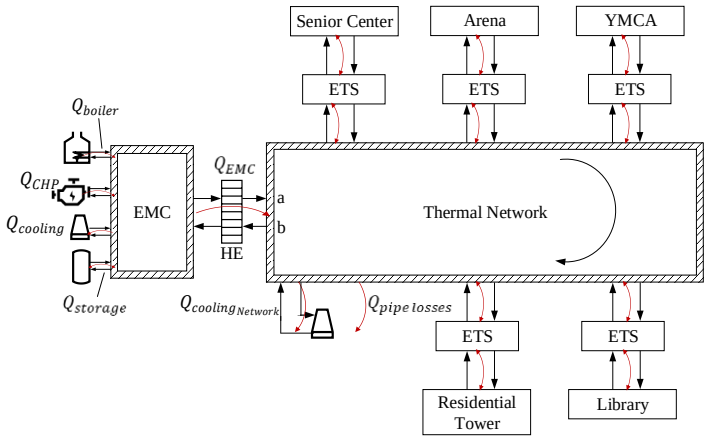

Figure 3.34: Network model with a centralized cooling tower

3.6.1.2 Selective Harvesting

Selective harvesting only harvests heat when it is required. The MTN temperature is used to determine if heat should be harvested. If the MTN temperature is below it's set point than heat will be harvested by the harvesting ETSs and if the MTN temperature is greater than or equal to it's set point no heat will be harvested. The rejected heat from the building cooling system that is not utilized/needed instantaneously based on the thermal network temperature is expelled at the buildings with the decentralized ETS cooling towers as described in Section 3.4.3. Since the heat is selectively harvested no additional equipment is required on the thermal network.

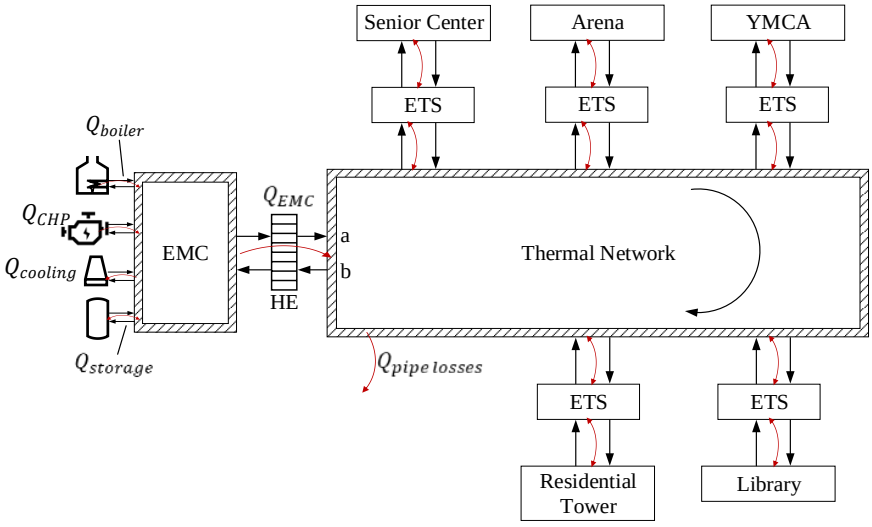

Figure 3.35: Network model with decentralized cooling towers

3.6.1.3 Network Thermal Energy Storage

The network thermal energy storage model is operated in a similar fashion to the network cooling tower model. All rejected heat is harvested from the buildings. The heat that is not used to meet the instantaneous heating loads is stored centrally in the network thermal storage tank. Like previous models, the thermal storage tank is the *StratifiedEnhanced* model from the Buildings Library with the control strategy developed by [78] and the heat pump is the heating HP from Section 3.3.4.1.

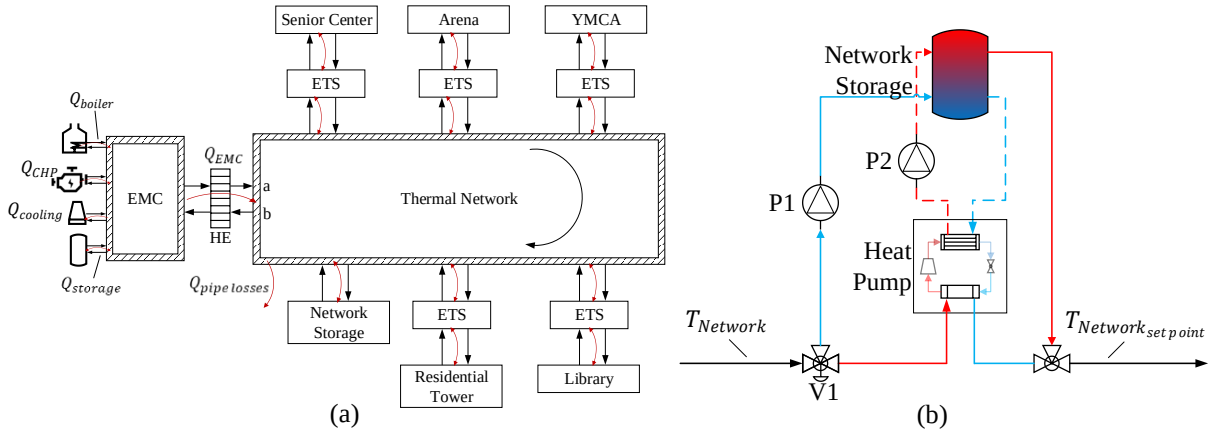

Figure 3.36: Network storage model schematic
(a) MTN schematic with the location of network storage and (b) the network thermal storage model

In Figure 3.36 (a) provides the overall network schematic with the network thermal storage included and Figure 3.36 (b) outlines the specifics of the network storage model used. When the CHP is on, V1 directs the thermal network fluid to the bottom of the storage tank. If $T_{Network}$ is less than the set point and the thermal storage is charged, the fluid will exit the network storage tank at $T_{Network_{setpoint}}$. If the CHP is off and the temperature of the network is greater than the network set point, the heat pump will remove heat from the network and it will use off-peak electricity to charge the storage at the desired set point. There is also an additional layer of control to stop harvesting heat at the buildings when the storage tank is full ($T_{storage_{bottom}} = T_{storage_{setpoint}}$) and the heat is then rejected at each building through the ETS cooling towers.

3.6.2 Verification

The developed network cooling tower model was used as the representative model and was verified against an in house Matlab code created to determine system behavior [81]. The Dymola model developed was run with a 10 minute time step and then post processed to average hourly data to compare with the hourly data received from the Matlab code developed by Abdelsalam.

Load profiles and simulation details are discussed in more detail in Section 5.1. Operation of the heating and harvesting ETS is as described in previous sections along the with the EMC operation for a constant temperature network. Simulation parameters utilized are outlined in Table 3.15.

Table 3.15: Verification simulation parameters

Pipe Length [m]	Network Set Point [°C]	Diameter [m]	$\dot{m}_N$ [kg/s]	CHP Size [kW_{th}]	Boiler Size [kW]
900	70	0.2	120	3,500	3,000

Key parameters from both models were compared. Labeling of the x-axis in Figure 3.37 corresponds to Figure 3.34. The energy flows not listed in Figure 3.34 are within the ETSs, such as the total building chiller power, heating HP power, harvesting HP power, the heat delivered by the thermal network to the buildings (the heat removed by the HP or heat exchanger to provide the building with its heating demand), and the heat harvested from the building and added to the thermal network. The data labels are the differences between the yearly energy values.

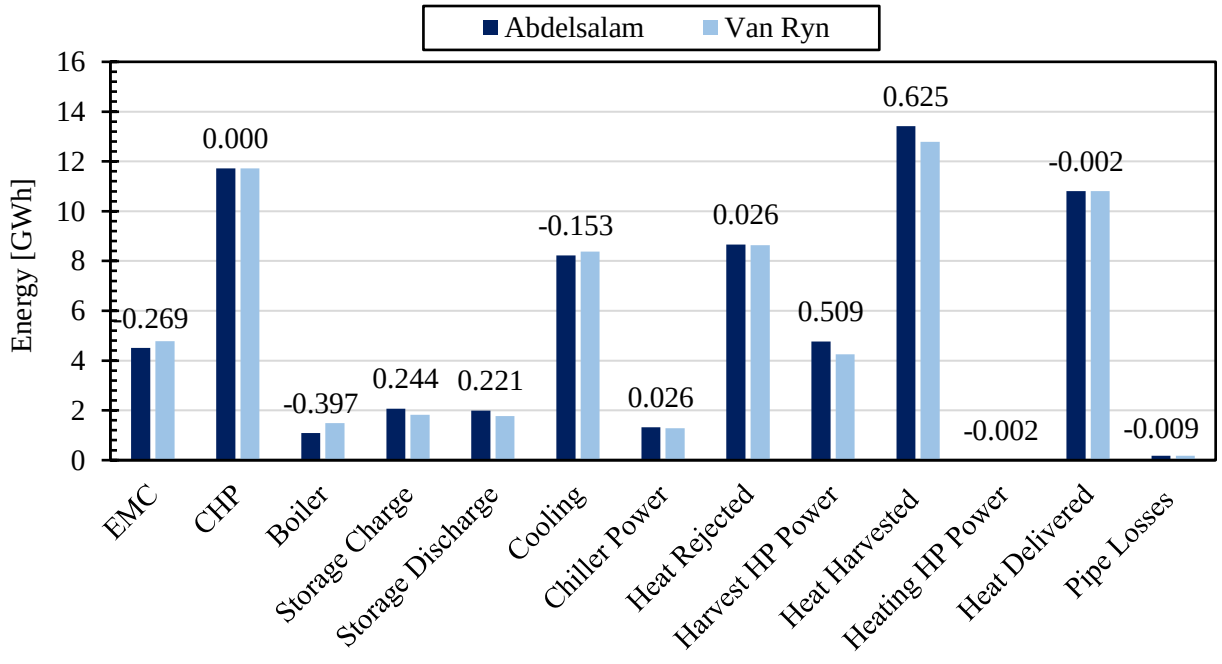

Figure 3.37: Verification results for main simulation parameters and the difference in yearly energy between both models

Table 3.16: The RMSE between model parameters by Abdelsalam and Van Ryn

	RMSE [kW]
EMC	72
CHP	0
Boiler	199
Storage Charge	234
Storage Discharge	194
Cooling	234
Chiller Power	33
Heat Rejected	47
Harvest HP Power	112
Heat Harvested	141
Heating HP Power	3
Heat Delivered	45
Pipe Losses	2

The largest difference between the two models is the quantity of heat harvested. To model the harvesting HP, both models use COP correlations developed with manufacturer performance data. The Dymola model COP equation, as described in Section 3.3.4.1, is a function of evaporator mass flowrate, the evaporator entering water temperature (EWT), and the temperature exiting the condenser. Abdelsalam's HP model uses a COP equation developed from a different HP manufacturer and the COP equation is a function of the evaporator EWT and the condenser EWT. The equation used by Abelsalam is presented in Equation 3.14.

$$COP = -0.0082183 * x^2 + 0.4364849 * x + 0.3390187 \quad (3.14)$$

Where x is defined below in degrees Kelvin,

$$x = \frac{EWT_{condenser}}{EWT_{condenser} - EWT_{evaporator}}$$

The harvesting HP model used in Dymola utilizes less power to harvest the rejected energy than the model in Abdelsalam's work. Due to the reduction in power input, there is less heat harvested by the HP and added to the thermal network.

Another area of difference is within the EMC. The amount of heat transferred to the network from the EMC, Q_{EMC}, is greater in Dymola. The increase in heat required from the EMC is due to the reduction in harvested heat. The main difference in the EMC comes from the thermal storage. The utilization of different storage models causes the differences in the yearly energy. Abdelsalam's storage model assumes a perfectly insulated tank with the storage medium discretized spatially into two fully mixed layers, a hot layer at the top and cold layer at the bottom. The tank begins initially fully mixed at 20°C. A plug flow approach is used through the storage tank during charging and discharging. The Dymola *StratifiedEnhanced* model from the Buildings Library uses stratification with 40 control volumes to compute the temperature of the fluid within the tank. The Dymola model also begins with the storage at a uniform temperature of 20°C. A third order upwind scheme is used to determine the outlet temperatures of the control volumes during the charging and discharging of the storage. Energy stored or not stored in the thermal storage then dictates the energy expelled through the cooling tower and what discharged or not discharged is required from the boiler.

Overall, the models showed good agreement providing confidence in the application of the Dymola model.

Chapter 4

4. Response Time

4.1 Definition and Background

The response time of the micro-thermal network characterizes the time it takes for the MTN to achieve a temperature change. The temperature change of the network can be deemed complete when the fluid returning to the starting point has reached the desired temperature or has reached steady state.

Changing the temperature of the network within a timely manner allows for controllability. Controllability of the temperature of the network gives the ability to manage the electricity consumption at the buildings at any given time.

The response time is comprised of two main components, the thermal time and the transit time. The thermal time component is dependant on the thermal mass of the network and the heat transfer rates to the network. The transit time component represents the time it takes for the fluid to travel the length of the network at the given flowrate. Therefore, the response time equation is as follows.

$$t_{response} = t_{transit} + t_{thermal} \tag{4.1}$$

A changing temperature network between a hot and cool temperature also eliminates the concern for Legionella growth expressed in [82]. As long as the hot temperature is greater than 50°C, bacteria formed during the low temperature periods will die off.

4.2 Response Time Equation

4.2.1 Transit Time

The transit time represents the time it takes for the fluid to go from point a to b in Figure 4.1. The transit time equation, Equation 4.2, utilizes the mass of fluid in the network and the mass flowrate of the fluid.

$$t_{transit} = \frac{M_N}{\dot{m}_N} \tag{4.2}$$

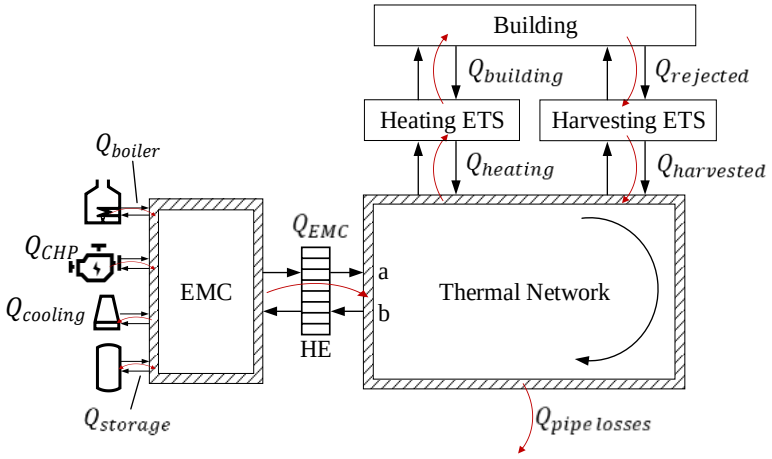

Figure 4.1: Thermal network schematic indicating points used for the response time equation

4.2.2 Thermal Time

The thermal time component can be defined as the time it takes for the temperature at point ‘a’ in Figure 4.1 to reach the desired set point. In order to determine the thermal component, an energy balance needs to be conducted on both the EMC and the MTN. All heat sources and areas of heat loss are examined. Figure 4.1 summarizes the heat flows of the system for a thermal network with clockwise water flow.

4.2.2.1 EMC Energy Balance

Within the EMC there is energy generated from the CHP and the boiler. The energy out of the EMC will be transferred to the thermal network through the heat exchanger. The heat transferred through the heat exchanger is calculated based on the heat transfer coefficient of the heat exchanger and the difference between the EMC header temperature and the network temperature. The stored energy will be in the thermal mass of the components within the EMC; the equipment and the piping.

Short-term thermal energy storage at the EMC is not considered in the EMC energy balance during the loop temperature transition. Moreover, the cooling tower at the EMC will also not operate. The key operating components during the loop temperature transition are thus the CHP, boiler, and heat exchanger. Therefore, the energy balance for the EMC is as follows with the final equation as Equation 4.3.

$$E_{in} + E_{generated} - E_{out} = E_{stored} \quad \begin{cases} E_{in} = 0 \\ E_{generated} = Q_{CHP} + Q_{boiler} \\ E_{out} = Q_{EMC} \\ E_{stored} = M_{EMC} c_p \dfrac{dT_{EMC}(t)}{dt} \end{cases}$$

$$M_{EMC} c_p \frac{dT_{EMC}(t)}{dt} = Q_{CHP} + Q_{boiler} - Q_{EMC} \tag{4.3}$$

4.2.2.2 Thermal Network Energy Balance

Sources of heat for the thermal network come from the EMC and the harvesting ETS. The EMC interacts with the thermal network through the heat exchanger. In the harvesting ETS the heat rejected from the buildings cooling system is harvested by either a heat pump or heat exchanger and added to the thermal network.

Heat is also removed in the thermal network through the heating of the buildings and the thermal losses of the network pipes. To heat the building, the thermal network interfaces with a heat pump or a heat exchanger. The amount of heat extracted from the network depends on the heating load of the building and either the COP of the heat pump or the effectiveness of the heat exchanger. The energy balance is as follows and the final equation is Equation 4.4.

$$E_{in} + E_{generated} - E_{out} = E_{stored} \quad \begin{cases} E_{in} = Q_{EMC} + Q_{harvested} \\ E_{generated} = 0 \\ E_{out} = Q_{pipe\ losses} + Q_{heating} \\ E_{stored} = M_N c_p \dfrac{dT_N(t)}{dt} \end{cases}$$

$$M_N c_p \frac{dT_N(t)}{dt} = Q_{EMC} + Q_{harvested} - Q_{pipe\ losses} - Q_{heating} \tag{4.4}$$

4.2.2.3 Thermal Time Equation

The EMC and thermal network energy balances were combined by substituting for Q_{EMC}. The resulting equation is Equation 4.5.

$$M_{EMC} c_p \frac{dT_{EMC}(t)}{dt} + M_N c_p \frac{dT_N(t)}{dt} = Q_{CHP} + Q_{boiler} + Q_{harvested} - Q_{pipe\ losses} - Q_{heating} \tag{4.5}$$

To simplify Equation 4.5, it is assumed that the temperature of the fluid at the EMC is equal to the temperature of the network plus a temperature difference, $T_{EMC}(t) = T_N(t) + \Delta T$. When substitution for the EMC temperature is incorporated, Equation 4.6 is formed. The temperature difference between the EMC and thermal network is assumed to remain constant throughout the temperature transition and therefore the derivative can go to zero.

$$(M_{EMC} + M_N) c_p \frac{dT_N(t)}{dt} + \overbrace{M_{EMC} c_p \frac{d\Delta T}{dt}}^{0} = Q_{CHP} + Q_{boiler} + Q_{harvested} - Q_{pipe\ losses} - Q_{heating} \tag{4.6}$$

Now that Equation 4.6 has been simplified, it can be integrated. The dt term integrated to Δt or $t_{thermal}$, representing the time for the temperature to go from its initial value to the desired set point. The $dT_N(t)$ term integrated to the temperature difference between the temperature of the thermal network at the start of the temperature transition and the temperature at the desired set point. The temperature difference can be simplified to the hot temperature of the network subtract the cool temperature. Further assumptions were made in integrating Equation 4.6:

- Heat flowrates are constant over the thermal time,
- Thermal losses are negligible in comparison to the other heat flows, and
- M_{EMC} is negligible if it is less than 2-10% of the network mass (further detail in Section 4.3.1)

The final thermal time equation is Equation 4.7. The equation gives an approximate value to the thermal time.

$$t_{thermal} = \frac{(M_{EMC} + M_N)c_p\left(T_{N_h} - T_{N_c}\right)}{Q_{CHP} + Q_{boiler} + Q_{harvested} - Q_{heating}} \tag{4.7}$$

4.2.3 Response Time

Combining equations 4.2 and 4.7 results in the response time equation, Equation 4.8. The equation has been simplified further with the use of more general terms. One variable, $Q_{available}$, now represents the total heat available from any heat source to raise the temperature of the network and ΔT_N is the desired network temperature difference.

$$t_{response} = \overbrace{\frac{\tilde{M}_N}{\dot{m}_N}}^{t_{transit}} + \overbrace{\frac{(M_{EMC} + \hat{M}_N)c_p\Delta T_N}{Q_{available}}}^{t_{thermal}} \tag{4.8}$$

4.3 Analysis, Modeling, and Verification

4.3.1 Parameter Analysis

Using the response time equation outlined in Equation 4.8, the effects of different parameters on the response time were analyzed. In testing the response time equation parameters, each parameter was varied while holding the remainder constant. The quantity M_{EMC} represents the mass of piping at the EMC, 87.15 kg, and the mass of the CHP, as these are the only thermal mass components utilized in the testing simulation. The CHP sizes and corresponding masses are listed in Table 4.1. The mass of the CHP was determined by a simple regression analysis conducted in Excel with data retrieved from the AixLib CHP database. The resulting equation is Equation 4.9 and provides the volume of the CHP, then utilizing the density of water, the mass can be determined.

$$V = 4x10^{-5}Q_{CHP} + 0.0025 \tag{4.9}$$

Table 4.1: CHP sizes corresponding mass

Size [kW_{th}]	Mass [kg]
566	25
847	36
1700	71
2000	83
2500	103
3500	143
5000	203

The main parameters utilized in testing are listed in Table 4.2 for each sub figure in Figure 4.2. A constant network length was used throughout the testing of 1,500 m.

Table 4.2: Response time parameter analysis methodoolgy

	L_N $[m]$	D $[m]$	M_N [kg]	ΔT_N [℃]	$\dot{m}_N$ $[kg/s]$
Figure 4.2 (a)	1,500	Varied	Varied	30	100
Figure 4.2 (b)	1,500	0.2	47,030	30	Varied
Figure 4.2 (c)	1,500	0.2	47,030	Varied	100

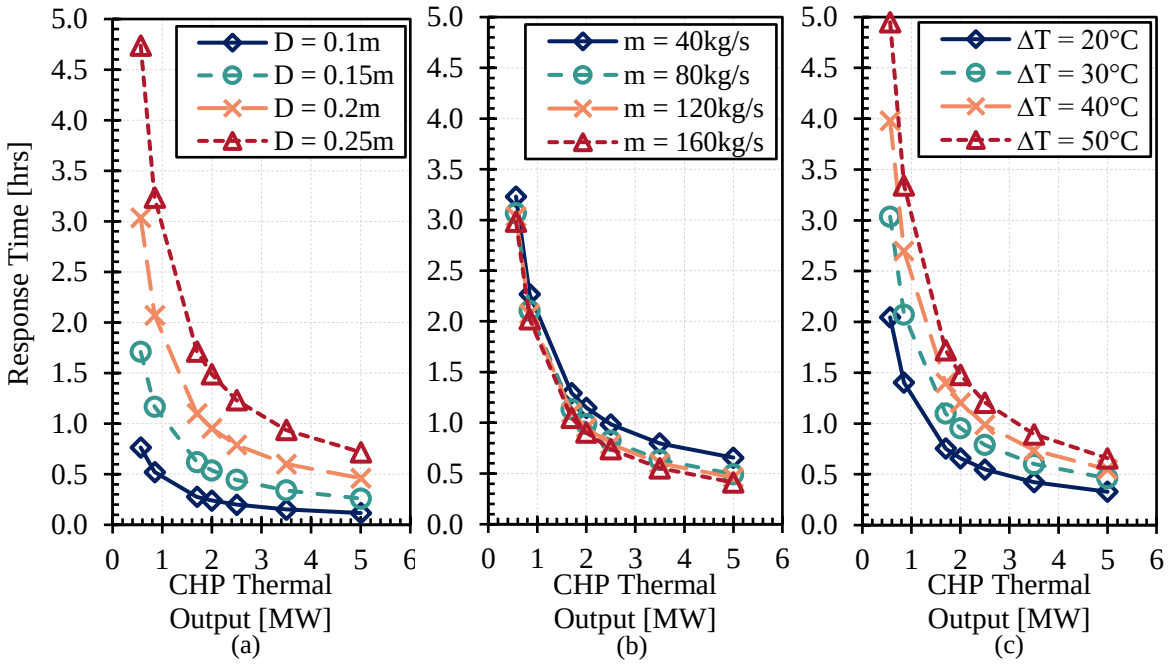

Figure 4.2: Response time equation parameter analysis
(a) thermal mass analysis, (b) mass flowrate analysis, and (c) temperature difference analysis

The diameter has a large effect on response time, presented in Figure 4.2 (a), because a small change in pipe diameter has a non-linear impact on the network thermal mass. The resulting masses of the network used in testing are 11,747 kg, 26,454 kg, 47,030 kg, and 73,484 kg. The thermal mass is a dominant parameter as it is in both the transit and thermal time components.

The overall response time is determined based on the sum of the transit time and the time scale associated with the thermal mass of the system. At very low flowrates, the transit time will dominate. As the flowrate is increased, the impact of the transit time on the overall response time will diminish. As shown in Figure 4.2 (b), for a change in flowrate between 40 and 80 kg/s the response time difference across all CHP thermal outputs improved by 589 seconds, but between the 120 to 160 kg/s mass flowrates the response time only improved by 98 seconds. Therefore, an increase in mass flowrate will eventually begin to have a negligible affect as the thermal time becomes the dominant term in the response time equation.

An increase in temperature difference is linearly correlated to the response time for a given heat input as seen in Figure 4.2 (c). The heat available is inversely related to the response time, demonstrated across all three plots in Figure 4.2. If the CHP thermal output were to keep increasing, eventually the response time would plateau as the transit time would become the dominant factor in the equation.

Affect of the EMC mass on the response time was also analyzed. Using the test cases above, the response time was calculated with no mass in the EMC. On average, the difference in response time between the incorporation of the mass at the EMC between the exclusion of the EMC mass was an increase of 14 seconds. In the EMC, the mass increased when the CHP size increased and inherently so did the quantity of available heat. Since the heat available increased with the mass of the EMC there was no significant impact on the response time. The EMC mass never exceeded 2% of the network thermal mass.

When the available heat is the dominant term the EMC mass becomes less significant, when the thermal mass is the dominant term the EMC mass has a larger impact on the response time. Figure 4.3 portrays the difference in response time between zero EMC thermal mass to the corresponding percentage of the network thermal mass on the x-axis. Network mass and available heat values used are at the two extremes of the ranges presented in this work, although a large thermal mass would typically not be paired with a small quantity of available heat as it would be difficult to increase the temperature of the network in a reasonable time frame. Therefore, depending on the amount of heat available, the EMC mass may be considered negligible if it is less than 2 to 10% of the network mass to keep the impact of the EMC thermal mass below 5 minutes.

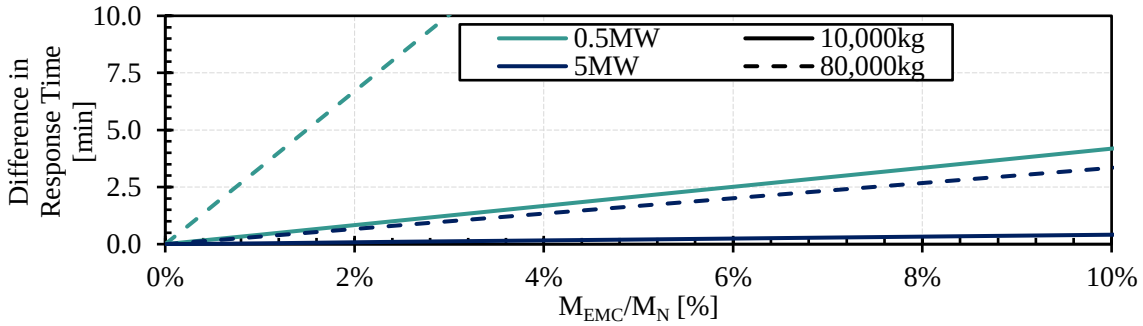

Figure 4.3: Relationship between the increase in response time and increase in EMC mass as a percentage of the network mass

4.3.2 Dymola Verification

Simulations were run in Dymola to confirm that the response time equation developed was accurately able to predict the time it would take for the thermal network to change temperature.

First, a simulation was conducted to look at the temperature profile during the temperature transition. The simulation was run with a 566 kW_{th} CHP and a one second time step to see the behavior of the fluid. A 30°C temperature difference was simulated using the plug flow pipe with no heat losses. Additional parameters used in the testing simulation are listed in Table 4.3. The simulation results along with the calculated temperature profile are plotted in Figure 4.4.

Table 4.3: Response time equation verification parameters

$L_N\ [m]$	$D\ [m]$	M_N [kg]	M_{CHP} [kg]	$\dot{m}_N\ [ks/s]$
1000	0.125	12,297	25	40

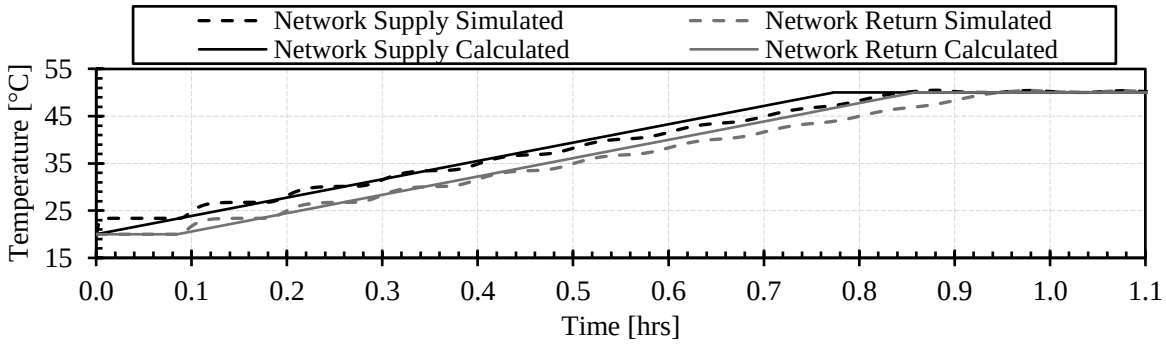

Figure 4.4: Temperature versus time plot simulated in Dymola and calculated with the response time equation

The Dymola simulation shows the number of times the fluid had travelled the length of the network. Each bump in the temperature profile signifies that the fluid has done one lap through the network piping. Since the response time equation does not take into account the dynamics of the fluid, it inherently predicts the response time to be quicker than the Dymola simulation. The results do show good agreement as the simulated and calculated response time differs by approximately 5 minutes. The response time for each case is presented in Table 4.4.

Table 4.4: Response time verification results compared with Dymola

Response Time Simulated [hrs]	Response Time Calculated [hrs]
0.95	0.86

Secondly, for various CHP sizes the calculated response times were compared to the response time simulated in Dymola. Simulation parameters utilized are the same as the previous simulation and listed in Table 4.3. The calculated values using the response time equation agree very well with the values from the Dymola simulation, displayed in Figure 4.5. Multiple scenarios were simulated where the thermal mass, mass flowrates, and CHP sizes were varried, 28 in total, and the RMSE between the simulated and calculated values is 4.4 minutes.

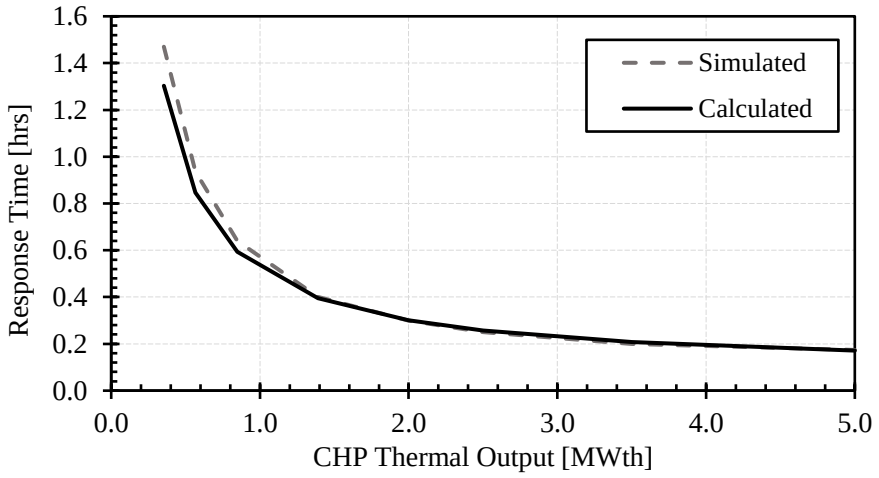

Figure 4.5: Response time simulated and calculated with varying CHP thermal output

4.4 Thermal Network Design Strategy Utilizing Response Time

The response time of the thermal network to changes in operating conditions can strongly influence the overall system performance. Careful design is thus required to ensure that the thermal network is able to achieve the desired temperature difference in the desired time frame.

This section presents a design strategy for micro-thermal networks that incorporates the distribution network response time. For each parameter in the response time equation, a graphical representation of the parameter was created and the relation to the other parameters is displayed. The figures created are used together as the design map for the micro-thermal network.

To begin the design process, the length of the MTN will be determined by the ICE-Harvest site clustering technique as described in [83]. Once the length of the site has been decided, the thermal mass of the network will be determined through the selection of a pipe diameter in Figure 4.6. Inner diameters of commercially available HDPE piping have been added to the plot, in dark grey lines, to indicate what sizes of piping would be feasible in a real application [84]. The inner diameter is subject to small changes depending on the pressure class of piping required and the pipe thickness.

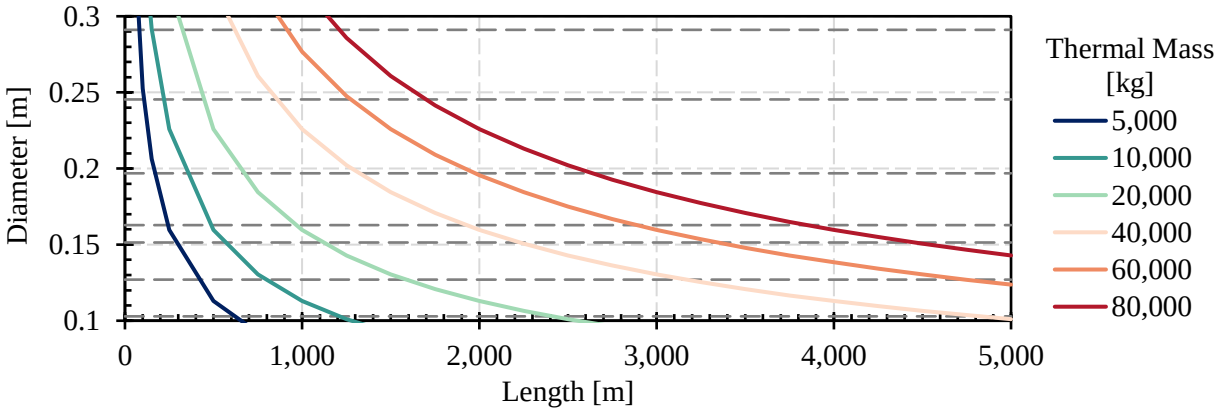

Figure 4.6: Length vs Diameter plot to determine the thermal mass of the network with commercially available pipe diameters indicated by the dashed horizontal lines for reference [84]

Utilizing the thermal mass, Figure 4.7 is used to determine the remaining MTN parameters. In Figure 4.7, there are three plots, each plot represents a value of the response time from 15, 30, and 60 minutes (left to right). The designer can approach these plots from a few different perspectives. Based on the desired outcome, whether it be a specific network temperature difference or quantity of heat available, the remaining parameters can be chosen to meet the desired goal. Outside constraints can also play a role, for example if there is a minimum mass flowrate required to meet the heating demands of the buildings.

After the network parameters have been chosen, the pumping power required of the system is considered in Figure 4.8. As a basis, if the pumping power is greater than approximately 10% of the CHPs electrical output, the pumping power is not considered as this exceeds the high end of the electrical distribution and transmission line losses. A previous step in the design process is explored to try reduce the pumping power, for example increasing the pipe diameter or decreasing the mass flowrate. It was established in Section 4.3.1 that the mass flowrate has a minimal impact on the response time when the thermal mass is the dominant parameter, but it does have a large impact on the pumping power.

All parameters are interrelated and changing one parameter can have a negative or positive effect on the end design goal. Figure 4.9 shows a design flow chart with with a suggested sequential design method, but with many opportunities to revert back to a previous stage to make adjustments to a parameter. The design process is iterative, it will require multiple tries until an optimal design is reached.

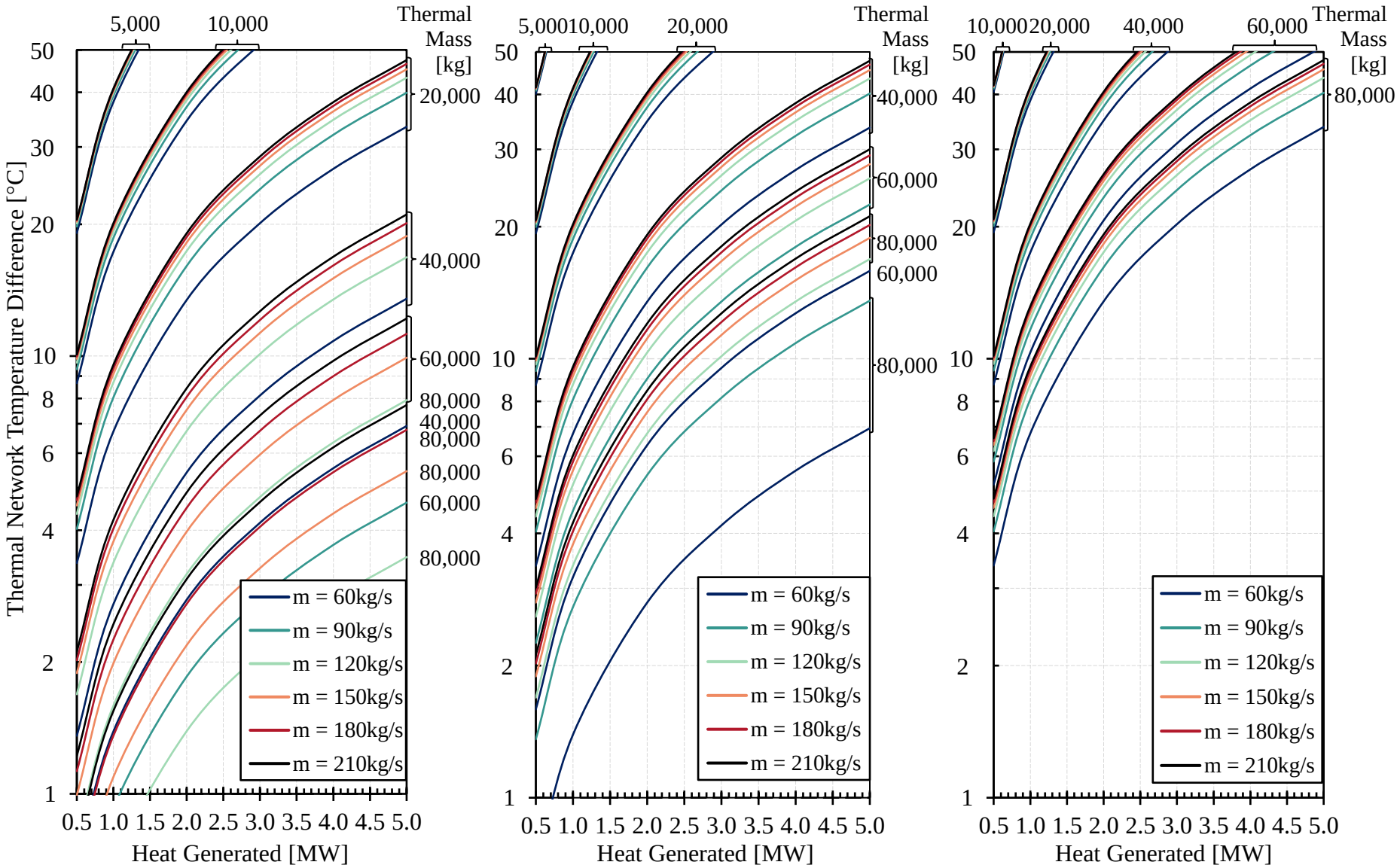

Figure 4.7: Left to right 15 minute, 30 minute, 60 minute response time

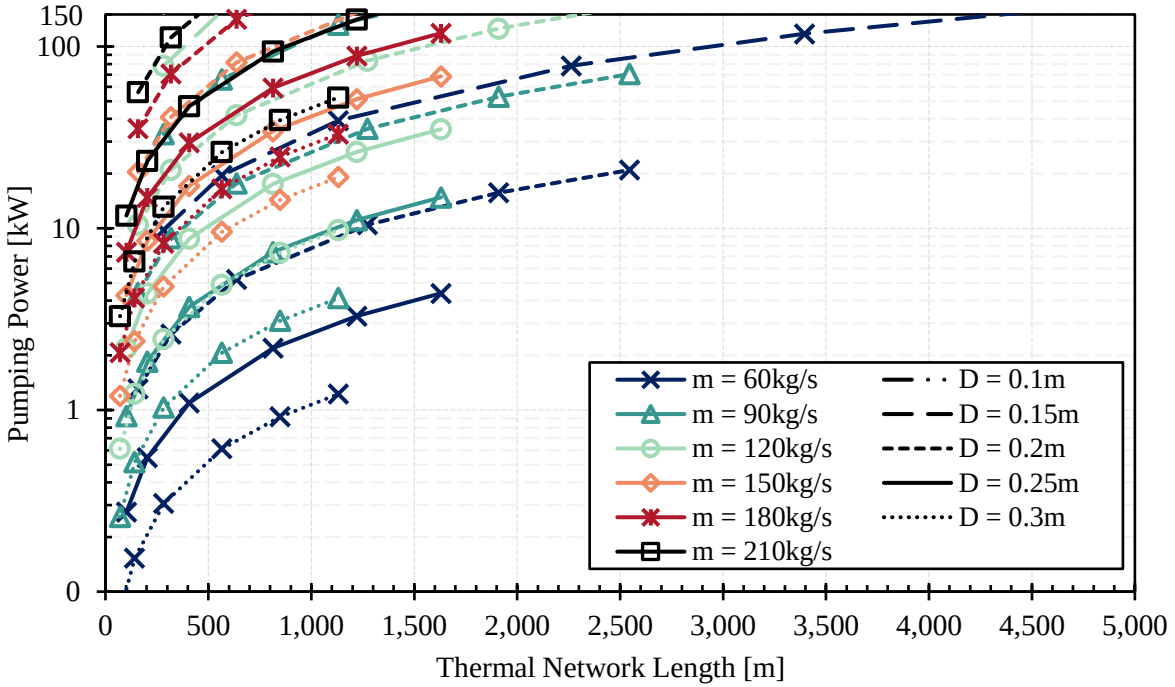

Figure 4.8: Pumping power map of the central pump
related to the thermal network length, mass flowrate, and diameter

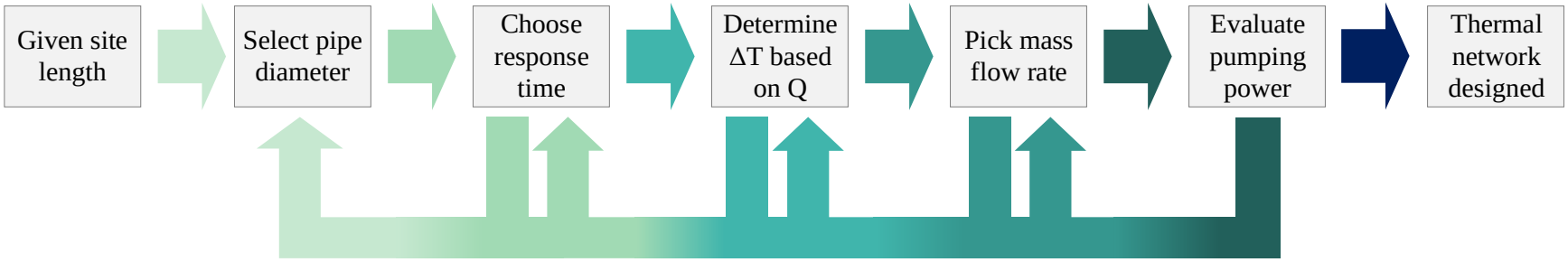

Figure 4.9: Network design process flow chart

Chapter 5

5. Results and Discussion

In this chapter, a spectrum of computational simulations were conducted in Dymola utilizing the models and operational strategies described in the previous sections. The aim of these simulations was to identify operational strategies for the MTN that reduce GHG emissions and provide necessary demand response to the electrical grid. Presented results will be analyzed and discussed in each section.

5.1 Background

As the basis for the computational simulations, a micro-thermal network was established using real-world data from the IESO and ICE-Harvest's industry partners. The MTN schematic and simulation model is displayed in Figure 5.1. Details regarding the building load profiles, piping configuration, emission factors, and general assumptions are provided in the succeeding sub-sections.

The operation of the MTN is as follows. During off-peak periods, electricity will be used from the provincial grid. During on-peak periods, the CHP will be activated. Ontario natural gas peaking power plant generation data was used to establish a general definition for the on-peak and off-peak periods. For the analysis conducted, the year 2017 was used. In 2017, there was minimal hours of natural gas peaking power plants operating on the Ontario electrical grid, only 3,347 hours of the year [54]. This provides a conservative estimate of the emissions reduction potential of the ICE-Harvest system. The hours that natural gas peaking plants were operational are considered to be on-peak periods and the on-site CHP is run to offset this generation. The remainder of the year is

presumed to be an off-peak period. Carbon free electrical generation and potential curtailed electricity is assumed to be available in off-peak times to meet the electrical demands of the site.

The micro-thermal network model in Dymola, displayed in Figure 5.1 (b), demonstrates how all of the constructed component models are incorporated. The system schematic of the MTN is also shown in Figure 5.1 (a) for reference. In the Dymola model, each component is connected with an equal length of pipe. The ground temperature model provides the network piping with the ground temperature conditions and sends the ambient air temperature to the ETSs. The EMC provides the ETSs with the CHP schedule and the network temperature set point for use in the ETS control strategy. The network model displayed is the selective harvesting model described in Section 3.6.1.2.

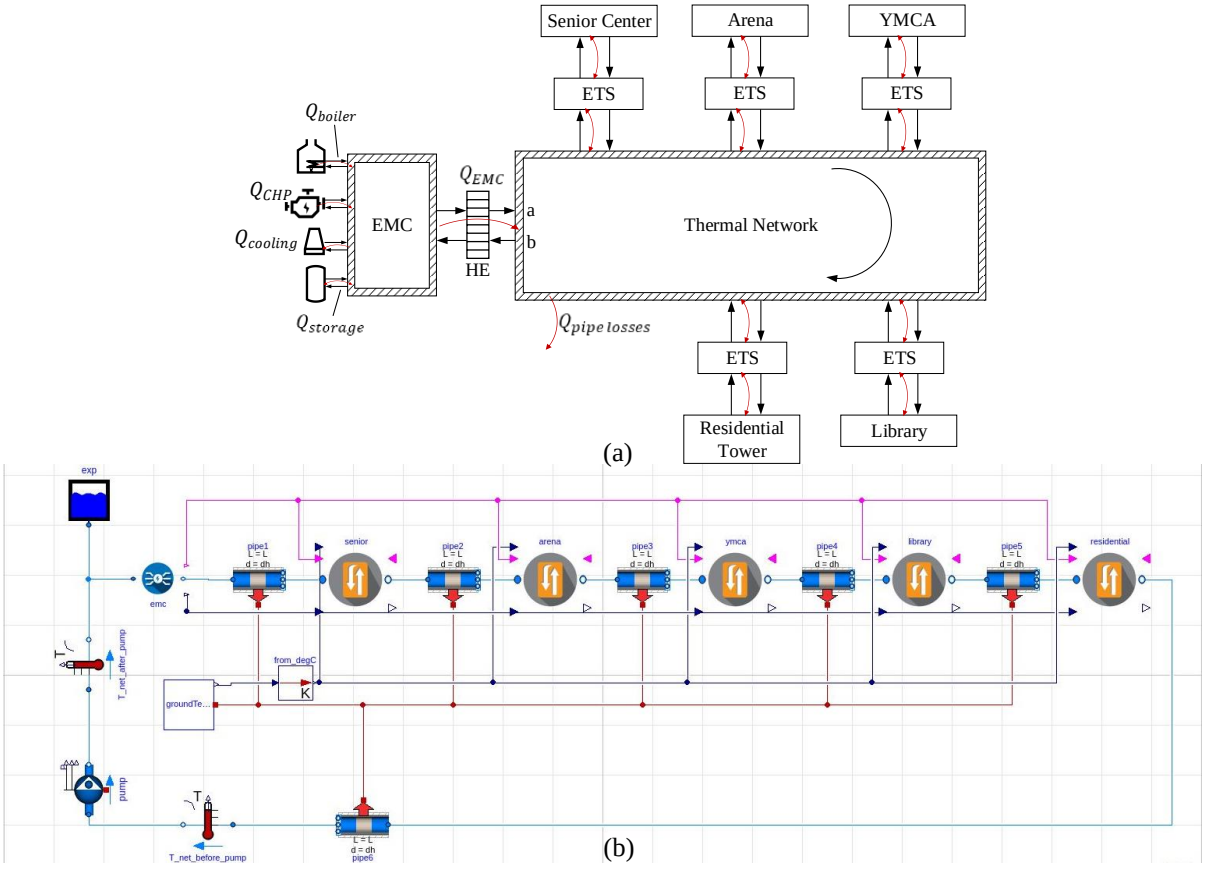

Figure 5.1: Micro-thermal network schematic (a) and model in Dymola (b)

5.1.1 Building Load Profiles

A cluster of five existing buildings in the Greater Toronto-Hamilton Area, for which industrial partners on the ICE-Harvest project have provided hourly information, were selected for the simulation of the community energy system. The simulation site consists of a senior center, arena, YMCA, library, and residential tower. The cumulative load profiles for the buildings are outlined in Figure 5.2 and the load profiles for the individual buildings are presented in Appendix C. The electrical demand includes the building plug loads and cooling electricity. Heating loads are a combination of space heating (SH) and domestic hot water (DHW). In the system simulations, building temperature set points of 60 and 45°C are explored. For the 60°C cases, the 60°C water can meet the SH and DHW demands. For the 45°C cases, additional heating to reach DHW temperatures may be required but is not considered in this study.

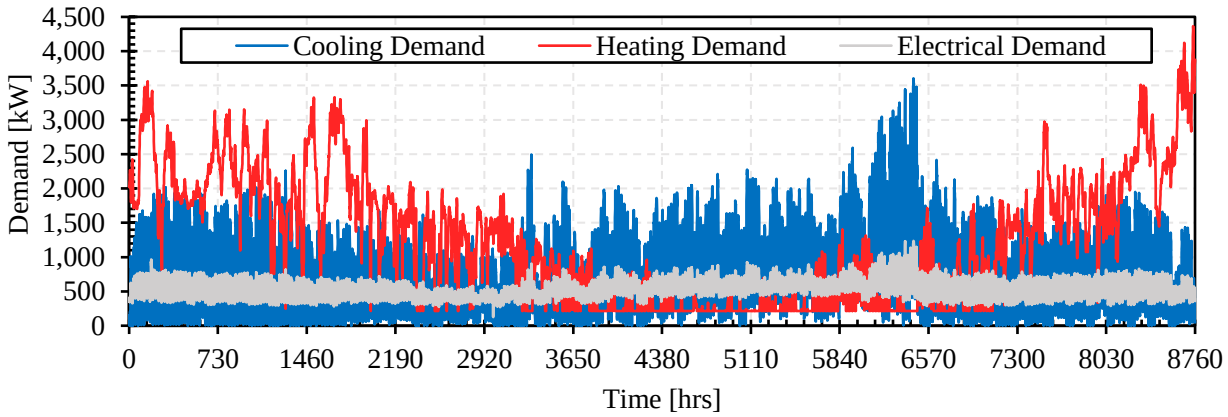

Figure 5.2: Site wide hourly heating, cooling, and building electrical demands

From analyzing the yearly energy requirements of the site, there is a balanced heating and cooling load. Abdalla et al. define a node to be balanced if the ratio of the annual cooling load to the sum of the annual heating and cooling load is in the range of 40 to 50% [83]. For this node, the cooling load is 40% of the total thermal energy demand, therefore classifying this node balanced. The balanced heating and cooling load also make this site suitable for GSHP systems.

Table 5.1: Total heating and cooling energy

Yearly	Energy [MWh]
Heating Demand	10,808
Cooling Demand	7,341
Rejected Heat	8,630
On-peak	4,703
Off-peak	3,926
Harvestable Heat	10,786

The building chillers produce rejected heat that is typically expelled into the atmosphere, Table 5.1 outlines the amount of heat rejected. There is more heat rejected during on-peak periods even though the on-peak period only comprises 38% of the year. On hot summer days the electrical demand increases significantly due to the operation of air conditioners. The increase in electrical demand causes the grid to dispatch natural gas peaking power plants, creating an on-peak period. The majority of rejected heat is in the summer months, corresponding to the on-peak periods, when all buildings are in cooling mode and the heating demand is low. Buildings such as the arena and the library/data center have a cooling load year-round and provide useful heat in the winter. Even in the winter months the harvestable heat may not fully align with the heating demand, the majority of cooling takes place during the day and the heating demands are greatest in the morning and evening.

An estimate of how much heat could be harvested from the system was calculated using an average COP of 5. The COP was obtained from the harvesting HP in the 40 and 50°C constant temperature network preliminary simulations, as these temperatures are the mid point of the range tested. The average COP was used with the quantity of rejected heat to estimate the harvested heat available, which is approximately equal to the heating load. Two harvesting strategies can be implemented: instantaneous harvesting and seasonal storage utilization. With instantaneous harvesting, a simultaneous heating and cooling load is required. The instantaneous harvesting heating demand

profile displayed in Figure 5.3 represents the heating load after the incorporation of harvested heat. All harvestable heat that coincided with the heating load was used to meet the demand. The heating yearly energy decreased to 5,159 MWh utilizing 52% of the harvestable heat. In the seasonal storage case, the large amounts of harvestable heat in the spring and summer months that were not utilized in the instantaneous case (the remaining 48%) are stored for use in the fall and winter. The harvested heat that was stored was assumed to have a 45% efficiency [85]. The seasonal storage heating demand profile has decreased in the winter and fall months as the seasonal storage was used to meet a portion of the demand. With seasonal storage, the heating load decreases to 2,824 MWh.

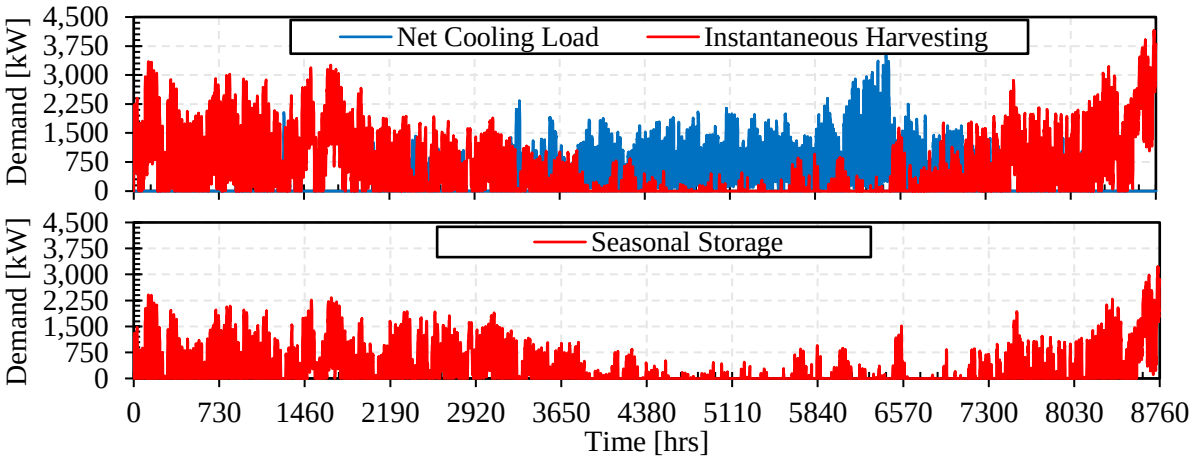

Figure 5.3: Cooling and heating load profiles after harvesting thermal energy

Figure 5.4 provides a closer look at the instantaneous harvesting profiles for a week in the winter and the summer. The quantity of heat harvested was retrieved from a 40°C constant temperature network simulation in Dymola. Previously, it was assumed that all harvestable heat meets the heating load, where as in Figure 5.4 only a portion of the heat was actually harvested. The instantaneous harvesting of heat is heavily reliant on the temperature of the micro-thermal network. If the temperature of the thermal network was not below its set point than the ETS would

not harvest heat. In the summer, large quantities of harvestable heat are visible. Only a small portion of the heat was actually harvested due to the very small heating demand. The remainder of the heat could be stored for use in the winter months.

The simulation results presented in the following sections only harvest heat when it is required, therefore, the actual amount of heat harvested from the system is less than in the instantaneous harvesting case.

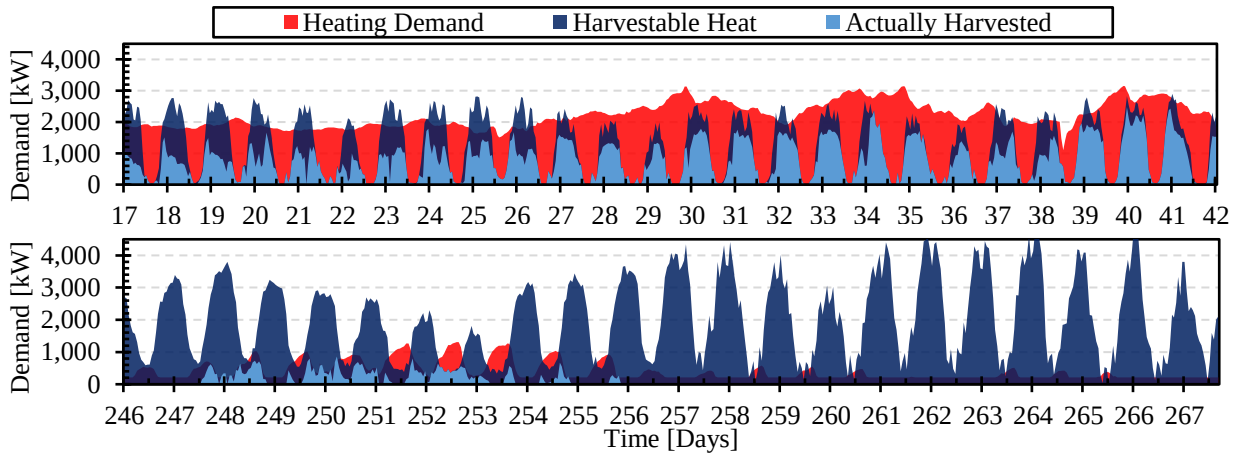

Figure 5.4: Harvestable heat and what was actually harvested
for a 40°C constant temperature network in the winter (top) and the summer (bottom)

5.1.2 Piping

High-density polyethylene (HDPE) 3408 grade P34 piping was chosen as the micro-thermal network piping due to its tough nature and typical use in large pipelines. HDPE has a maximum allowable temperature of 82°C making it suitable for the full range of thermal network temperatures explored [52]. The insulation and pipe properties used in the model are listed in Table 5.2. The EMC piping, outlined in Section 3.5, was modeled as steel due to the hotter temperatures of the EMC loop and the pipes were modeled with no thermal losses.

Table 5.2: Piping parameters required as inputs in Dymola

Pipe - HDPE		Pipe Insulation – Urethane Foam	
Pipe Roughness [m]	Density [kg/m^3]	Thermal Conductivity [W/mK]	Thickness [m]
1.5e-6[a]	960[b]	0.022[c]	0.051[b]

[a] Handbook of Polyethylene Pipe, Chapter 6: Design of PE Piping Systems [86]

[b] 2017 AHRAE Handbook – Fundamentals, Chapters 22 and 23 [52]

[c] 2020 AHRAE Handbook – HVAC Systems and Equipment, Chapter 12: District Heating and Cooling [87]

The micro-thermal network pipes are buried at 1.7 m, which is the average depth obtained from the district heating and cooling system in downtown Hamilton, ON. Each pipe length in the model is 150 m, totaling 900 m for the entirety of the network. The outdoor ambient air temperature for the year 2017 was retrieved from the McMaster weather station due to close proximity to the site modeled. Data with a 15 minute time resolution was used as an input to the model. The thermal diffusivity of the soil, for input to the ground temperature model, is based on the work from Judd et al. [88] and is 6.967x10^{-7} m^2/s.

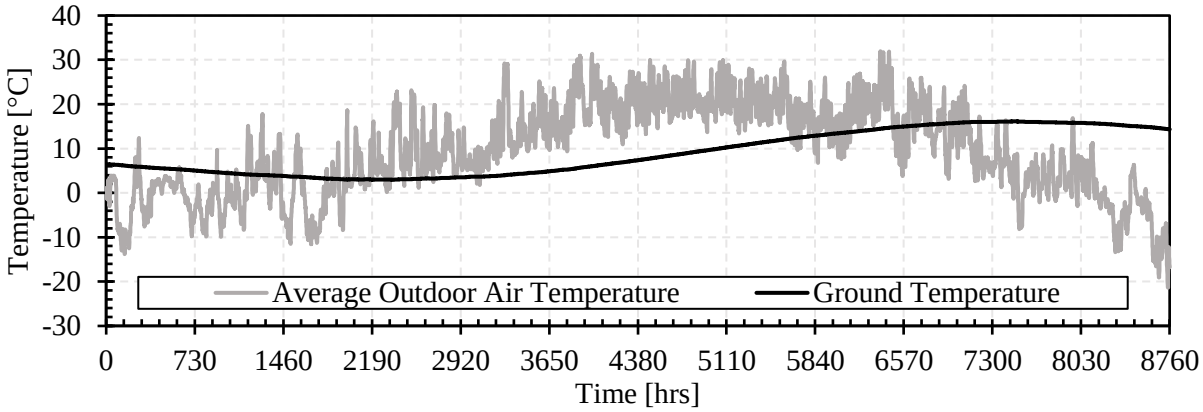

Figure 5.5: Average outdoor air temperature and ground temperature at 1.7 m below the surface for the year 2017

5.1.3 Equipment Sizing and Parameter Selection

Three different CHP sizes are explored. Table 5.3 outlines the thermal and electrical output for each CHP size, along with the mass of the cooling fluid required. The CHP was modeled without part loading capabilities; therefore, the CHP operates at full capacity when it is running.

Table 5.3: CHP thermal and electrical power output

CHP Electrical Capacity [kW_e]	CHP Thermal Capacity [kW_{th}]	Mass [kg]
750	900	38.5
1,000	1,200	50.5
1,250	1,500	62.5

The boiler is sized at 3 MW for the 1,200 and 1,500 kW_{th} CHP scenarios. A size of 3.5 MW was required with the 900 kW_{th} CHP in order to meet the peak heating load of approximately 4.5 MW. The heat exchangers used in the system were set to have a nominal effectiveness of 0.7, no specific size was set.

In development of the system model, all components were modeled with minimal thermal mass. Within each component, the thermal mass or time delay was set to a value that resulted in a negligible quantity of thermal mass without causing system instabilities. Having very little thermal mass in the model components allowed for easy identification of all heat flows throughout the system. All components in the EMC, with the exception of the CHP and piping, have very small mass that totals to less than 2 to 10% of the network mass for each scenario. Therefore, the mass of the EMC was not incorporated in the response time calculations.

The EMC short-term thermal storage tank is sized at 1,000 m^3 in the majority of cases. Sizing for the short-term storage at the ETSs, utilized during the network temperature transitions, was determined for a response time of 30 and 60 minutes as described in Section 3.4.2 and listed in Table 5.4.

Table 5.4: ETS storage sizes for a response time of 30 and 60 minutes

Building	ETS Thermal Storage Size [m^3]	
	30 minute Response Time	60 minute Response Time
Arena	13	26
Library	15	30
Residential Tower	33	66
Senior Center	9	18
YMCA	33	33

The mass flowrate going into each ETS from the thermal network is calculated in real time based on the building heating and harvesting loads. Flowrates were obtained from a preliminary simulation and the maximum mass flowrates required for each component in the ETS was obtained. The maximum mass flowrate of the heat exchangers is constrained by the micro-thermal network flowrate due to the PI controller used. Therefore, the flowrate required for the heat pumps was used in determining the network flowrate. The maximum required flowrates for the heating HP and the harvesting HP can be seen in Table 5.5. The maximum overall flowrate required is 128.2 kg/s, for the peak heating demand of the residential building. Therefore, a flowrate of 140 kg/s was utilized in the response time equation as the flowrate for the network to ensure all buildings had sufficient flow.

Table 5.5: Heat pump maximum mass flowrates

Building	Mass Flowrate [kg/s]	
	Heating HP	Harvesting HP
Arena	14.5	46.0
Library	15.8	95.5
Residential Tower	128.2	44.8
Senior Center	10.4	29.9
YMCA	39.8	50.8

5.1.4 Emission Factor

The grid hourly average emission factor (AEF) was used to determine the emissions for all baseload electricity, building loads and chillers, and for off-peak electrical consumption.

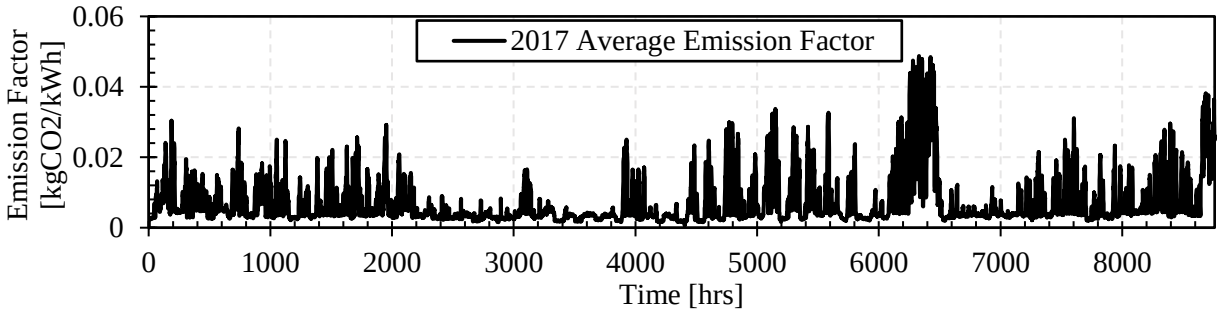

Figure 5.6: Average hourly emission factor for the year 2017 [54]

A calculated marginal emission factor (MEF) was used to determine the emissions for any additional electricity consumed on-peak outside of the baseload consumption. The baseload consumption is the existing electrical demands before the addition of the ICE-Harvest system. This consists of the building electrical demands and the electrical requirements for the building chiller. Any additional electricity consumed whether it is met by the CHP or on-peak grid electricity will have the marginal emission factor applied to account for the additional natural gas generation used to meet the new loads. The MEF is utilized because whether it is centrally or decentrally a natural gas generator will operate, the bonus with the ICE-Harvest system is that the heat is captured and delivered to buildings. The natural gas emission factor is from the RETScreen software developed by Natural Resources Canada [89] and was used in Equation 5.1 to calculate the MEF. An efficiency of 42% was used to represent the efficiency of grid level natural gas generators, providing a conservative estimate of the ICE-Harvest emissions.

$$MEF = \frac{NGEF}{Eff} = \frac{0.1794\ kgCO_{2e}/kWh}{42\%} = 0.4271\ kgCO_{2e}/kWh \tag{5.1}$$

The natural gas emission factor encompasses the emissions due to methane (CH_4) and nitrous oxide (N_2O). To determine the CO_2 equivalence value, a global warming potential of 28 tCO_2/tCH_4 was used for methane and a factor of 265 tCO_2/tN_2O was used for nitrous oxide [90]. Emissions from the non-energy uses of fuel, such as mining, transportation, and line losses, are not included in this analysis [91]. Updating the emission factor to include the life cycle emissions from natural gas production would not change the trends seen in the results, only the value of total emissions.

5.1.5 Assumptions

In all presented simulations, the pumping power requirements of the ETS pumps and the pump at the EMC are not considered in the analysis. The pump arrangements may not reflect the actual

implementation of the system and therefore do not provide an accurate representation of the electrical consumption required.

In the simulation conducted for the verification study, outlined in Section 3.6.2, all available rejected heat was harvested. The harvested heat that was not used to meet the building heating loads was then expelled through the network cooling tower. Since the rejected heat requires electricity to be harvested, it is not viable to use electricity, harvest heat, and ultimately remove it with the cooling tower. For the remainder of simulations in this thesis, the network cooling tower model was not considered. Heat was only harvested selectively when it was required or when there was means to store the additional harvested heat.

The pipe thickness is constant for the changing pipe diameters in all simulations. The change in thickness is minimal for the relatively small changes in diameter explored. Therefore, a thickness of 0.0104 m was used for all simulations and obtained from a HDPE piping manufacturer data sheet [84].

The operational temperature ranges chosen for the micro-thermal network simulations reach bounds that are outside the operational limitations for the heating HP model developed, described in Section 3.3.4.1. A heat pump that met all of the required temperature ranges was not found in commercially available heat pumps. Due to the wide range of temperatures explored in the simulations, two different heat pumps would be required to switch back and forth depending on the network temperature. Therefore, only one heating HP was modeled for computational efficiency. Depending on the temperature of the network, the resulting COP may not be representative of the temperature ranges utilized. Appendix B provides greater detail.

5.2 Reference Scenarios

For comparison, the yearly performance for two reference cases was calculated. The first case is the conventional scenario where the heating loads are met purely by a boiler at 90% efficiency, the cooling loads are met by chillers, and the electrical loads are met by the Ontario grid. In the second scenario, the building heating and cooling loads will be met with a ground source heat pump (GSHP). The electrical requirements for the GSHP are approximated by determining the COP using the heating, cooling, and refrigeration COP equations outlined in Section 3.3.4. The ground temperature at 1.7 m below the surface (seen in Figure 5.3) was used as the temperature of the fluid entering the source side of the heat pump and the fluid outlet temperature on the load side was the building set point temperature of 60°C for heating, 12°C for cooling, and -12°C for refrigeration. A GSHP case can be utilized in this scenario because the heating and cooling loads are balanced and will not cause a change in ground temperature over time. The results of the reference scenarios are presented in the following sections with comparison to the simulated cases.

5.3 Constant Temperature Simulations

The system was simulated by maintaining a constant micro-thermal network temperature year round to assess the performance of the thermal network with different temperature set points. In the simulations, a constant temperature network EMC model was used along with the selective harvesting network model. With the selective harvesting model, heat is harvested only when required based on the MTN temperature. The simulations were run with a one hour time step. The parameters of the thermal network were held constant for all simulations and are outlined in Table 5.6. The results of the constant temperature simulations are then compared to the reference scenarios described in Section 5.2.

Table 5.6: Simulation parameters for the constant temperature network

Diameter [m]	Length [m]	Mass Flowrate [kg/s]	CHP Size [kW_{th}]	Boiler Size [kW]	EMC Storage [m^3]
0.285	900	140	1,500	3,000	1,000

A breakdown of how the building heating loads are met for each case is displayed in Figure 5.7. For the constant temperature network cases, the heating loads are provided by multiple sources. From the EMC, the heating load can be met by the CHP and/or the boiler. Heat generated by the CHP is separated into heat provided instantaneously and heat that was stored and later provided by the EMC storage. The harvested energy is a summation of the rejected heat from the building chiller and the electricity consumption of the harvesting HP. Heat provided by the heating HP is determined based on the electricity consumption of the heating HP.

The 20°C network temperature simulation is similar to a 5GDHC network and the 70°C network is close to a 4GDH network. The downside of the ultra-low, 20°C, temperature distribution is that the heating HP is required to operate regardless of an on-peak or off-peak period in order to meet the building heating demands, consuming a large amount of on-peak electricity. Comparatively, the 70°C network heating HPs consume no electricity for heating since the heating demand can be met through direct heat exchange. The 70°C network, therefore, has the largest boiler utilization because direct heat exchange pulls more heat from the network as there is no electrical consumption from the HPs providing heat to the buildings. The boiler then supplies greater amounts of heat to the network to account for the larger amount of heat removed. As the temperature of the network increases from 20 to 70°C, the trend is apparent, reduced heating HP use causes an increase in boiler utilization. The quantity of heat harvested also increases with temperature of the network due to the increase in power consumption of the harvesting HPs. At higher network temperatures more power is required to lift the building chiller rejection

temperature to the temperature of the thermal network. Additional power required is added to the quantity of rejected heat which increases the amount of harvested heat. The rejected heat from the building chillers is constant throughout all cases.

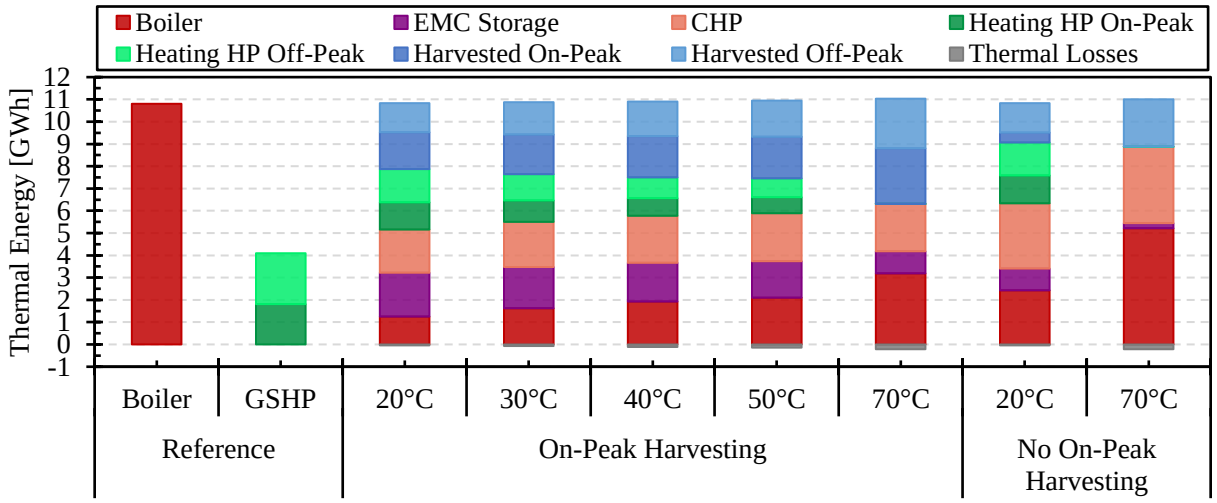

Figure 5.7: Annual thermal energy requirements for constant temperature thermal networks

Within the constant temperature simulations, two scenarios were explored. The first scenario harvests rejected heat throughout the year regardless of on-peak and off-peak times and the second only harvests heat off-peak. When heat is harvested on-peak, more on-peak electricity is consumed from the harvesting HPs. To compare the energy required from the generating equipment in the two scenarios, two temperatures were run without harvesting rejected energy during on-peak periods to decrease on-peak electrical consumption, labeled *No On-peak Harvesting*. For the No On-Peak Harvesting (NOPH) cases, the boiler consumption increases to compensate for the heat that is no longer being harvested. In the 20°C NOPH case, a small portion of heat is still harvested on-peak, in the dark blue. Electricity is not consumed to harvest this heat as there is a direct heat exchange option at the harvesting ETS. With the low temperature network, heat can still be harvested on-peak through direct heat exchange with no electrical consumption.

The temperature of the thermal network after each building and the supply and return to the EMC are plotted in Figure 5.8. The network has a floating temperature, therefore when heat is harvested the temperature can reach above the set point and when a building removes heat the temperature can drop below the set point. The 20°C network is displayed for both scenarios of harvesting on-peak and not harvesting on-peak. In the bottom plot, an overall lower temperature is seen throughout the network due to the reduction in heat harvested. The temperature leaving the residential building's ETS is the lowest since it is the last building on the network and has the highest heating loads. When there is harvesting on-peak, the temperature of the network is seen to frequently increase after the library due to it's large cooling load in the winter months.

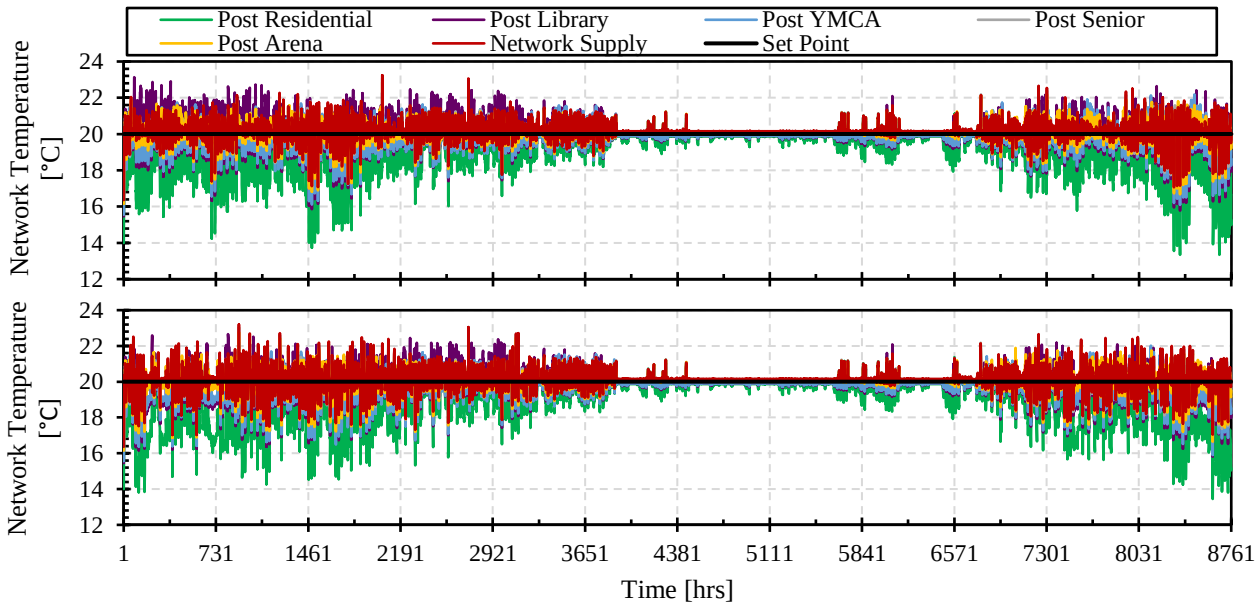

Figure 5.8: Temperature profiles at different locations across the micro-thermal network
for a set point of 20°C, the top plot includes on-peak harvesting and the bottom plot harvests heat off-peak only

The trends discussed for the thermal energy are also apparent in the electrical energy breakdown in Figure 5.9. As the network temperature increases, less electricity is consumed by the heating HPs and electricity consumed by the harvesting HPs increases. In the NOPH cases, the electricity from the harvesting HPs is reduced by 57 and 55% compared to the on-peak harvesting values for

the 20 and 70°C networks, respectively. All constant temperature network cases consume greater amounts of electricity compared to the traditional boiler scenario and less electricity than the GSHP. The source of electricity is also shown in Figure 5.9. In the constant temperature network scenarios, there is the use of the CHP. The *CHP Electricity* category is the CHP electricity that is used instantaneously to meet the electrical demand. If the CHP electricity produced is greater than the demand it is considered *Additional CHP Electricity*. The additional CHP electricity can be stored, exported to the grid, shared with the surrounding community, or an advanced control system can operate equipment to ensure that all CHP electricity produced is consumed on-site.

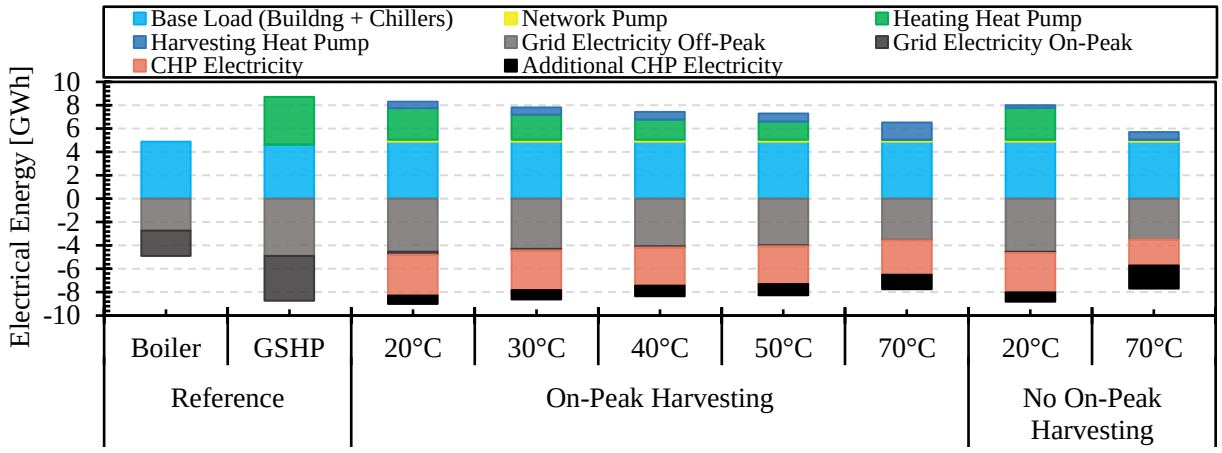

Figure 5.9: Electrical energy consumption by individual equipment in positive y-axis and electrical energy generation in the negative y-axis

Unrecovered thermal energy for the different cases is presented in Figure 5.10. Greater quantities of rejected heat are utilized with an increase in network temperature. As the network temperature increases less heating HP power is required and more heat is being pulled from the MTN. With the increased removal of heat from the MTN there is additional opportunity to harvest rejected heat. With the increase in network temperature it is also apparent that the unrecovered CHP heat increases. At lower MTN temperatures, the temperature difference between the EMC storage and the network is greater than at high MTN temperatures. The larger temperature difference allows

for greater EMC storage utilization during off-peak periods. When the EMC storage discharges off-peak, the quantity of additional CHP heat that can be stored during on-peak periods increases. If there is not an opportunity to charge the EMC storage on-peak the CHP heat is unrecovered.

The constant temperature networks do not see a drastic decrease in the amount of unrecovered thermal energy compared to the reference scenarios. If there was the inclusion of long-term seasonal storage, the unrecovered heat would decrease significantly.

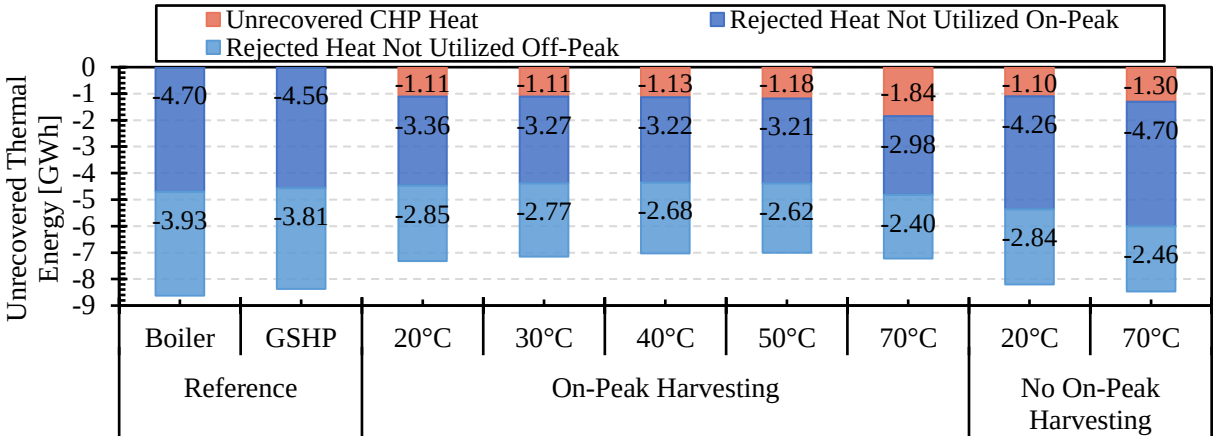

Figure 5.10: Unrecovered thermal energy for constant temperature networks

GHG emissions across all constant temperature simulations are approximately equal and demonstrate emissions reductions compared to the conventional boiler scenario. The emissions for all cases are outlined in Figure 5.11. The 70°C network shows the least reduction in GHG emissions compared to the conventional boiler case because of the additional boiler use. When no heat is harvested on-peak, the emissions of the system increase and the gap in emissions between the 20°C and 70°C scenarios decrease. In the 20°C cases, there is greater EMC storage utilization due to the larger temperature difference between the MTN and the CHP heat. Since the CHP heat, instantaneously and through the EMC storage, has been utilized as much as possible, when there is NOPH the boiler compensates for the lack of harvested energy. This is also demonstrated in Figure 5.10, the unrecovered CHP heat does not significantly change from the harvesting to NOPH

case. In the 70°C cases the EMC storage is not able be utilized to the extent of the 20°C case because of the smaller temperature difference between the MTN and the CHP heat. Therefore, when NOPH was simulated with the 70°C network, there was previously unrecovered CHP heat that was able to make up for the heat not harvested. The unrecovered CHP heat in the 70°C NOPH case decreased 29%. Due to the greater boiler utilization to make up for the reduction in harvested heat, in the 20°C NOPH case the emissions reductions decreased by 5%. Whereas in the 70°C NOPH case, since the CHP was able to compensate for a larger portion of the reduction in harvested heat, the emissions reductions only decreased by 3% compared to harvesting on-peak.

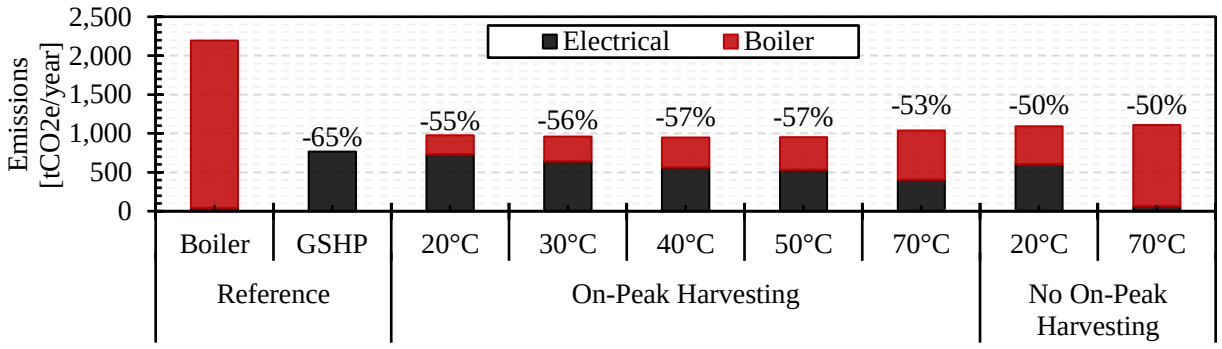

Figure 5.11: GHG emissions and percentage emissions reduction from the boiler case for a constant temperature network

The benefits of the CHP and on-site electrical generation can be seen when looking at the electrical demands of the system. Figure 5.12 displays the electrical demands of all cases with and without the incorporation of a CHP. The GSHP case has the largest demand on-peak, almost double the conventional boiler case. With the GSHP, there is no CHP available to offset the demand, therefore the grid is responsible to meet the entirety. In the constant temperature network cases, the on-peak demand is relatively large but with the CHP, the grid only has to meet a fraction of the demand. All constant temperature cases have a reduced on-peak demand compared to the conventional boiler case. When there is no heat harvested on-peak, the 70°C case requires minimal electricity from the grid on-peak at 5 kW. With the CHP there is also electricity that is not used on-site, the

use of this electricity can be explored for export to the grid, use by the surrounding community, or to be stored on-site with battery storage.

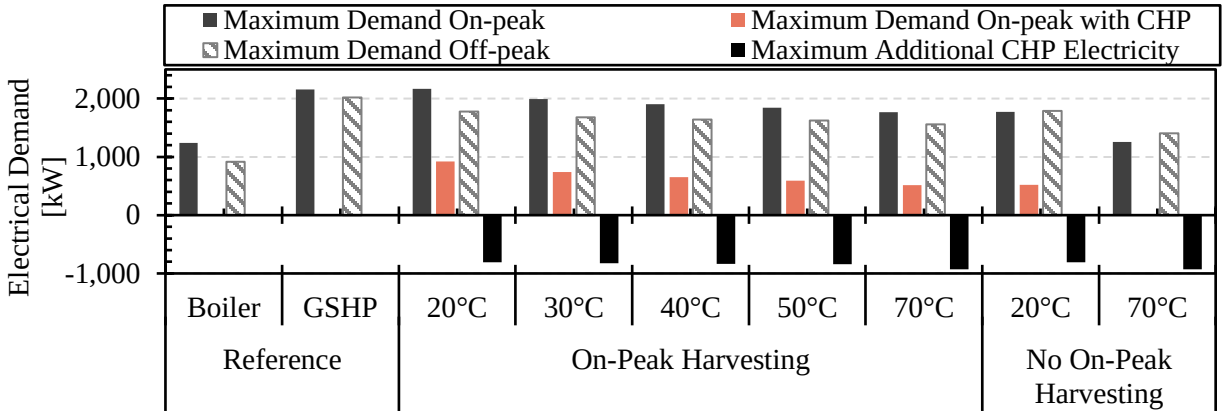

Figure 5.12: System maximum electrical demands for constant temperature networks

The combination of the low temperature off-peak and high temperature on-peak behaviour would result in the best of both cases.

5.3.1 Summary

In the low temperature networks, which closely resemble 5GDHC systems, electricity from the heating HPs is required throughout the year to provide heat to the buildings. This consumes electricity during on-peak periods. But in the low temperature network, there is less energy required from the boiler and the storage utilization increases. The emissions for the 20°C case are greater than the emissions for the 30, 40, and 50°C networks. Although the boiler required increases as the temperature of the network increases, the large electricity requirement from the heating HPs on-peak for the 20°C network generates the greatest electricity emissions. Emissions for the lower temperature cases are still close in value, providing a 55 to 57% reduction in emissions from the boiler scenario.

The hot temperature network at 70°C, similar to a 4GDH system, uses direct heat exchange to provide heat to the buildings, therefore, no electricity was required from the heating HPs. To

maintain the hot temperature all year, the boiler was required to meet the majority of the load as the storage utilization decreased. A summary of how the heating load is met is outlined in Table 5.7. The 70°C network had the greatest emissions when heat was harvested on-peak, but still created a 53% reduction in emission compared to the boiler scenario.

Table 5.7: Contribution to meeting the heating demand

	Boiler	EMC Storage	CHP	Heating HP	Harvesting
20°C	12%	18%	18%	25%	27%
70°C	29%	9%	19%	0%	43%

When heat is not harvested on-peak, the 20 and 70°C produce nearly identical emissions. Both cases provided a 50% reduction in emissions compared to the boiler scenario. The emissions increased due to the greater boiler utilization to compensate for the heat that was not harvested during peak periods.

5.4 Variable Temperature Simulations

The ICE-Harvest system was simulated with a variable temperature micro-thermal network, where the temperature difference from cool to hot ranges from 20 to 50°C. A variable temperature network was investigated to provide demand response to the electrical grid and to reduce GHG emissions compared to full boiler operation and a constant temperature network.

The range of temperature differences was tested with different sizes of CHP to analyze the operational behavior for the system. Along with various CHP sizes, different modes of operation and control strategies were used to change the temperature of the thermal network and the results are presented and analyzed. All changing temperature simulations in the following sections were run with a ten-minute time step in order for Dymola to capture the change in network temperature. The ten-minute data was then averaged hourly for analysis purposes.

5.4.1 Using ETS Thermal Storage

5.4.1.1 Simulation Set Up

To change the temperature of the thermal network, the CHP will be used as the only heat source. The state of charge of the EMC storage at a given time of the year is difficult to quantify and boiler use is undesirable due to increased GHG emissions. The response time is therefore calculated with the thermal power of the CHP and desired temperature difference of the network; it will represent the maximum time it will take for the network to change temperature as occasionally there will be thermal storage to assist the transition depending on the state of charge.

Different temperature differences were explored. For each temperature difference and CHP size, a constant mass flowrate of 140 kg/s was used and the diameter of the network pipes was adjusted in order to obtain a thermal mass where the response time of network was 15, 30, and 60 minutes. The viability of the scenario was determined by the resulting pumping power. If the pumping power was less than 10% of the CHPs electrical output than the simulation was deemed viable, anything over 12% was not simulated, and between 10 and 12% was simulated to analyze and compare the results. Figure 5.13 displays the corresponding pumping power for each temperature difference, response time, and CHP thermal output. The simulations conducted are identified with a green or yellow marker, corresponding to the colour coding in Table 5.8. Figure 5.13 only displays the range of pumping power that was in a permissible range to highlight the viable simulations. No 15 minute response time simulations made it into the plot as the pumping power required was too large. The parameters for the conducted simulations are outlined in Table 5.9, including the pipe design values, velocity, and pressure drop.

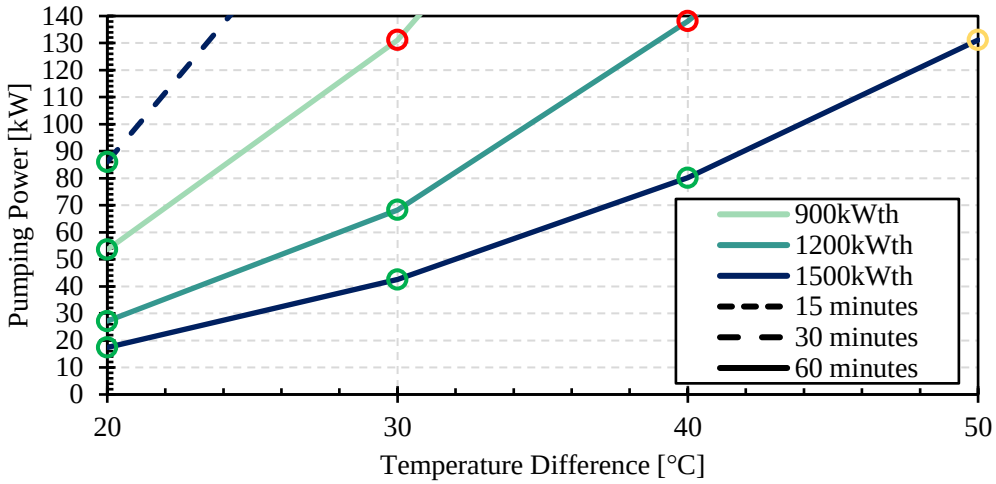

Figure 5.13: Network temperature difference and resulting pumping power

Table 5.8: Range of acceptable pumping power

	Range		
$\frac{Pumping\ Power}{CHP\ Electrical\ Output} x100\%$	< 10%	≥10% and ≤12%	>12%

Table 5.9: Thermal network parameters for final simulation cases

Scenario		Pipe Diameter [m]	Thermal Mass [kg]	Pumping Power [kW]	Velocity [m/s]	Pressure Drop [Pa/m]
CHP Size [kW_{th}]	Network Temperature Difference					
900	50-70°C	0.226	36,031	54	3.50	325
1,200	50-70°C	0.26	47,688	27	2.64	165
	40-70°C	0.215	32,609	68	3.86	420
1,500	50-70°C	0.285	57,300	17	2.20	105
	50-70°C (30 mins)	0.205	29,646	86	4.25	530
	40-70°C	0.237	39,624	43	3.18	255
	30-70°C	0.208	30,520	80	4.13	495
	20-70°C	0.187	24,669	135	5.12	835

In total, 8 simulations were conducted. For these simulations, the pre-heating and boiler delay EMC model was used along with the selective harvesting network model. The boiler delay ensures that the boiler is not operating during the temperature transitions. The pre-heating takes advantage of rejected heat available and carbon free electricity to assist in the MTN temperature transition. Only one 30-minute response time case was deemed viable and the remaining cases have a 60 minute response time. For the 900 kW_{th} CHP scenario, a 3.5 MW boiler was required in order to meet peak demand, in all other cases a 3 MW boiler was used.

5.4.1.2 Yearly Results

The results of the simulations are compared with the reference scenarios of using a conventional boiler for heating and a GSHP for both heating and cooling. Figure 5.14 summarizes the thermal energy supply of the cases. The building heating demands can be met by the EMC storage, CHP, boiler, heating HP, or harvested energy. The *EMC storage* represents heat that was charged with additional CHP heat and was utilized off-peak. *CHP* is the portion of the CHP heat that is used instantaneously. In all scenarios, heat was harvested on-peak. The overall trend of how the heating load is met across the various temperature differences does not see a large change. With an increase in CHP thermal output, the amount of boiler utilization decreases and the amount of EMC storage increases. The heating HP power increased in the 20-70°C case because of the lower temperature off-peak. The thermal losses increased when higher temperatures were simulated and in cases with larger thermal masses.

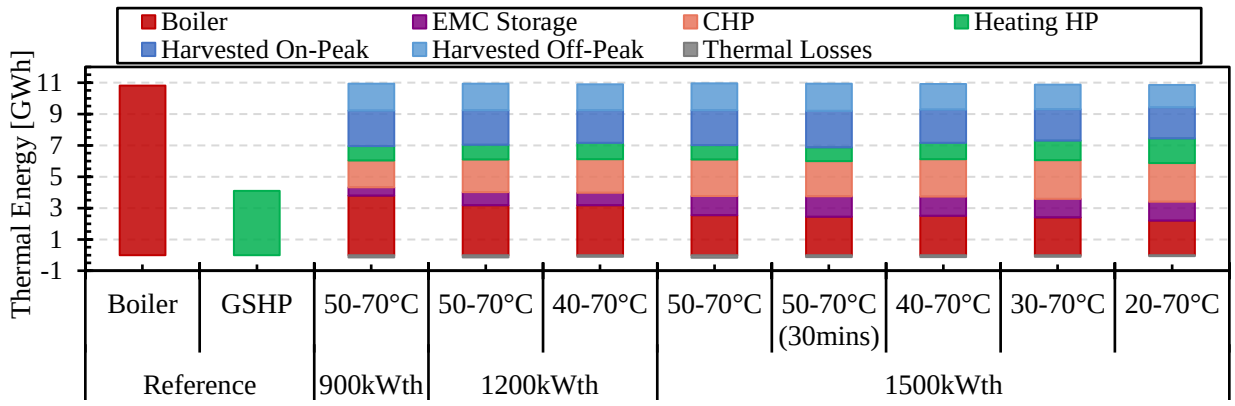

Figure 5.14: Changing temperature network thermal energy distribution

The behaviour of the equipment in the EMC throughout the year is displayed in Figure 5.15. There is large boiler utilization in the winter months and no boiler is needed in the summer. The light purple indicates the EMC storage is being charged with heat from the CHP that is not used instantaneously. The heat from the CHP in the summer months is unrecovered as there is only a small heating demand and the EMC storage is not sized large enough to store all of the heat.

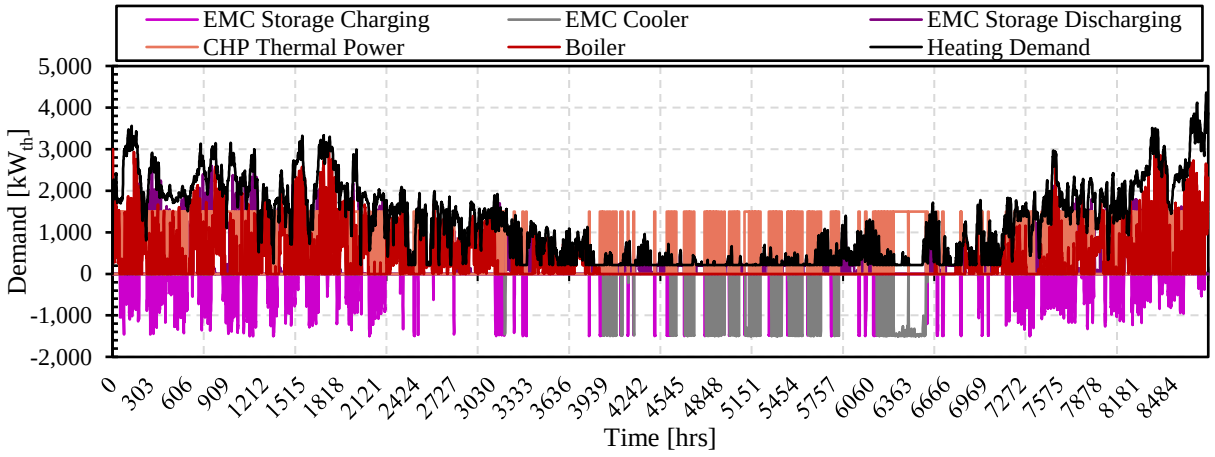

Figure 5.15: EMC equipment operation for a 50-70°C network with a 1,500 kW_{th} CHP

The smaller CHP sizes have less unrecovered heat compared to the larger CHPs, presented in Figure 5.16. The unrecovered heat is fairly constant across CHP sizes with the same temperature differences. In the conventional boiler and GSHP scenarios, no heat is recovered from the building chillers.

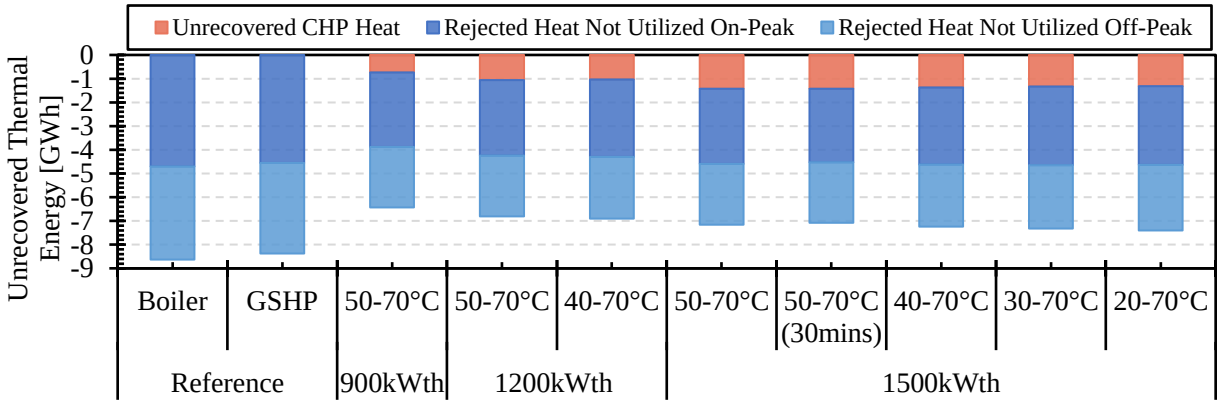

Figure 5.16: Unrecovered thermal energy for changing temperature network simulations

Relative importance of pumping consumptions (RIE_{pump}) is defined as the ratio between the electricity consumption for pumping and the heat delivered to the substations or ETSs, as found in literature. Due to the ETSs also providing heat to the buildings and the incorporation of energy harvesting, two ratios were calculated, one with the heat delivered just from the EMC ($RIE_{pump_{EMC}}$) and the other with the EMC, heating heat pumps, and harvesting (RIE_{pump}). The

same ratio was calculated for the thermal losses. In Table 5.10, the cells in green represent ratios less than 3% and are within permissible limits based on values reported in literature. The ratios highlighted in yellow are between 3 and 6%, representing pumping energy that is reaching a large percentage of the total heating energy but may still be viable for implementation. Ratios in red are greater than 6% and would require additional justification to be implemented. All thermal loss ratios are less than 3% and do not pose concern.

Table 5.10: Pumping power and thermal loss percentage of heat delivered

	900 kW_{th}	1,200 kW_{th}		1,500 kW_{th}				
	50-70°C	50-70°C	40-70°C	50-70°C	50-70°C (30mins)	40-70°C	30-70°C	20-70°C
RIE_{pump}	4.20%	2.13%	5.37%	1.36%	6.74%	3.34%	6.3%	10.3%
$RIE_{pump_{EMC}}$	7.61%	3.82%	9.55%	2.45%	12.3%	5.96%	11.3%	19.1%
$RIE_{thermal}$	1.31%	1.47%	1.11%	1.60%	1.21%	1.21%	0.94%	0.73%
$RIE_{thermal_{All}}$	2.37%	2.65%	1.97%	2.87%	2.20%	2.15%	1.68%	1.35%

The pumping requirements with respect to the total electrical consumption of the system are displayed in Figure 5.17. There is varying pumping energy for all cases, the largest being for the 20-70°C network temperature change. Heating heat pump electricity is all used off-peak because of the hot network temperature direct heat exchange is now used on-peak.

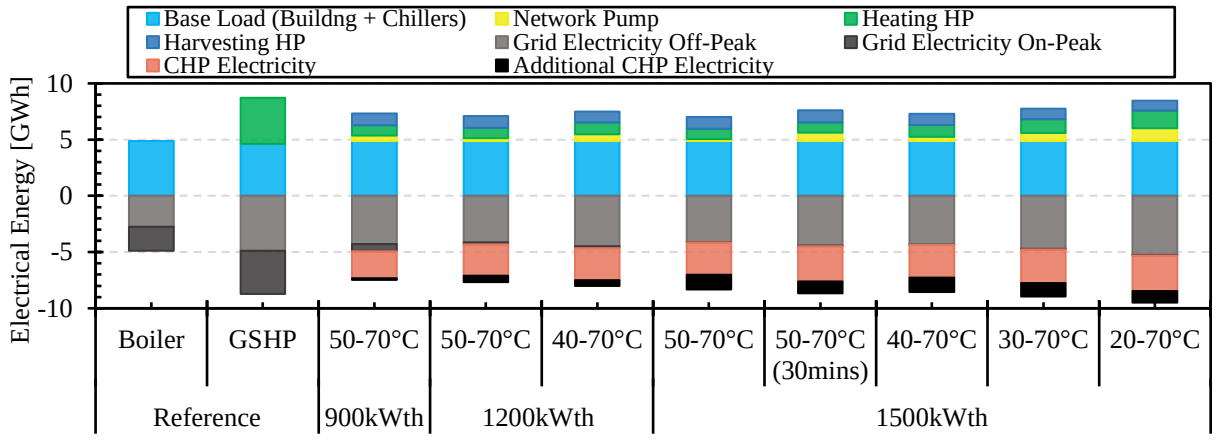

Figure 5.17: Electrical consumption and generation for changing temperature network simulations

Emissions for the changing temperature micro-thermal networks all show reduction from traditional boiler case. All changing temperature simulations, with a 60 minute response time and 1,500 kW_{th} CHP, show a larger GHG emissions reduction compared to the constant temperature cases. The emissions for the 50-70°C and 40-70°C scenarios with a 1,500 kW_{th} CHP are comparable to the GSHP scenario.

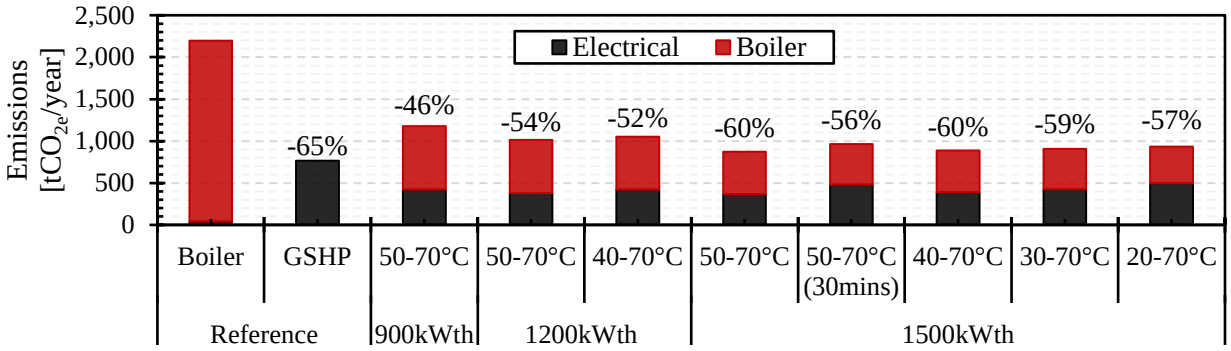

Figure 5.18: GHG emissions for changing temperature micro-thermal network scenarios

Due to the charging of the ETS storage during off-peak periods, the off-peak electrical demand has increased in the changing temperature cases. The production of off-peak demand allows for the utilization of carbon free electricity generation sources and avoids curtailment. With the larger CHP sizes, the electrical demand the grid is required to meet on-peak is lower than with the smaller CHPs, but all changing temperature cases reduce the on-peak demand compared to the boiler and GSHP scenario.

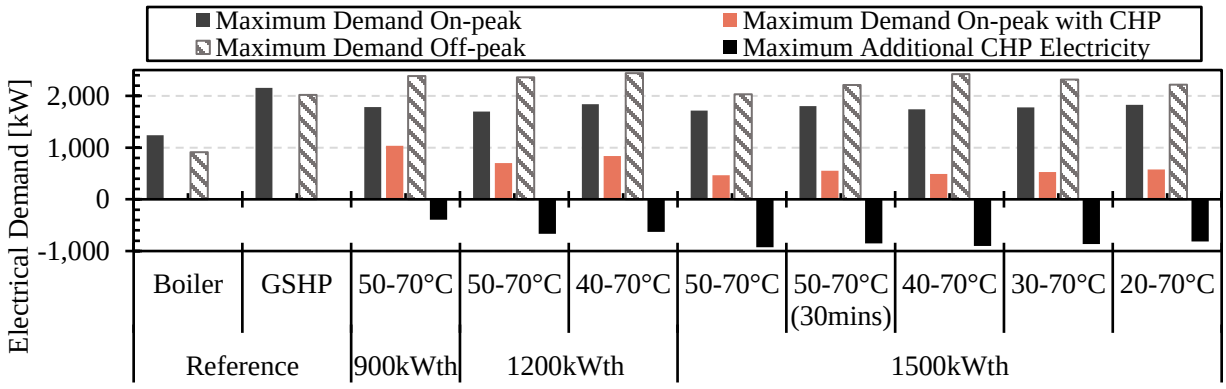

Figure 5.19: Electrical demands for changing temperature thermal network

5.4.1.3 Hourly Load Profiles

For a week at the end of September and the beginning of October, where the hottest outdoor temperatures of the year occurred, the performance of the systems are plotted. Figure 5.20 compares the operational differences between the 50-70°C case and the 20-70°C case. The electrical peak on September 26th is the largest of the year as temperatures reached 32°C. Electrical requirements for building chillers increased due to the large cooling load, therefore, grid electricity on-peak is required.

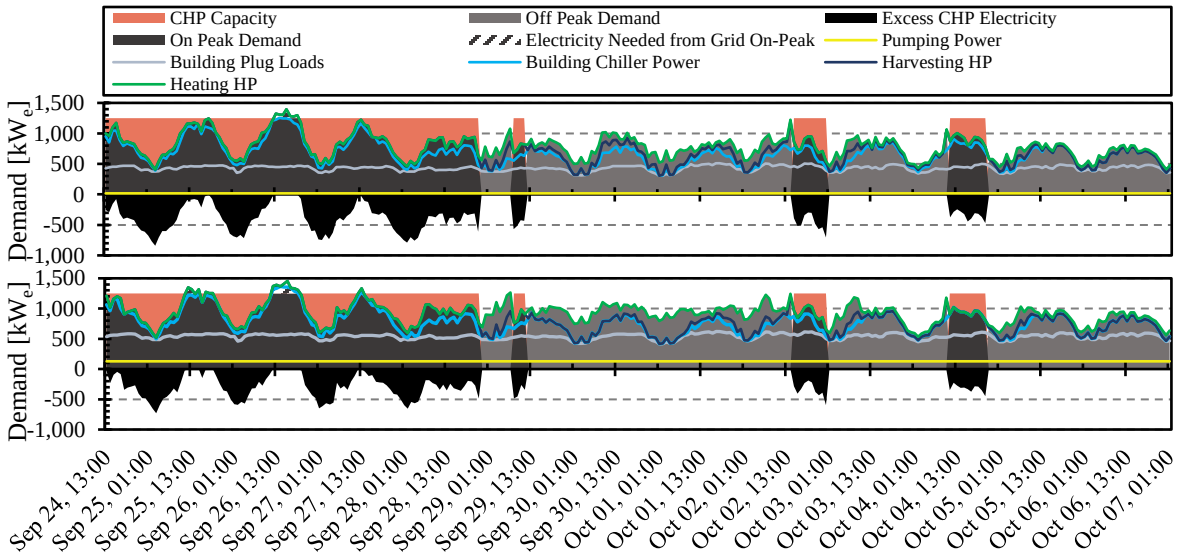

Figure 5.20: Hourly electricity profiles for a 20 and 50°C network temperature difference. The 50-70°C case is displayed in the top plot and the 20-70°C case on the bottom.

The electrical loads are greater for the 20-70°C case (50°C temperature difference) in comparison to the 50-70°C case (20°C temperature difference). During on-peak periods it is due to the larger pumping power requirements and off-peak from the increase in heating HP power. The increase in heating HP power is much greater than the decrease in the harvesting HP power. Although the outdoor air temperature is hot, the heating HP still operates because of the domestic hot water load the buildings experience. Harvesting HP spikes occur before the CHP turns on, this is the pre-heating of the network. Heat is harvested to increase the temperature as much as possible to

improve the response time of the network. During the summer months when rejected heat is abundant, the temperature of the network can reach the hot set point before the CHP comes on.

Due to the large temperature difference between the network temperature off-peak and the temperature of the ETS storage (80°C), the utilization of storage is much greater in the 20-70°C case. In Figure 5.21, during the off-peak stretch from Sept. 29th to Oct. 2nd zero boiler is required, whereas in the 50-70°C case the boiler is required because the temperature of the EMC loop has come within 5°C of the thermal network temperature and can no longer utilize the EMC thermal storage. The highlighted area on October 3rd at 1pm, where nothing seems to be meeting the heating load, is the time it takes for the network temperature to reduce to the cool temperature and only a small amount of heating HP power is required.

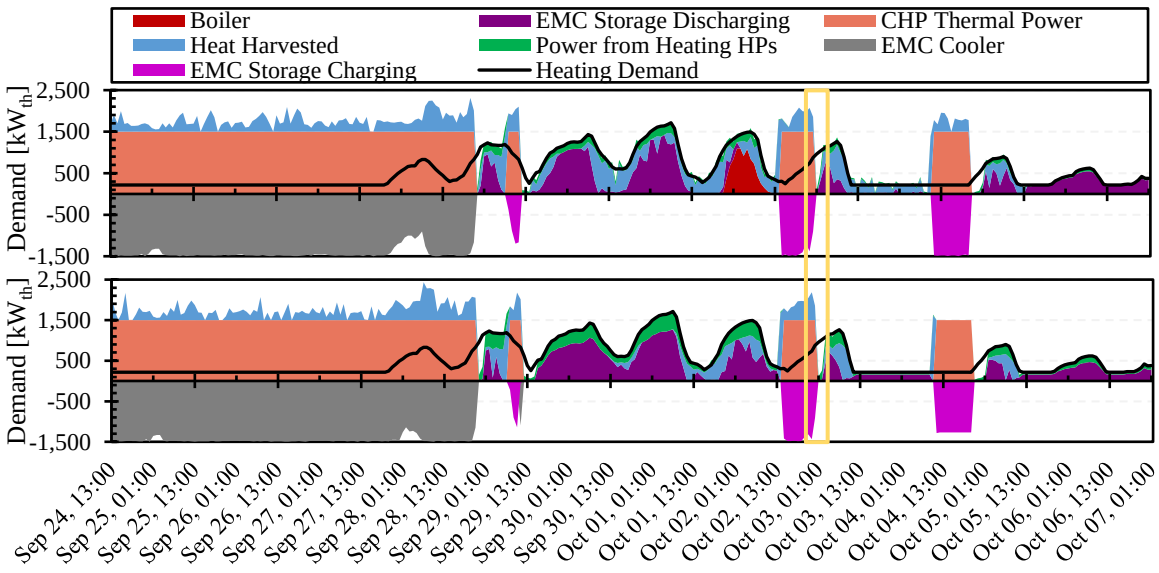

Figure 5.21: Hourly thermal system behaviour for a 20 and 50°C network temperature difference. The 50-70°C case is displayed in the top plot and the 20-70°C case on the bottom.

The temperature profiles in Figure 5.22, display the large temperature difference between the storage and the network. Therefore, the storage is used the entirety of the off-peak period. During off-peak periods the bottom of the storage tank is approximately equal to the EMC return

temperature. The storage is discharging and meeting a portion of the heating load, until the EMC return temperature is greater than the bottom of the storage tank and the boiler is used to meet the heating load.

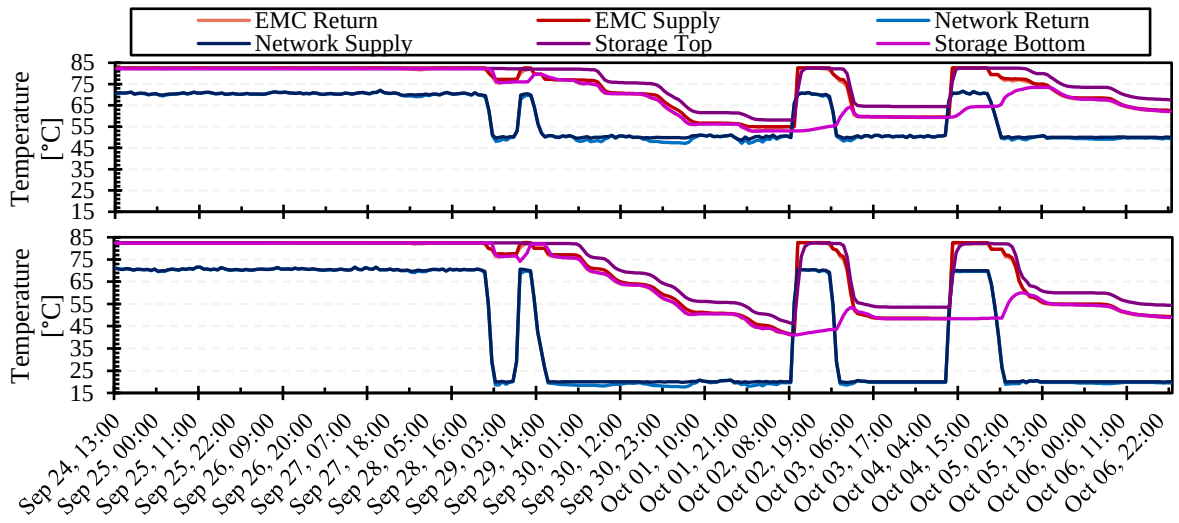

Figure 5.22: Temperature profile for a 20 and 50°C network temperature difference

5.4.1.4 Summary

The changing temperature network outperformed the constant temperature networks and the traditional boiler system in terms of demand response and GHG emissions, demonstrating the viability of the changing temperature. The changing temperature network incorporates the behaviour from the low temperature networks in off-peak periods, utilizing heating HPs to consume carbon free electricity. In on-peak periods the hot network temperature is used to eliminate the use of heating HPs so no additional load is added to the grid. The simulations conducted excluded seasonal/long-term thermal storage and optimization (discussed in Section 6.2), with the inclusion of those, the performance is expected to surpass that of the GSHP for GHG emissions.

With a constant yearly mass flowrate, the 40 and 50°C temperature differences were not feasible. The design of the micro-thermal network, to achieve the 60 minute response time, required a

decrease in pipe diameter which caused a large pumping power requirement. The 0.098m decrease in network diameter from the 20 to 50°C temperature difference resulted in an increase in pumping power of 973 MWh. Although the diameter decreased by a factor of 1.5, the pumping power increased by a factor of 7.5. Out of the 973 MWh, 372 MWh of electricity was consumed on-peak, translating to an additional 159 tCO_{2e} emitted. Therefore, due to the excess pumping electricity, the large network temperature differences are not suitable for a constant yearly mass flowrate.

A simulation with the response time of 30 minutes was explored, no large overall difference was seen between the 60 minute case. The ETS storage was sized appropriately in both cases so no heating HP electricity was used on-peak. The 30 minute response time required a reduction in thermal mass of the network demonstrating the same problems encountered with the large temperature differences; large pumping requirements.

5.4.2 Comparing ETS Thermal Storage to the Boiler

Due to the large pumping power requirements in the Section 5.4.1 results, a different control strategy was explored. Previously, the boiler was not used for the network temperature transition, but in the following cases it is primarily used in order to increase the thermal power available for changing the temperature of the network. An increase in the thermal power allows for the network to contain greater quantities of thermal mass, resulting in larger pipe diameters and less pumping power. In the boiler simulations, the pre-heating EMC model and the selective harvesting network model was used. Since the boiler in now used for the temperature transition, it does not need to be delayed when the CHP initially turns on. Before temperature transitions, heat is harvested to pre-heat the network as much as possible to alleviate the boiler load and the remainder of the time it is only harvested when additional heat is required on the MTN. The ETS storage cases were

previously outlined in Section 5.4.1. The pipe diameters used in the simulations discussed in this section are listed in Table 5.11.

Table 5.11: Pipe diameters used in the decentralized storage and boiler simulations

Scenario		Pipe Diameter [m]
Control Strategy	Network Temperature Difference	
ETS Storage	50-70°C	0.285
	20-70°C	0.187
Boiler	50-70°C	0.285
	20-70°C	0.285

For the 50-70°C network, in the boiler case the overall boiler utilization decreases. Thermal energy requirements are outlined in Table 5.12. When looking further into the on and off-peak boiler use, the on-peak boiler increases because it is used to increase the temperature of the network and meet the heating loads of the buildings during the temperature transition, but the off-peak use decreases. The decrease in boiler use off-peak demonstrates that when charging the ETS thermal storage tanks off-peak, a portion of that heat is coming from the boiler. The trend in the on and off-peak periods is also seen in the 20-70°C case, but the increase in boiler use on-peak outweighs the decrease off-peak and leads to an overall increase in boiler use. The large boiler increase on-peak comes from the increase in thermal mass of the network, compared to the ETS storage case, in order to decrease the pumping power. That additional mass in the pipes requires an increase in boiler utilization to lift the temperature of the network. The thermal losses for the 20-70°C case also increase because of the increase in thermal mass/pipe diameter creating a larger heat transfer area. Heating HP electrical consumption decreases in both scenarios from not having to charge the ETS storage tanks.

Table 5.12: Thermal energy requirements to meet the heating demand

	Decentralized Storage [MWh]		Boiler [MWh]	
	50-70°C	20-70°C	50-70°C	20-70°C
Boiler	2,540	2,189	2,514	2,336
Boiler On-peak	447	517	522	879
Boiler Off-peak	2,094	1,673	1,992	1,458
CHP	2,327	2,479	2,309	2,503
EMC Storage	1,228	1,204	1,253	1,161
Heating HP	927	1,563	847	1,449
Heating HP On-Peak	0	0	12	40
Heating HP Off-Peak	927	1,563	835	1,409
Harvested Heat	3,932	3,426	4,025	3,396
Harvested On-peak	2,226	1,997	2,312	2,059
Harvested Off-peak	1,707	1,428	1,713	1,337
Thermal Losses	-175	-79	-175	-117

In the boiler case for the 50-70°C and the 20-70°C cases, there is the addition of on-peak electrical consumption of the heating HPs. Since the ETS storage tanks are not used, there is nothing to alleviate the heating load from the thermal network. Until the temperature of the network reaches the point of direct heat exchange, the heating HP is required to meet the building heating demands. In the 20-70°C boiler case, there is a large reduction in pumping power due to the increase in diameter of the pipes.

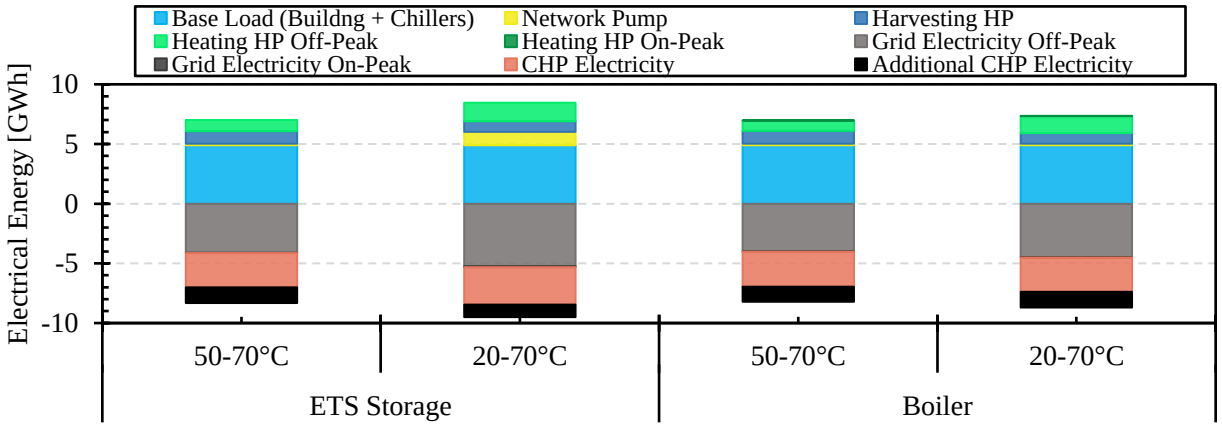

Figure 5.23: Electrical energy consumed by the system in the positive y-axis and electrical energy used to meet the demand in the negative y-axis

The total emissions are presented in Figure 5.24 for each case. Although the boiler utilization increased, the boiler scenario for the 20-70°C case has fewer total emissions due to the large reduction in on-peak electrical consumption from the pumping power decrease. The emissions decreased by 109 tCO_{2e} and reduced emissions by 62% compared to the conventional boiler scenario. The emissions for the boiler 50-70°C case increased by 11 tCO_{2e} due to the increase in on-peak electrical consumption from the heating heat pumps.

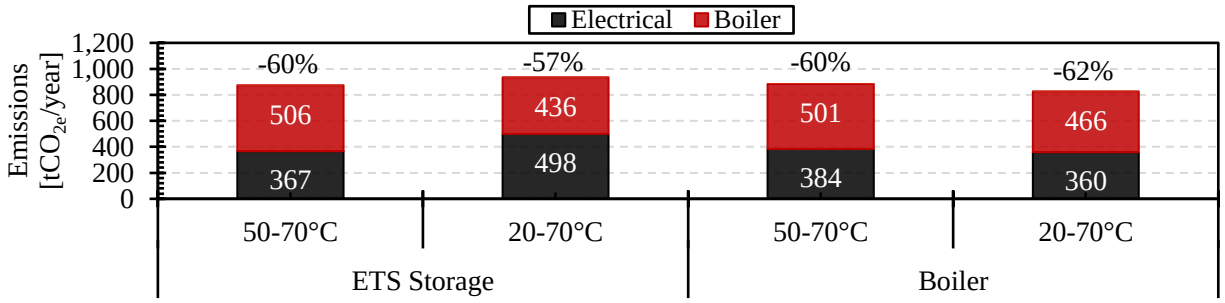

Figure 5.24: GHG emissions for each case with the values displayed and percentage reduction from the boiler scenario

The on-peak demand seen by the grid remains constant in the 50-70°C cases but the off-peak demand decreases. The boiler case does not experience as large of an off-peak electrical demand due to the elimination of charging the ETS storage. Therefore, the potential for reducing curtailed electricity is not as great in the boiler case. Due to the power decrease in the 20-70°C boiler scenario, the on-peak demand met by the grid decreased and the off-peak demand also decreased.

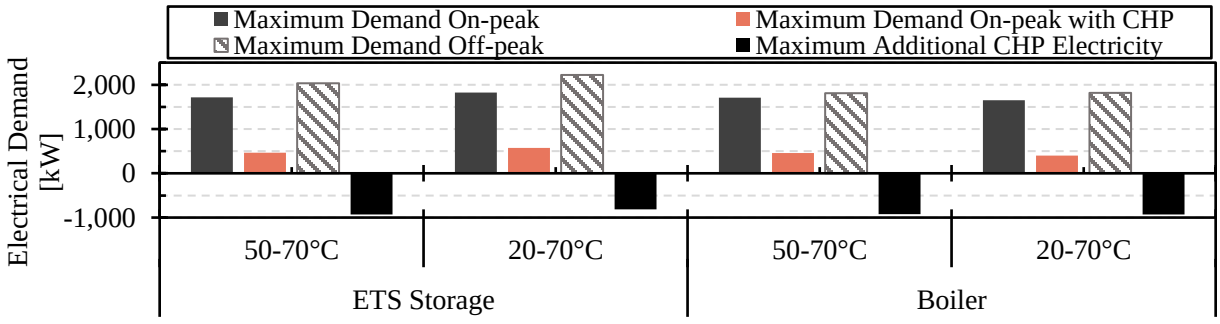

Figure 5.25: Electrical demands for the decentralized storage and boiler scenarios

5.4.2.1 Summary

The comparison to the boiler operational strategy to transition the temperature of the network demonstrated the promise of utilizing lower temperatures during off-peak periods. The 20-70°C boiler case recorded one of the lowest GHG emissions of the changing temperature network simulations. Utilizing lower temperatures (20 and 30°C) in the off-peak periods has shown reduced GHG emissions due to an increase in EMC storage utilization. The larger temperature difference between the lower off-peak MTN temperatures and the EMC storage set point allows for extended use of the EMC storage and reduces boiler use. Low temperatures in off-peak periods are also beneficial due to the increase in heating HP power from the larger temperature difference between the building set point and the MTN. The higher power requirement of the heating HPs reduces boiler utilization by providing greater electrification of the heating demand with carbon free electricity. Unfortunately, to have a low temperature in the off-peak periods and maintain the hot temperature in on-peak periods, the temperature difference between the low and hot temperature increases. The large temperature difference requires a small thermal mass in the network and creates large pumping power requirements in scenarios where only the CHP is used to increase the temperature of the network. The boiler is not recommended to be used as an operational strategy in implementations of the ICE-Harvest system, as decarbonization strategies are drifting away from boiler use, but it demonstrated the capability of large temperature differences with a lower pumping power requirement.

For the 50-70°C boiler scenario, the emissions increased compared to the ETS storage case. The increase in on-peak electricity consumed by the heating HPs leads to an increase in the overall emissions. The ETS storage provides benefits in demand response, versatility, and resiliency. Using ETS storage at each of the buildings eliminates on-peak electricity consumption by the

heating HPs and increases electrical demand off-peak, creating potential to utilize curtailed electricity. The comparison also showed a decrease in boiler usage in the boiler scenario. When the boiler consumption was broken down into on and off-peak, there was a decrease in the off-peak period. This was an indication that the boiler is being used as a heat source when the ETS storage tanks are charging.

5.4.3 On-peak Vs. No On-peak Harvesting

When heat is harvested during on-peak periods it consumes grid electricity. In order for the system to provide greater demand response, cases were simulated where heat was not harvested on-peak. To explore the system behavior, differences between not harvesting and harvesting heat on-peak for the 50-70°C case was explored for all three sizes of CHP. The pre-heating and boiler delay EMC model was used along with the selective harvesting network model. The harvesting on-peak cases were taken from Section 5.4.1.

5.4.3.1 Yearly Results

Analyzing the thermal energy distribution in Figure 5.26, in the NOPH cases the on-peak electricity consumed by the harvesting HPs goes to zero and the boiler compensates. The boiler utilization on-peak triples when heat in not harvested. The instantaneous use of the CHP increases on-peak as well but leads to less CHP heat to charge the EMC storage for availability in off-peak times. With less storage available off-peak, there is additional compensation by the boiler. In off-peak periods the boiler increases on average by a factor of 1.3 when heat is not harvested.

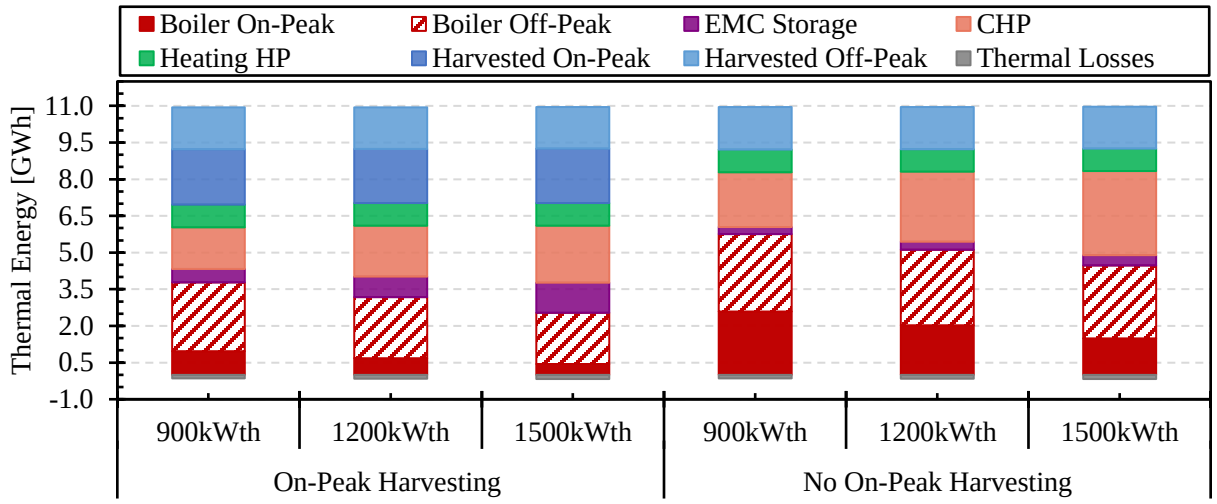

Figure 5.26: Thermal energy distribution comparing harvesting and not harvesting on-peak

The increase in instantaneous CHP utilization when heat is not harvested on-peak leads to less heat from the CHP unrecovered. The amount of unrecovered heat by the CHP decreased on average by 27% with NOPH. The distribution of the CHP heat as a percentage of the total energy is seen in Figure 5.27.

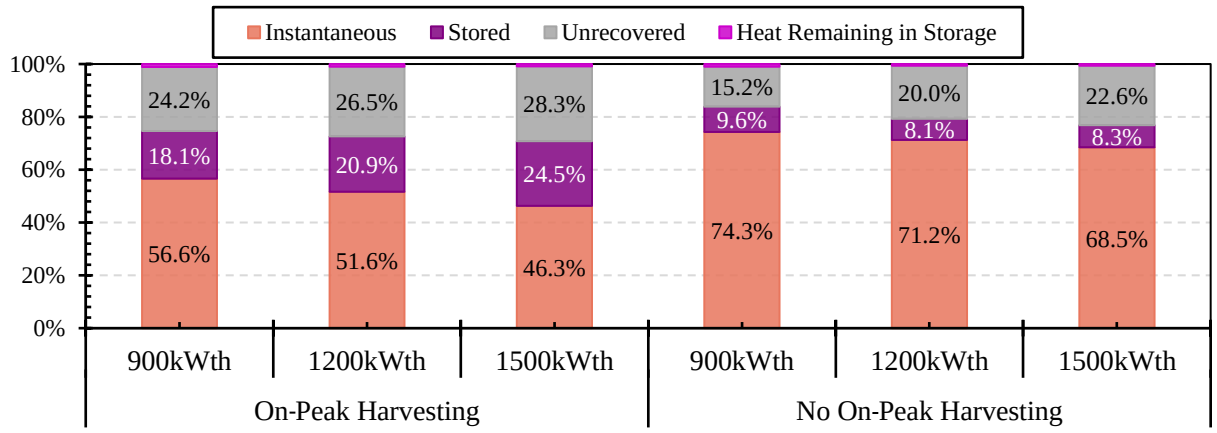

Figure 5.27: Utilization of CHP heat in harvesting and not harvesting on-peak cases

The increased boiler utilization, to compensate for the heat not harvested on-peak, results in an increase in emissions. Although the on-peak electrical consumption decreased, the boiler increase surpassed the electrical emissions avoided as shown in Figure 5.28.

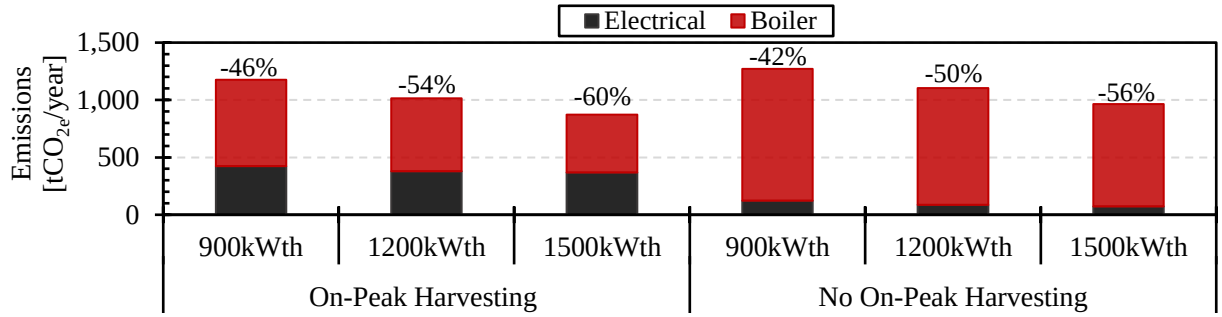

Figure 5.28: GHG Emissions for the harvesting and not harvesting on-peak cases

From an electricity stand point, in the NOPH cases, the on-peak electricity demand decreased resulting in greater quantities of excess electricity from the CHP. The electrical parameters that fluctuate the most between the two scenarios are highlighted in Table 5.11, which is located beside Figure 5.29 where all parameters are displayed. The electricity consumed by the harvesting HP decreases significantly. The majority of the electricity consumed by the harvesting HP was on-peak due to the large temperature difference between the rejected heat and the 70°C hot temperature of the network. The decrease in harvesting HP electricity equals the difference in the grid electricity consumed on-peak and the additional CHP electricity.

Table 5.11: Main electrical parameters between harvesting and not harvesting heat on-peak

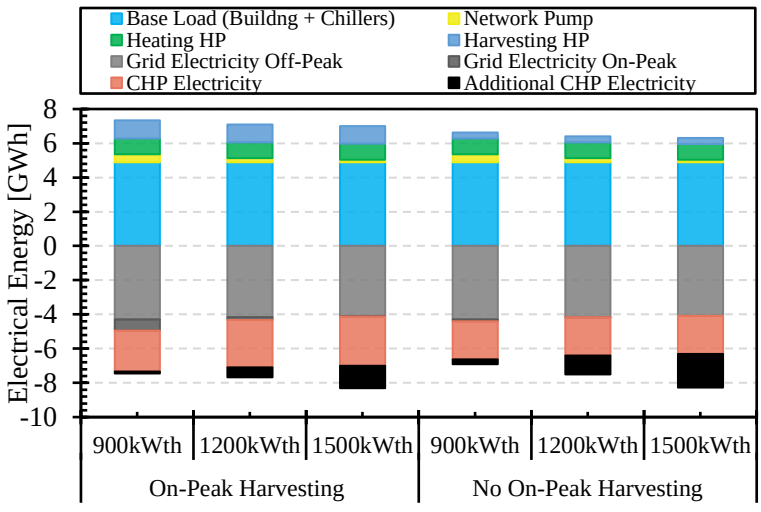

	CHP Size [kW_{th}]	[MWh_e]		
		Grid On-peak	Excess	Har. HP
On-peak Harvesting	900	651	124	1054
	1,200	164	574	1037
	1,500	29	1305	1041
No On-peak Harvesting	900	100	277	353
	1,200	5	1106	352
	1,500	0.005	1969	350

Figure 5.29: Electrical energy distribution for harvesting and not harvesting on-peak cases

Although the NOPH cases result in an increase in emissions, they have a greater demand response. When there is no electrical requirement from the harvesting HPs on-peak, the CHP only has to offset the building load, the chillers, and the pumping power, resulting in a significant decrease in electricity required from the grid. In the 1,500 kW_{th} CHP case the maximum on-peak demand essentially disappears as only 5 kW is required by the grid. The remaining cases are displayed in Figure 5.30.

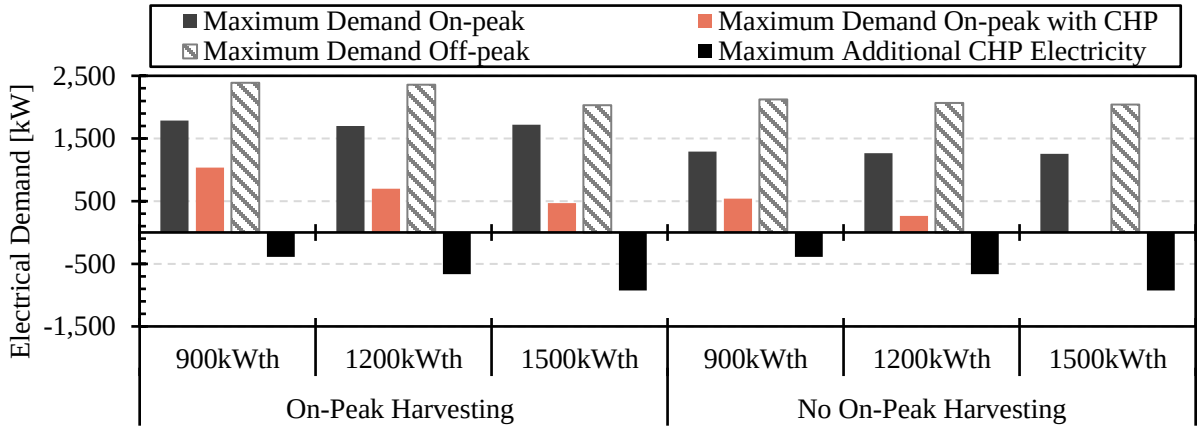

Figure 5.30: Electrical demands for harvesting and not harvesting on-peak cases

5.4.3.2 Hourly Demand Profiles

The last two weeks of December have the coldest temperatures of the year and are plotted hourly to see the behavior of the different equipment at different times. With the hourly profiles, the dynamics of the system can be seen when comparing on-peak harvesting and NOPH for cases run with a 1,500 kW_{th} CHP. Figure 5.31 (a) represents the electrical demands and how they are met with harvesting heat on-peak and (b) shows the case where heat is not harvested on-peak. In Figure 5.33 (a) more of the CHP electricity is utilized, the CHP can cover the majority of electricity consumed by the harvesting HPs. Within the 2 week period, a maximum of 234 kW was needed from the grid when heat was harvested on-peak. The profiles for the off-peak periods are the same in both scenarios. When heat is not harvested on-peak there is much more excess CHP electricity.

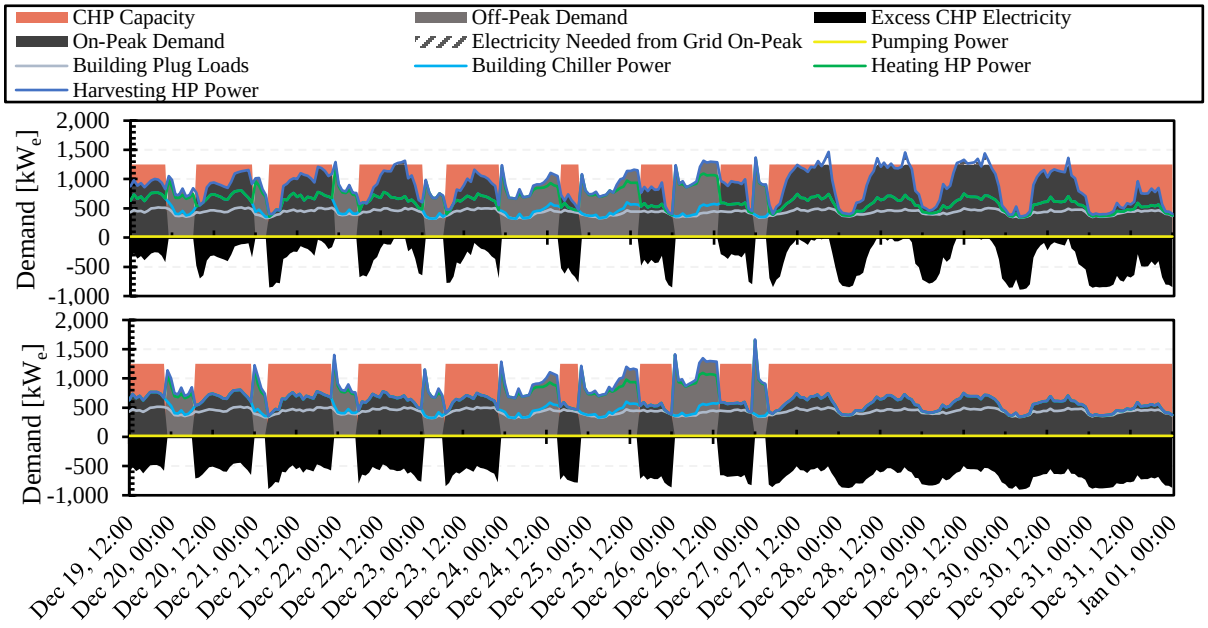

Figure 5.31: Hourly electrical profiles for harvesting and no harvesting on-peak
the top (a) is harvesting energy on-peak and the bottom (b) does not harvest on-peak for a CHP size of 1250kW$_e$

The thermal demand profiles are displayed in Figure 5.32. When heat is harvested on-peak, the boiler usage decreases significantly. There is also opportunity for the harvested energy and the CHP to exceed the heating demand on-peak, which allows for the CHP heat to be stored. The heat stored on-peak is then used to reduce boiler use off-peak. Occurrences of heat stored on-peak are portrayed in the temperature profiles in Figure 5.33 as well. When the heat harvested can meet a portion of the heating load, the EMC loop can reach temperatures greater than 80°C and the EMC storage can be charged. The EMC loop temperature in Figure 5.33 (b) stays at 75°C as it is just producing enough heat to meet the heating load.

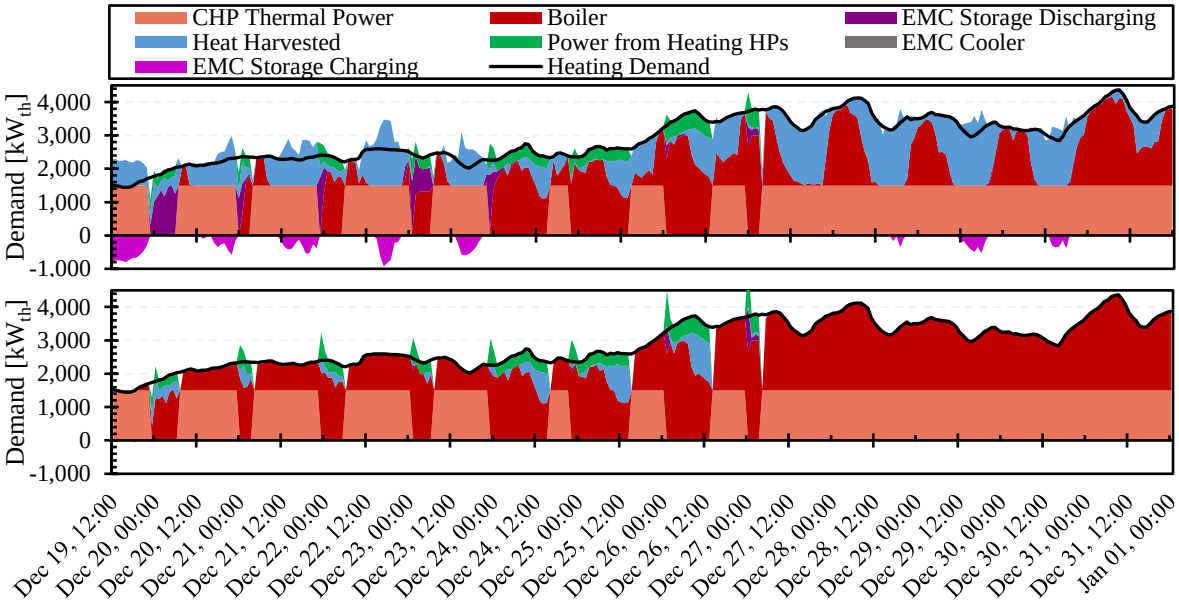

Figure 5.32: Hourly thermal profiles for harvesting and no harvesting on-peak
the top (a) is harvesting energy on-peak and the bottom (b) does not harvest on-peak for a CHP size of 1,500 kWth

The electrical and thermal loads do not coincide, there is a large thermal load but not electrical, from an electrical standpoint the CHP looks oversized but for thermal it is only meeting a third of the winter heating demand. To even the load distribution, long-term thermal storage would help in reducing the winter heating demands heat that was stored from the CHP in the summertime when heating demands are low.

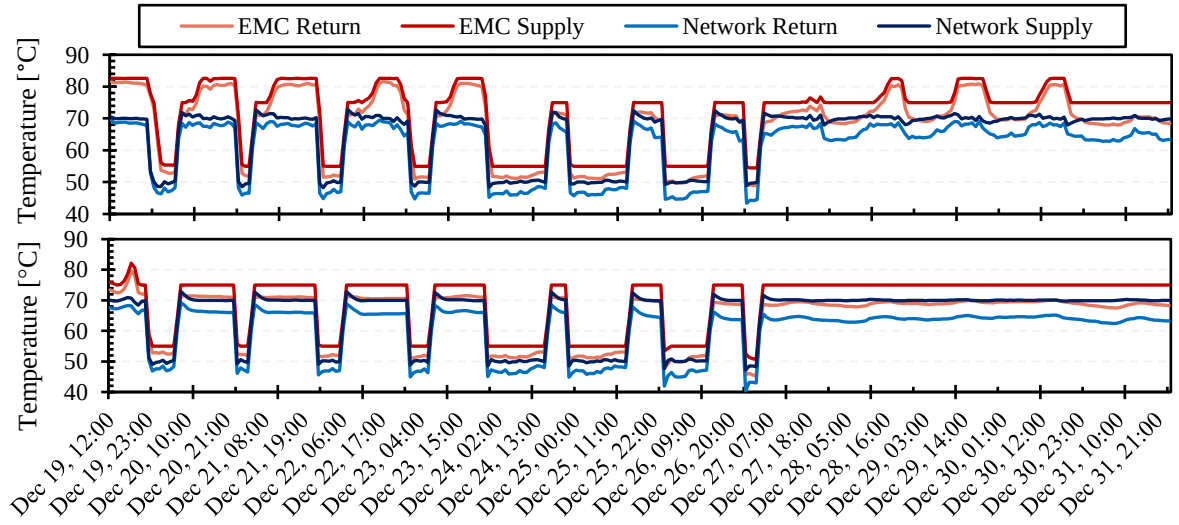

Figure 5.33: Temperature profiles for harvesting and not harvesting heat on-peak

As presented in Figure 5.34, there is a shift in electrical peak. Traditionally the electrical peak occurs in the summer months but with the ICE-Harvest system the peak is seen in the winter. Looking at the dark grey line representing on-peak electrical demand, the maximum demand required from the grid on-peak is now in January, and other larger demands are also seen in the winter months due to the harvesting of heat on-peak.

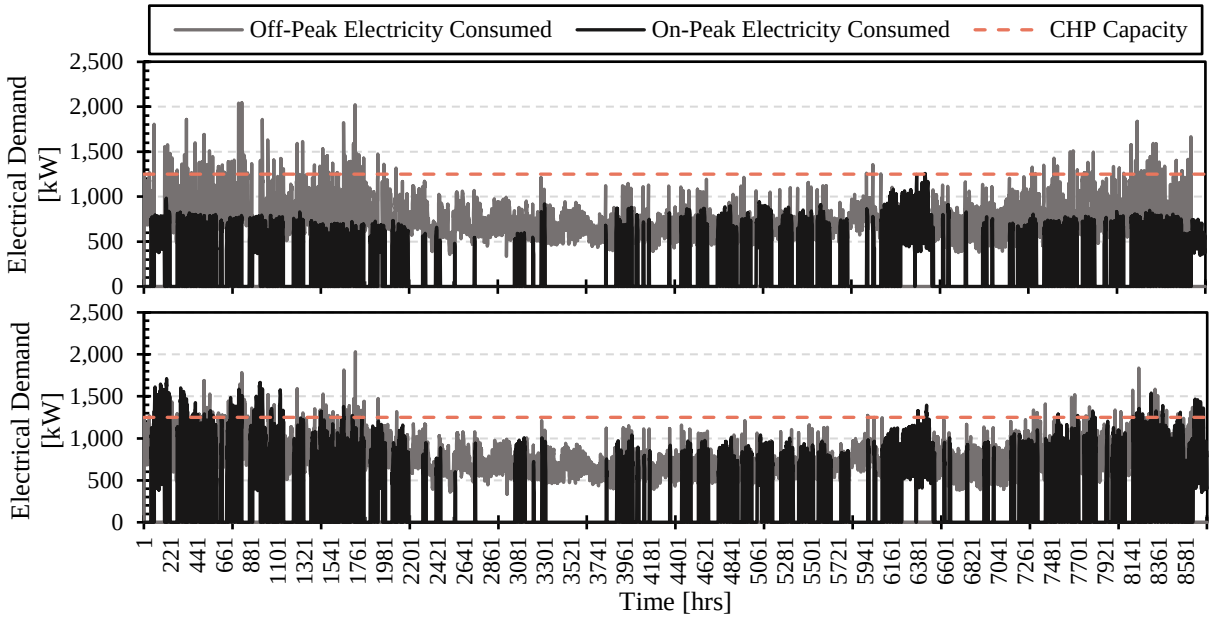

Figure 5.34: Hourly electrical demands over the year
for harvesting (bottom) and not harvesting heat on-peak (top)

5.4.3.3 Summary

The impact of when harvesting heat occurs was explored in the *On-peak Vs. No On-peak Harvesting* analysis. Both options provide significant GHG reductions from the traditional boiler scenario and have come close but not surpassed the emissions reductions of the GSHP case. They also demonstrate less electricity consumed during on-peak periods compared to the traditional boiler and GSHP case. The main goals of both strategies and key takeaways are outlined below:

Harvesting heat on-peak – The focus on harvesting decreases the energy required from the boiler, resulting in emissions reductions of up to 60% from the conventional boiler scenario.

The reduction the peak electrical demand during on-peak periods is 16%, 44%, and 62% for CHP sizes 900, 1,200, and 1,500 kW_{th}.

No harvesting on-peak – The focus is on demand response and reducing on-peak electrical consumption. The reduction in electrical demands in on-peak periods is 56%, 79%, and 99.6% for CHP sizes 900, 1,200, and 1,500 kW_{th}. With emissions reductions up to 56% from the conventional boiler scenario.

Both harvesting and not harvesting on-peak reduced the on-peak electrical demand required by the grid. Whereas in the GSHP case, peak electrical demand increased by 174% compared to the conventional boiler case.

The CHP size has a large impact on GHG emissions and system behaviour. A large CHP is beneficial for meeting the thermal demand and the unrecovered heat can size long-term storage, but there are large quantities of additional electricity. Depending on the site constraints, if the CHP is not allowed to export the electricity to the grid, share within the local community, or there is too much electricity for battery storage, the CHP sizing will be constrained by its electrical output. The downside with the small CHP sizes is the reduction in peak demand compared to the traditional boiler is not significant as the larger CHP sizes, but compared to the GSHP it created a larger impact. If increased demand response is required, the large CHP size can be used with additional layers of control. A limit can be placed on harvesting electricity on-peak as to not exceed the CHP electrical output, instead of an on/off control. The demand response achieved can still be significant without having additional electricity required from the grid. The incorporation of harvested heat, even in reduced quantities, will reduce boiler use and GHG emissions.

5.4.4 Thermal Storage Analysis

A key component to the ICE-Harvest system is thermal storage. Different storage locations and capacities will be explored in this section. Displayed in the previous results, there is still a large quantity of unrecovered rejected heat from the building chillers and an opportunity to harvest and employ that heat throughout the year. To try increase the amount of harvested heat, the network storage model was implemented. The network storage is located on the MTN and stores the harvested heat. When the network storage is being charged, all available rejected heat is harvested and the excess that is not required by the building heating demand is stored. When the network storage is full, the building ETSs will stop harvesting heat. Discharging of the storage occurs during on-peak periods when the temperature of the MTN is below it's set point. More detail on the network storage model is presented in Section 3.6.1.3. Figure 5.35 displays the network storage system schematic and model in Dymola. The EMC model used for the network storage simulations was the fundamental changing temperature model. To initiate the network temperature transition the CHP is operated, indicating an on-peak period. Heat is added to the network from the CHP, boiler, or the network storage (if heat is available) to change the network temperature. The network storage simulations were compared to cases with ETS storage. Different storage capacities were also explored for the EMC storage and the network storage.

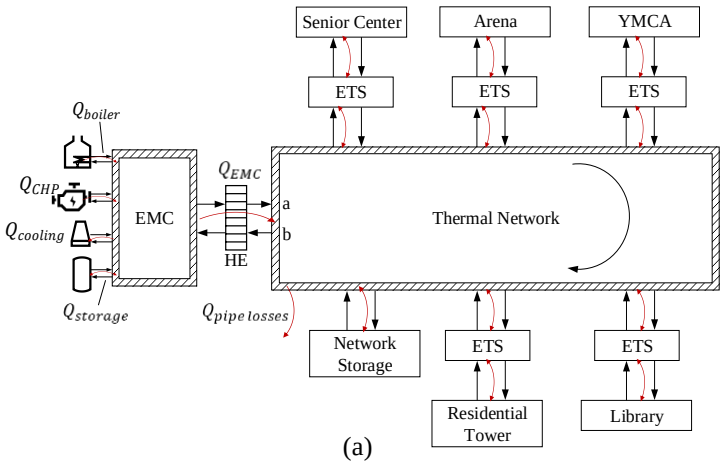

(a)

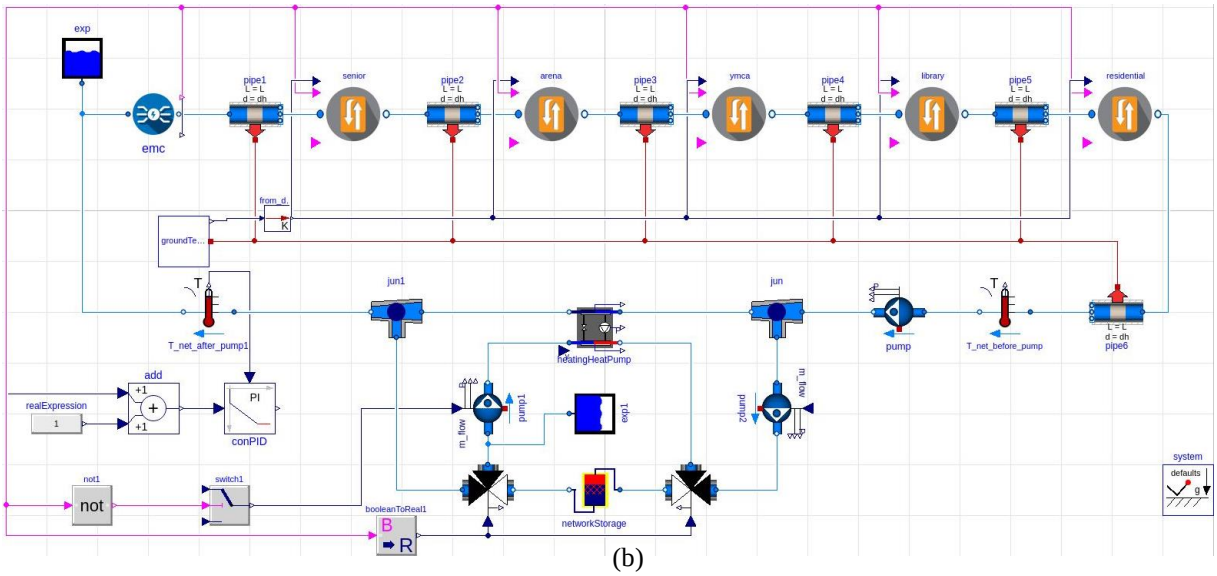

(b)

Figure 5.35: Network storage system schematic (a) and Dymola model (b)

Along with various storage locations and capacities, lower distribution and building temperatures were tested. A 30-60°C case was run for all options explored. The building temperature set point was lowered to 45°C (previously 60°C) and the set point of the storage tanks at the ETSs was lowered to 55°C (previously 70°C), remaining at 10°C above the building set point.

For a given network temperature range, different storage combinations are simulated, as described in Table 5.13. For cases where ETS storage is utilized, two different EMC storage capacities are investigated. In the network storage cases, the EMC storage is constant at 1,000 m^3 and the network storage capacity is either 5,000 or 10,000 m^3. The diameter for the 30°C temperature differences is 0.237 m and the 20°C temperature difference cases is 0.285 m. All simulations contained a 1,500 kW_{th} CHP.

Table 5.13: Simulation cases for different capacities and locations of thermal storage

	Storage Volume [m^3]			
	EMC	ETS	Network	Total Storage Capacity
ETS Storage 1	1,000	172	-	1,172
ETS Storage 2	10,000	172	-	10,172
Network Storage 1	1,000	-	5,000	6,000
Network Storage 2	1,000	-	10,000	11,000

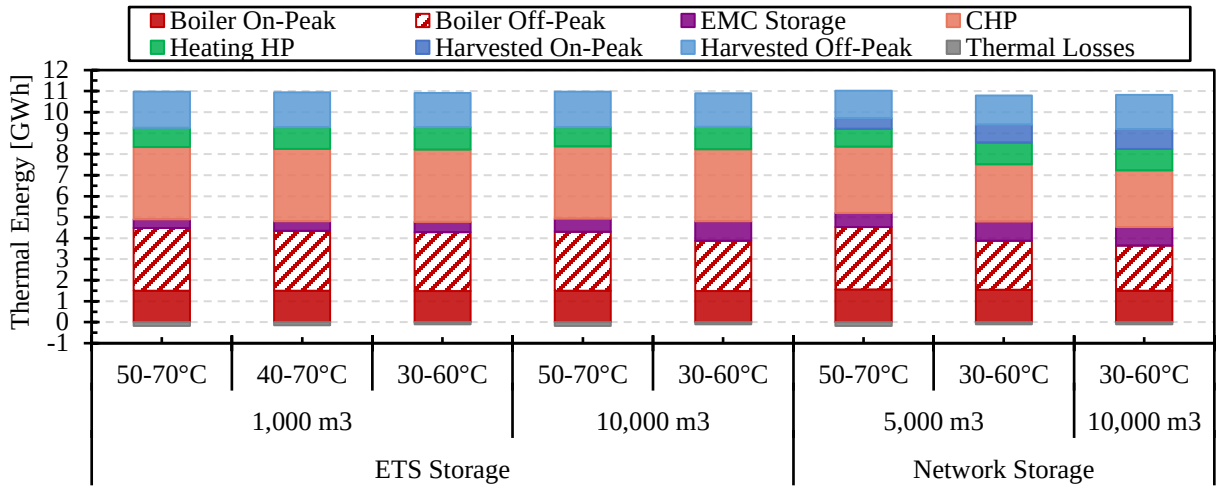

Figure 5.36: Thermal distribution results for the thermal storage analysis

Thermal energy distribution for all cases is outlined in Figure 5.36. The main differences noticed across the ETS storage cases with the varying EMC storage capacity, is the use of the boiler during off-peak periods. With the larger storage capacities, more heat is stored from the CHP and is able to offset the boiler during off-peak periods with no change to the instantaneous use of the CHP. The system behavior for the larger EMC storage mimics that of seasonal/long-term thermal storage but on a smaller scale. Although different control strategies to discharge the storage would be implemented in a seasonal storage scenario, there is less heat from the CHP unrecovered and overall boiler use is reduced. With seasonal storage capacities, all of the unutilized heat from the CHP would be stored.

In Figure 5.36, the comparison to network storage is also presented. The rejected heat from the building chillers is harvested and stored during off-peak periods for use in the network temperature transition and meeting the heating demand on-peak. The network storage is charged at 70°C as to not exceed the temperature limitations on the heat pump. The larger temperature difference between the hot network temperature in the 30-60°C case and the network storage, allows for greater storage utilization compared to the 50-70°C case. Harvested energy is separated into

Harvested On-Peak and *Harvested Off-Peak.* For the network storage case, the differentiation between on and off-peak energy harvesting represents when the energy was used. All heat was actually harvested in the off-peak period, a portion was used to meet the heating loads instantaneously and the remainder was stored. The stored energy is then discharged on-peak, resulting in the *Harvested On-Peak* value. The harvested energy utilized on-peak required no additional electrical requirement as the heat was elevated off-peak with carbon free electricity. There is a reduction in the boiler use off-peak from the increased quantities of energy harvested. Even though there is harvested energy being used on-peak, the boiler use increases as it is required to assist in the network temperature transition. When ETS storage is used, the boiler can be completely non-operational for the temperature transitions allowing the boiler use to decrease.

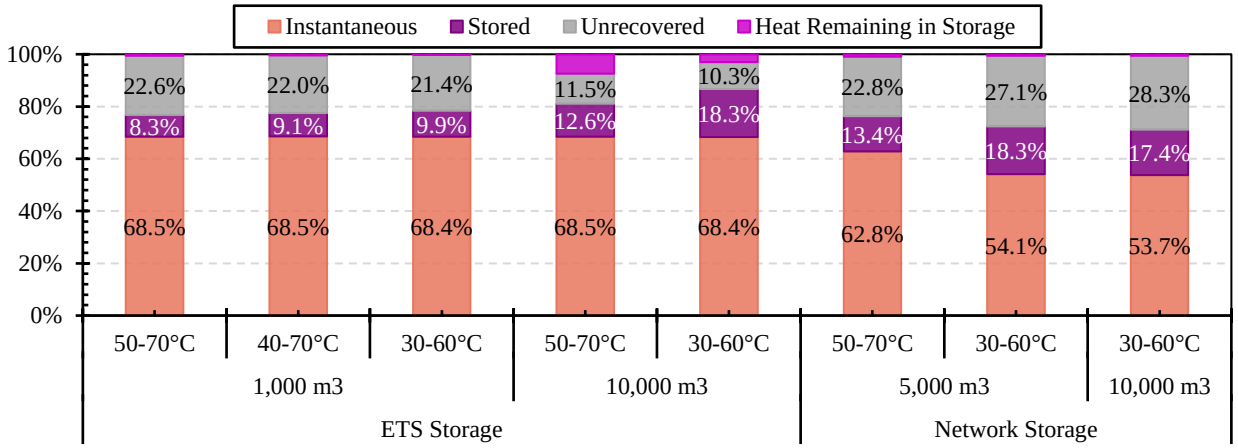

Figure 5.37: Utilization of CHP heat out of a total 5,021 MWh produced

A breakdown of the EMC storage utilization is presented in Figure 5.37. The initial state of the EMC storage, at the beginning of the simulation on January 1st, is discharged at 20°C. The energy required to charge the storage to a useful temperature is not able to be recovered as the system temperatures do not operate that low. Therefore, there is heat remaining in the storage at the end of the year. Due to the increase in harvesting in the network storage case compared to the ETS

storage, the EMC storage requirement off-peak declines. When all heat is harvested and the excess stored, the temperature returning to the EMC is at the set point of the network and therefore does not require any heat. Previously, when only a select quantity of heat was harvested the temperature returning to the EMC was, the majority of the time, below the MTN set point. Since the rejected heat is stored off-peak for use in on-peak periods, the instantaneous use of the CHP decreases since a portion of the heating demand is now being met by the network storage. Overall, more CHP heat is unrecovered because when the CHP heat is not used instantaneously and the EMC storage is full the heat is removed through the cooler.

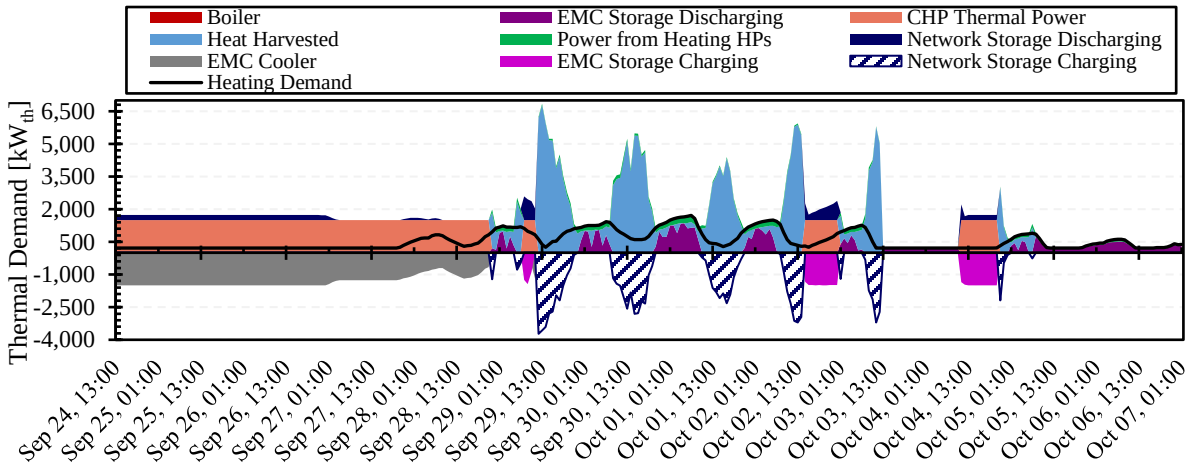

Figure 5.38: Hourly thermal demand profiles for 30-60°C with 5,000 m^3 network storage capacity

The hourly thermal demand profiles are displayed in Figure 5.38. During peak periods, the network storage is able to meet the majority of the heating load. Therefore, the CHP heat is either stored in the EMC storage or unrecovered if the storage is full. In off-peak periods, all rejected heat is harvested into the MTN and the heat that is not used to meet the heating load is stored in the network storage. When the network supply and return temperatures are equal, presented in Figure 5.39, harvested heat from the network has been stored. The heat pump that interfaces with the network storage removes heat from the network and returns the temperature of the network back

to the set point. Therefore, no heat is required from the EMC during these periods. On Oct. 4th, no heat is harvested because the network storage is full and the heating load is met by the EMC storage.

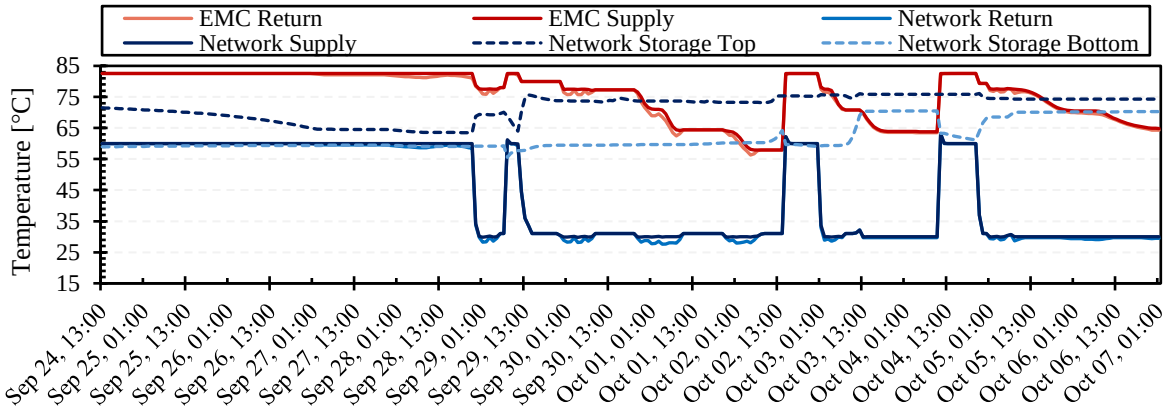

Figure 5.39: Temperature profiles for 30-60°C with 5,000m^3 network storage capacity

Unrecovered thermal energy for the simulations is displayed in Figure 5.40. Only a small change in heat harvested was seen comparing the 5,000 to 10,000 m^3 network storage cases. The discharging control strategy was not optimal and therefore the energy was not being discharged enough for the storage to be replenished. There is still a large opportunity to store rejected heat given the correct operational strategy. With the 10,000 m^3 case there is still 45% of heat rejected that is not utilized off-peak and with 5,000 m^3 there is 54% available. Comparing all cases, the 10,000 m^3 EMC storage case shows the least amount of unrecovered heat.

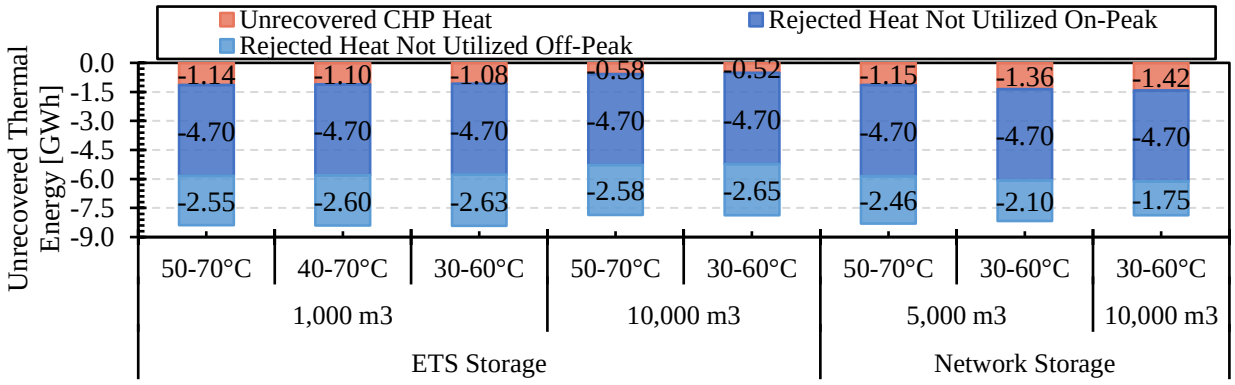

Figure 5.40: Unrecovered thermal energy for the storage analysis

The decrease in network temperature does not have a large impact on emissions reductions in the ETS storage cases where the EMC storage is 1,000 m^3. Where the benefits are seen from the lower temperatures is the incorporation of large storage capacities due to the larger temperature differences. With the 30-60°C network, the emissions between the 10,000 m^3 EMC storage and the 5,000 m^3 network storage are very close and the network storage case has an overall storage capacity system wide of 59% of the large EMC storage case.

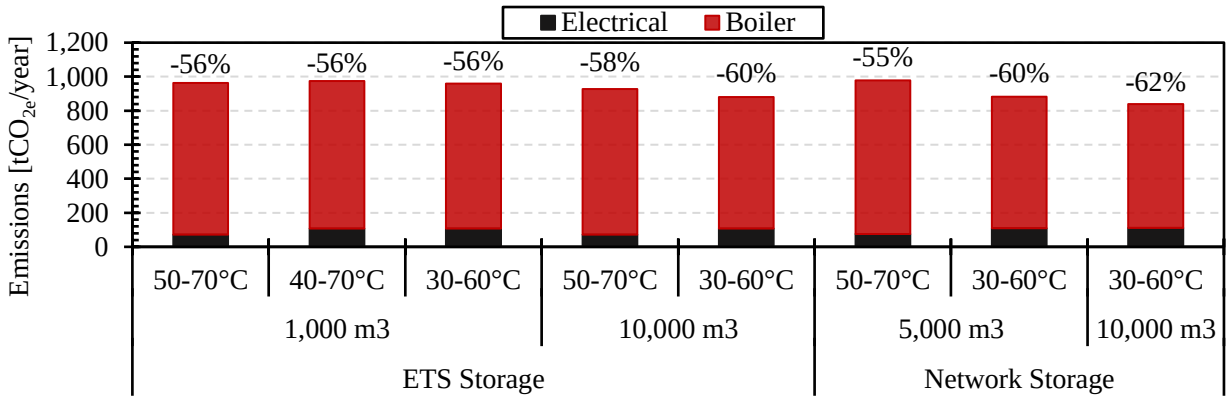

Figure 5.41: Emissions for the storage analysis with emissions reductions from the conventional boiler scenario

In the network storage cases, to meet the heating demand of the buildings during the network temperature transition the heating heat pump is required. The heating HP on-peak electrical consumption in the network storage cases is called out in Figure 5.42. In all ETS storage cases the on-peak electricity consumed by the heating HPs is zero. The pumping power varies between the 20 and 30°C temperature differences, the larger pumping requirements being for the 30°C temperature difference. The harvesting HP electricity consumed increases as the network storage capacity increase due to more energy being harvested.

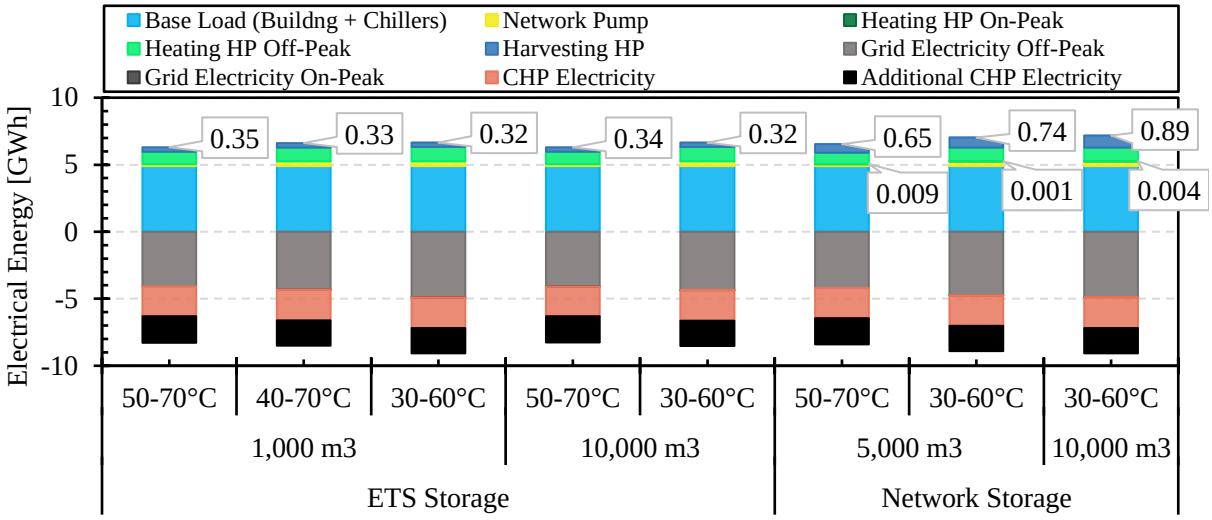

Figure 5.42: Electrical energy for the storage analysis

Hourly electrical profiles are presented in Figure 5.43. During on-peak periods for the network storage case the CHP can meet the majority of the electrical demand. The only demands are the building plug loads, the building chillers, and the pumping power. During off-peak periods, the electrical demand doubles when heat is being harvested. The electrical demands reach such high values off-peak due to the two-step harvesting that is necessary to charge the storage. First step is to use the harvesting HP at the ETS to capture the rejected heat, and second is to use the network HP to increase the temperature of the harvested energy to 70°C to charge the storage.

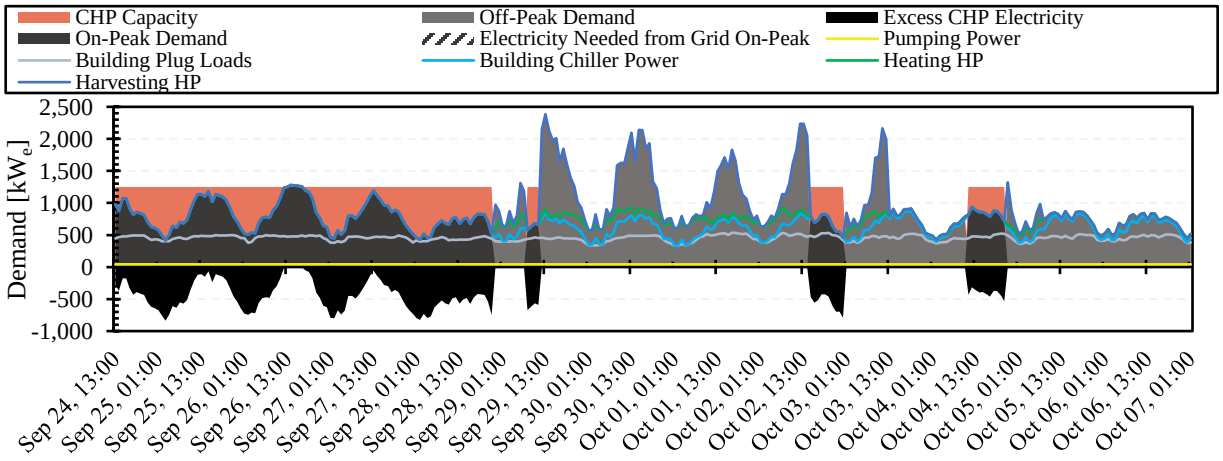

Figure 5.43: Hourly electrical profiles for 30-60°C with 5,000 m^3 network storage capacity

Due to the higher pumping power, in the 30°C temperature difference cases the on-peak demand required from the grid is 30 kW as opposed to 5 kW for the 20°C temperature difference cases. All of the demands required from the grid are very small. Off-peak, when network storage is used the maximum demand seen off-peak is 2.5 MW, providing significant demand response potential for the use of curtailed renewable electricity sources.

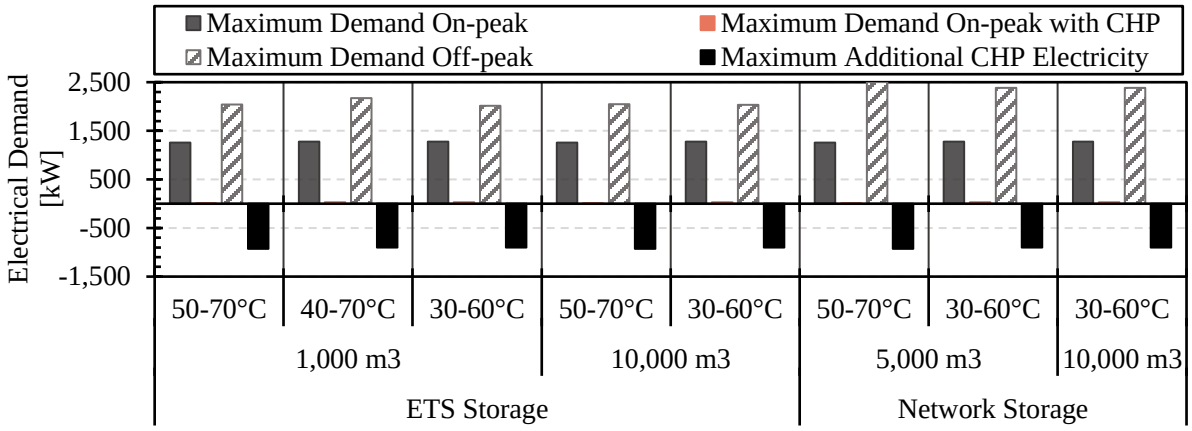

Figure 5.44: Electrical demands for the storage analysis cases

5.4.4.1 Summary

In the network storage cases, the positive effects of harvesting heat are seen. The network storage case with a 5,000 m^3 volume had approximately the same emissions as the EMC storage capacity of 10,000 m^3. The network storage achieved the same results but with just over half of the overall thermal storage volume. With the network storage, the electricity requirements are large during off-peak periods, generating more electrical demand to utilize curtailed renewable generation.

When the network storage volume was increased from 5,000 m^3 to 10,000 m^3, the rejected heat harvested only increased by 13%. The network storage is set to discharge during peak periods where the temperature of the micro-thermal network is either 60 or 70°C. When the storage tank is charged to a set point of 70°C, there is not a large enough temperature difference, even in the 60°C case, for the utilization of storage on-peak. Following the control strategy used, the

temperature difference between the hot network temperature and the storage set point should be increased to make effective use of the harvested heat.

In the network harvesting cases, there was on-peak demand reduction of 98% compared to the conventional boiler case and emissions reductions of 60 and 62% for the 5,000 and 10,000 m^3 cases respectively. There is still rejected heat during on-peak periods that is not being captured and large amounts off-peak. Even with the 10,000 m^3 capacity only 25% of available rejected heat was harvested.

The recovered CHP heat and the harvested heat are stored separately, an improvement on the way this heat is stored will improve the utilization of the heat and reduce GHG emissions further.

5.5 Summary

The benefits and disadvantages of all system simulation cases and the reference scenarios have been summarized in Table 5.14.

Table 5.14: Simulation Summary

	Benefits	Disadvantages
Reference Scenarios		
Boiler	• Simple system • Already implemented in buildings	• Large consumption of natural gas leading to large emissions • No sharing of thermal energy between buildings
GSHP	• Large emissions reductions • No direct use of natural gas	• Generates large electrical demands • Large space requirement for drilling into the ground • No sharing of thermal energy between buildings
Constant Temperature Network		
Low Temperature Network	• Reduces GHGs • Good EMC storage utilization sue to the large temperature difference	• No demand response provided to the electrical grid • Additional demand throughout the year due to the Heating HP electrical requirements

	Benefits	Disadvantages
Hot Temperature Network	• No electrical requirements from the heating HPs	• Decrease in EMC storage utilization • Larger boiler use and GHG emissions
Variable Temperature Network		
ETS Storage		
Small CHP Capacity	• Small quantities of unrecovered CHP heat • Greater use of harvested heat • Minimal quantities of additional CHP electricity	• Increase in boiler use and GHG emissions • Not able to alleviate as much electrical demand from the grid
Large CHP Capacity	• Allows for very minimal electrical • CHP heat can meet a large portion of the heating demand	• Large quantities of unrecovered CHP heat • Large amounts of additional CHP electricity
Small Temperature Difference	• Low pumping power requirements	• Having higher temperatures in off-peak periods leads to an increase in GHG emissions
Large Temperature Difference	• Lower network temperatures during off-peak periods result in reduced GHG emissions	• Large pumping power requirements
Harvesting On-Peak	• Reduction in boiler use • Allows the CHP heat to be stored for off-peak periods	• Increase in on-peak electrical demand
No Harvesting On-Peak	• Virtually no electrical demand during on-peak periods	• Increase in boiler utilization on-peak due to the reduction in heat harvested
Boiler Network Transition	• Demonstrated the viability of large temperature differences • Having a lower temperature thermal network off-peak increases HP electricity and reduces boiler utilization	• Reliance on the boiler
Lower Building Set Point of 45°C (30-60°C Network)	• Lower network temperatures provide greater storage utilization	• Not a significant difference in results compared to the higher building temperature set point of 60°C
Large EMC Storage	• Very little heat from the CHP was unrecovered	• Large quantities of unrecovered heat from building chillers
Network Storage	• Increased the amount of usable harvested heat	• Small electricity requirement from the heating HPs on-peak • Increases the unrecovered heat from the CHP

Chapter 6

6. Conclusions and Recommendations

6.1 Conclusion

Based on the research conducted in this thesis, implementation of the ICE-Harvest system was demonstrated to be an effective way to provide demand response to the electrical grid and reduce GHG emissions. The electrical consumption of the community was controlled while still delivering the entirety of the heating load uninterrupted and unchanged. Various operational strategies were developed to determine the overall behaviour of the system and how the system components interact. This thesis has produced results that will aid in the sizing of equipment and long-term seasonal storage solutions.

The results presented in Chapter 5 display the operating range potential for the ICE-Harvest system. Various control strategies and operational scenarios of the ICE-Harvest system were explored to gauge the behavior of the system under different circumstances. The ICE-Harvest system is very flexible in nature and can be adjusted to the needs of many sites. Analysis was conducted on a range of CHP sizes. The larger CHP sizes provide the ability to deliver increased demand response to the electrical grid but necessitate a greater storage capacity so the additional energy generated is recovered. Storage bridges the temporal gap between when the energy is generated to when it is required and is a key component of the system. Multiple thermal storage locations and capacities were studied. It was concluded that long-term thermal storage would lead to further GHG reductions by the system and that proper control mechanisms are essential for the integration of thermal storage. Through simulating the different operation scenarios, trade-offs

between simulation parameters were discovered and a deeper understanding of system interactions was developed.

Simulations were conducted that are representative of a 4GDH and 5GDHC system. The 4GDH systems have adopted a low temperature thermal distribution network that can range from 30 to 70°C. The 70°C constant temperature thermal network operates at a temperature where direct heat exchange to the building can be performed to meet the heating demands. Maintaining the 70°C network temperature all year with no electrification of heating results in substantial energy from the boiler. Consequentially, there are significant GHG emissions. In 5GDHC systems, an ultra-low distribution temperature has been adopted to focus on the electrification of heating. The 20°C constant temperature thermal network created a considerable increase in electrical demand from operation of the heating HPs. Similarly, operation of the GSHP provided full electrification of heating and resulted in a 174% increase of peak demand. The electrification of heating requires a robust carbon free electrical generation source in order to see full benefits.

Behaviour of the 4GDH and 5GDHC systems validated the motivation for a changing temperature micro-thermal network. For electricity grids with mixed generation, such as Ontario, a changing temperature network takes advantage of carbon free sources when they are available and offsets natural gas generation by operating an efficient on-site CHP. At the low temperature of the MTN, electrification of heating is used to increase electrical demand and consume curtailed electricity. Operation of the MTN at the hot temperature exploits the heat generated from the CHP to provide direct heat exchange to the buildings, eliminating the electrical demand for heating. The efficacy of the system was demonstrated with emissions reductions of up to 62% and reduction in on-peak demand of up to 99% compared to a conventional boiler system. Ontario's goal of emissions

reductions by 2030 requires the implementation of smart energy systems such as the ICE-Harvest system.

6.2 Recommendations for Future Work

The key areas of future improvement for this implementation of the ICE-Harvest system are to address the pumping power requirements and the utilization of waste heat.

All of the unrecovered heat from the CHP is an opportunity for long-term seasonal storage, future models should include the seasonal storage to further reduce boiler use. A combined seasonal storage with CHP heat and harvested energy would eliminate the need for two large storages. The harvested heat would have to be increased in temperature to match the heat rejected from the CHP or it can be used as insulation at the lower temperature to prevent losses.

Pumping power requirements could be reduced through the implementation of a variable mass flowrate. From the response time analysis, the flowrate did not have a large effect on the response time. For network temperature transitions there would be a permissible flowrate range that would achieve the response time. For example, dropping the flowrate to 100 kg/s from a value of 140 kg/s for a 20°C temperature difference results in an approximate 3 minute increase in the response time but drops the pumping power by 11 kW which would have a large impact on yearly pumping power requirements. The fluctuating flowrate analysis would require a sophisticated control strategy especially with the implementation of harvested heat. With a variable flowrate network, the annual pumping power requirements would reduce, making the larger thermal network temperature differences a viable option.

System optimization, including the building set point temperatures, thermal network temperatures, equipment sizes, and flowrates, should be completed. If the building heating system could afford

a lower temperature of water to their heating system, then the loop hot temperature could be decreased and lead to further GHG savings.

Instead of using short-term thermal storage tanks (ETS storage) at the buildings, utilize the building thermal mass. In Dymola simulations, there was no thermal mass associated with the building, and therefore the temperature in the "building" would decrease significantly when the heating demand was not being met. In reality, a building should have enough thermal mass to sustain a comfortable temperature if no heat is added for the duration of the response time.

Further research areas to explore:

- Explore a GSHP system with thermal storage for comparison. The addition of thermal storge to the GSHP case could provide demand management and reduce electrical demands during on-peak periods.
- Adding a geo-exchange system to try utilize excess electricity generated by the CHP.
- Further investigation into the use of rejected heat on-peak. The addition of harvested heat on-peak would reduce boiler consumption. Harvesting of the heat could be controlled so that the demands of the site do not exceed the CHP electrical output.
- Incorporation of renewable resources. Solar thermal and solar PV could be incorporated to reduce the GHG emissions of the system and further reduce electrical demands.
- Utilizing a heat recovery chiller in the harvesting ETSs for heat harvesting in one stage instead of two. Removing the need for the harvesting HP and being able to reject heat from the building chiller at a high enough temperature to enter the thermal network could reduce the electrical consumption of the system.
- The implementation the ICE-Harvest system in different jurisdictions and provinces to analyze the behaviour of the system with different electrical grid generation sources.

Appendix D provides results for the ICE-Harvest system in Ontario for the year 2015. The significant impact of the electrical gid generation source on how the system should be operated was demonstrated.

References

[1] Pew Center on Global Climate Change, “Agenda for Climate Action,” 2006.

[2] Ministry of the Environment - Conservation and Parks, “Preserving and Protecting our Environment for Future Generations A Made-in-Ontario Environment Plan Ministry of the Environment, Conservation and Parks,” p. 53, 2018.

[3] Environment and Climate Change Canada, “National Inventory Report 1990 - 2019: Greenhouse Gas Sources and Sinks in Canada,” 2021.

[4] Natural Resources Canada, “Comprehensive Energy Use Database,” 2022. [Online]. Available: https://oee.nrcan.gc.ca/corporate/statistics/neud/dpa/menus/trends/comprehensive_tables/list.cfm. [Accessed: 05-Mar-2022].

[5] Government of Ontario, “Ontario’s Climate Change Update 2014,” 2017. [Online]. Available: https://www.ontario.ca/page/ontarios-climate-change-update-2014#section-3.

[6] IESO, “2021 Year in Review.” [Online]. Available: https://www.ieso.ca/en/Corporate-IESO/Media/Year-End-Data. [Accessed: 30-Mar-2022].

[7] Independent Electricity System Operator, “A Progress Report On Contracted Electricity Supply,” 2021.

[8] IESO, “Annual Planning Outlook,” 2021.

[9] T. Fawcett, R. Layberry, and N. Eyre, “Electrification of heating: the role of heat pumps,” in *BIEE Conference*, 2014, no. September, pp. 1–13.

[10] The National Academies, “Natural Gas,” 2022. [Online]. Available: http://needtoknow.nas.edu/energy/energy-sources/fossil-fuels/natural-gas/.

[11] Ontario Energy Board, “Ontario Electricity Distributor Practices Relating to Management of System Losses,” 2008.

[12] U.S. Department of Energy, "Furnaces and Boilers," 2022. [Online]. Available: https://www.energy.gov/energysaver/furnaces-and-boilers.

[13] B. Rezaie and M. A. Rosen, "District heating and cooling: Review of technology and potential enhancements," *Appl. Energy*, vol. 93, pp. 2–10, 2012.

[14] G. Simons and S. Barsun, "Chapter 23: Combined Heat and Power Evaluation Protocol," 2017.

[15] B. Tarroja, F. Chiang, A. AghaKouchak, S. Samuelsen, S. V. Raghavan, M. Wei, S. Sun, Kaiyu, T. Hong, "Translating climate change and heating system electrification impacts on building energy use to future greenhouse gas emissions and electric grid capacity requirements in California," *Appl. Energy*, vol. 225, no. January, pp. 522–534, 2018.

[16] J. Moraga González and M. Mulder, "Electrification of heating and transport: A scenario analysis for the Netherlands up to 2050," Netherlands, 2018.

[17] D. Fischer, K. B. Lindberg, S. Mueller, E. Wiemken, and B. Wille-Haussmann, "Potential for Balancing Wind And Solar Power Using Heat Pump Heating And Cooling Systems," *4th Sol. Integr. Work.*, no. February, pp. 263–271, 2014.

[18] W. Li, X. Li, Y. Wang, and J. Tu, "An integrated predictive model of the long-term performance of ground source heat pump (GSHP) systems," *Energy Build.*, vol. 159, pp. 309–318, 2018.

[19] J. Luo, J. Rohn, M. Bayer, A. Priess, L. Wilkmann, and W. Xiang, "Heating and cooling performance analysis of a ground source heat pump system in Southern Germany," *Geothermics*, vol. 53, pp. 57–66, 2015.

[20] S. Werner, "International review of district heating and cooling," *Energy*, vol. 137, pp. 617–631, 2017.

[21] J. F. Collins, "The History of District Heating," *Dist. Heat.*, pp. 154–161, 1959.

[22] H. Lund, S. Werner, R. Wiltshire, S. Svendsen, J. E. Thorsen, F. Hvelplund, B. V.

Mathiesen, “4th Generation District Heating (4GDH) Integrating smart thermal grids into future sustainable energy systems,” Energy, vol. 68, pp. 1–11, 2014.

[23] H. Lund, P. A. Østergaard, T. B. Nielsen, S. Werner, J. E. Thorsen, O. Gudmundsson, A. Arabkoohsar, B. V. Mathiesen, “Perspectives on fourth and fifth generation district heating,” *Energy*, vol. 227, no. 120520, 2021.

[24] L. Newman and Y. Herbert, “The use of deep water cooling systems: Two Canadian examples,” *Renew. Energy*, vol. 34, no. 3, pp. 727–730, 2009.

[25] IDEA, “Map of District Energy in North America,” 2015. [Online]. Available: https://www.districtenergy.org/resources/resources/system-maps. [Accessed: 21-Feb-2022].

[26] X. Liu and P. Mancarella, “Modelling, assessment and Sankey diagrams of integrated electricity-heat-gas networks in multi-vector district energy systems,” *Appl. Energy*, vol. 167, no. September, pp. 336–352, 2016.

[27] H. Lund, P. A. Østergaard, M. Chang, S. Werner, S. Svendsen, P. Sorknæs, J. E. Thorsen, F. Hvelplund, B. O. Gram Mortensen, B. Vad, C. Bojesen, N. Duic, X. Zhang, B. Moller, “The status of 4th generation district heating: Research and results,” *Energy*, vol. 164, pp. 147–159, 2018.

[28] H. Kauko, K. Husevåg, D. Rohde, and N. Nord, “Dynamic modeling of local district heating grids with prosumers: A case study for Norway,” *Energy*, vol. 151, pp. 261–271, 2018.

[29] H. Lund, P. A. Østergaard, D. Connolly, and B. V. Mathiesen, “Smart energy and smart energy systems,” *Energy*, vol. 137, pp. 556–565, 2017.

[30] H. Lund, N. Duic, P. A. Østergaard, and B. V. Mathiesen, “Future district heating systems and technologies: On the role of smart energy systems and 4th generation district heating,” *Energy*, vol. 165, pp. 614–619, 2018.

[31] FLEXYNETS, “FLEXYNETS Project,” 2020. [Online]. Available: http://www.flexynets.eu/en/Project.

[32] S. Boesten, W. Ivens, S. C. Dekker, and H. Eijdems, "5th Generation District Heating and Cooling Systems as a Solution for Renewable Urban Thermal Energy Supply," *Adv. Geosci.*, vol. 49, pp. 129–136, 2019.

[33] R. Zarin Pass, M. Wetter, and M. A. Piette, "A thermodynamic analysis of a novel bidirectional district heating and cooling network," *Energy*, vol. 144, pp. 20–30, 2018.

[34] S. Buffa, M. Cozzini, M. D. Antoni, M. Baratieri, and R. Fedrizzi, "5th generation district heating and cooling systems: A review of existing cases in Europe," *Renew. Sustain. Energy Rev.*, vol. 104, no. February, pp. 504–522, 2019.

[35] F. Bünning, M. Wetter, M. Fuchs, and D. Müller, "Bidirectional low temperature district energy systems with agent-based control: Performance comparison and operation optimization," *Appl. Energy*, pp. 502–515, 2018.

[36] T. Sommer, M. Sulzer, M. Wetter, A. Sotnikov, S. Mennel, and C. Stettler, "The reservoir network: A new network topology for district heating and cooling," *Energy*, vol. 199, p. 117418, 2020.

[37] R. Rogers, "Unidirectional Low Temperature Thermal Networks: Enabling Thermal Distributed Energy Resources," McMaster University, 2019.

[38] M. Wirtz, L. Kivilip, P. Remmen, and D. Müller, "5th Generation District Heating: A novel design approach based on mathematical optimization," *Appl. Energy*, vol. 260, no. November 2019, pp. 114–158, 2020.

[39] R. Verhoeven *et al.*, "Minewater 2.0 project in Heerlen the Netherlands: Transformation of a geothermal mine water pilot project into a full scale hybrid sustainable energy infrastructure for heating and cooling," *Energy Procedia*, vol. 46, pp. 58–67, 2014.

[40] N. Vetterli, M. Sulzer, and U. P. Menti, "Energy monitoring of a low temperature heating and cooling district network," *Energy Procedia*, vol. 122, pp. 62–67, 2017.

[41] T. Schluck, P. Kräuchi, and M. Sulzer, "Non-linear thermal networks - How can a meshed network improve energy efficiency?," in *CISBAT 2015 Lausanne*, 2015, pp. 779–785.

[42] M. Köfinger, D. Basciotti, R. R. Schmidt, E. Meissner, C. Doczekal, and A. Giovannini, "Low temperature district heating in Austria: Energetic, ecologic and economic comparison of four case studies," *Energy*, vol. 110, pp. 95–104, 2016.

[43] F. Ruesch, M. Rommel, and J. Scherer, "Pumping Power Prediction in Low Temperature District Heating Networks," *Proc. Int. Conf. CISBAT 2015*, no. November 2017, pp. 753–758, 2015.

[44] T. Ommen, J. E. Thorsen, W. B. Markussen, and B. Elmegaard, "Performance of ultra low temperature district heating systems with utility plant and booster heat pumps," *Energy*, vol. 137, pp. 544–555, 2017.

[45] N. Yildirim, M. Toksoy, and G. Gokcen, "Piping network design of geothermal district heating systems: Case study for a university campus," *Energy*, vol. 35, no. 8, pp. 3256–3262, 2010.

[46] O. Martin-du Pan, P. Woods, and R. Hanson-graville, "Optimising pipe sizing and operating temperatures for district heating networks to minimise operational energy consumption," *Build. Serv. Eng. Res. Technol.*, vol. 40, no. 2, pp. 237–255, 2019.

[47] V. D. Stevanovic, B. Zivkovic, S. Prica, B. Maslovaric, V. Karamarkovic, and V. Trkulja, "Prediction of thermal transients in district heating systems," *Energy Convers. Manag.*, vol. 50, no. 9, pp. 2167–2173, 2009.

[48] P. K. Olsen, C. H. Christiansen, M. Hofmeister, S. Svendsen, J. E. Thorsen, O. Gudmundsson, M. Brand, "Guidelines for Low-Temperature District Heating," *EUDP 2010-II Full-Scale Demonstration Low-Temperature District Heating in Existing Buildings*, no. April, pp. 1–43, 2014.

[49] T. Tereshchenko and N. Nord, "Importance of Increased Knowledge on Reliability of District Heating Pipes," *Procedia Eng.*, vol. 146, no. 1877, pp. 415–423, 2016.

[50] V. Kain, "Flow accelerated corrosion: Forms, mechanisms and case studies," *Procedia Eng.*, vol. 86, pp. 576–588, 2014.

[51] T. Satoh, Y. Shao, W. G. Cook, D. H. Lister, and S. Uchida, "Flow-assisted corrosion of carbon steel under neutral water conditions," *Corrosion*, vol. 63, no. 8, pp. 770–780, 2007.

[52] ASHRAE, *2017 ASHRAE Handbook —Fundamentals (SI)*. 2017.

[53] E. Guelpa and V. Verda, "Demand response and other demand side management techniques for district heating: A review," *Energy*, vol. 219, 2021.

[54] IESO, "IESO," 2022. [Online]. Available: https://www.ieso.ca/en/.

[55] E. Guelpa, L. Marincioni, S. Deputato, M. Capone, S. Amelio, E. Pochettino, V. Verda, "Demand side management in district heating networks: A real application," *Energy*, vol. 182, pp. 433–442, 2019.

[56] H. Cai, S. You, and J. Wu, "Agent-based distributed demand response in district heating systems," *Appl. Energy*, vol. 262, no. January, 2020.

[57] M. Leśko and W. Bujalski, "Operational optimization in district heating systems," *Rynek Energii*, 2016.

[58] M. Lesko and W. Bujalski, "Modeling of District Heating Networks for the Purpose of Operational Optimization with Thermal Energy Storage," *Arch. Thermodyn.*, vol. 38, no. 4, pp. 139–163, 2017.

[59] D. Basciotti, F. Judex, O. Pol, and R.-R. Schmidt, "Sensible heat storage in district heating networks: a novel control strategy using the network as storage," *IRES - 6th Int. Renew. Energy Storage Conf. Exhib.*, p. 4, 2011.

[60] A. Arteconi, N. J. Hewitt, and F. Polonara, "Domestic demand-side management (DSM): Role of heat pumps and thermal energy storage (TES) systems," *Appl. Therm. Eng.*, vol. 51, pp. 155–165, 2013.

[61] M. Miara, D. Günther, Z. L. Leitner, and J. Wapler, "Simulation of an Air-to-Water Heat Pump System to Evaluate the Impact of Demand-Side-Management Measures on Efficiency and Load-Shifting Potential," *Energy Technol.*, vol. 2, no. 1, pp. 90–99, 2014.

[62] H. Edtmayer, P. Nageler, R. Heimrath, T. Mach, and C. Hochenauer, "Investigation on sector coupling potentials of a 5th generation district heating and cooling network," *Energy*, vol. 230, p. 120836, 2021.

[63] Modelica Association, "Modelica — A unified object-oriented language for physical systems modeling — Language Specification," 2021.

[64] G. Schweiger, P. O. Larsson, F. Magnusson, P. Lauenburg, and S. Velut, "District heating and cooling systems – Framework for Modelica-based simulation and dynamic optimization," *Energy*, vol. 137, pp. 566–578, 2017.

[65] G. Schweiger, H. Nilsson, J. Schoeggl, W. Birk, and A. Posch, "Modeling and simulation of large-scale systems: A systematic comparison of modeling paradigms," *Appl. Math. Comput.*, vol. 365, 2019.

[66] L. Giraud, C. Paulus, and R. Baviere, "Modeling of Solar District Heating: A Comparison Between TRNSYS and MODELICA," in *ISES Conference Proceedings*, 2014.

[67] D. Basciotti and O. Pol, "A Theoretical Study of the Impact of Using Small Scale Thermo Chemical Storage Units in District Heating Networks," *Int. Sustain. Energy Conf.*, pp. 1–10, 2011.

[68] B. van der Heijde, M. Fuchs, C. Ribas Tugores, G. Schweiger, K. Sartor, D. Basciotti, D. Müller, C. Nytsch-Geusen, M. Wetter, L. Helsen, "Dynamic equation-based thermo-hydraulic pipe model for district heating and cooling systems," *Energy Convers. Manag.*, vol. 151, no. September, pp. 158–169, 2017.

[69] M. Ricci, P. Sdringola, S. Tamburrino, G. Puglisi, E. Di Donato, M. A. Ancona, F. Melino, "Efficient District Heating in a Decarbonisation Perspective: A Case Study in Italy," *Energies*, vol. 15, no. 3, 2022.

[70] Modelica Association, "Modelica Standard Library," 2019. [Online]. Available: https://doc.modelica.org/om/Modelica.html.

[71] M. Wetter, W. Zuo, T. S. Nouidui, and X. Pang, "Modelica Buildings Library," *J. Build.*

Perform. Simul., vol. 7, no. 4, pp. 253–270, 2014.

[72] D. Müller, M. Lauster, A. Constantin, M. Fuchs, and P. Remmen, "Aixlib - an Open-Source Modelica Library Within the IEA-EBC Annex 60 Framework," *Proc. CESBP Cent. Eur. Symp. Build. Phys. BauSIM 2016*, no. September, pp. 3–9, 2016.

[73] J. Benthin, A. Heyer, P. Huismann, M. Djukow, A. Hagemeier, and K. Görner, "Demand oriented Modelling of coupled Energy Grids Demand oriented Modelling coupled Energy Grids," pp. 59–66, 2019.

[74] M. Mans, T. Blacha, P. Remmen, and D. Müller, "Automated model generation and simplification for district heating networks cooling networks," pp. 179–186, 2019.

[75] F. Casella, M. Otter, K. Proelss, C. Richter, H. Tummescheit, and P. Milano, "The Modelica Fluid and Media library for modeling of incompressible and compressible thermo-fluid pipe networks," in *The Modelica Association*, 2006.

[76] Modelica Association, "Modelica.Fluid.Pipes.DynamicPipe," 2020. [Online]. Available: https://doc.modelica.org/om/Modelica.Fluid.Pipes.DynamicPipe.html.

[77] M. Wetter, "Buildings.Fluid.HeatPumps.Carnot_y," *Modelica Buildings Library*. [Online]. Available: https://simulationresearch.lbl.gov/modelica/releases/latest/help/Buildings_Fluid_HeatPumps.html#Buildings.Fluid.HeatPumps.Carnot_y.

[78] B. Sullivan, M. Lightstone, and J. Cotton, "A Comparison of Different Heating and Cooling Energy Delivery Systems and The Integrated Community Energy and Harvesting System in Heating Dominant Communities," McMaster University, 2020.

[79] H. Jin, "Parameter Estimation Based Models of Water Source Heat Pumps," 2002.

[80] Daikin Applied, "Catalog 1107-7 Daikin Water to Water Source Heat Pumps," 2019.

[81] M. Y. Abdelsalam, K. Friedrich, S. Mohamed, J. Chebeir, V. Lakhian, B. Sullivan, A. Abdalla, J. Van Ryn, J. Girard, M. F. Lightstone, S. Bucking, J. S. Cotton, J.S., "Integrated

Community Energy and Harvesting Systems: A Climate Action Strategy for Cold Climates," *Appl. Energy*, Under Review, 2022.

[82] M. A. Millar, B. Elrick, G. Jones, Z. Yu, and N. M. Burnside, "Roadblocks to low temperature district heating," *Energies*, vol. 13, no. 22, 2020.

[83] A. Abdalla, S. Mohamed, S. Bucking, and J. S. Cotton, "The impact of clustering strategies to site integrated community energy and harvesting systems on electrical demand and regional GHG reductions," *Energy*, Under Review.

[84] Uponor Infra Ltd., "Sclairpipe Versatile High Density Polyethylene Pipe," 2015.

[85] L. Mesquita, D. McClenahan, J. Thornton, J. Carriere, and B. Wong, "Drake Landing Solar Community: 10 Years of Pperation," in *IEA SHC International Conference on Solar Heating and Cooling for Buildings and Industry*, 2017, no. August, pp. 333–344.

[86] Plastics Pipe Institute (PPI), "Chapter 6 - Design of PE Piping Systems," in *PPI Handbook of Polyethylene Pipe*, 1950, pp. 155–264.

[87] ASHRAE, *2020 ASHRAE Handbook —HVAC Systems and Equipment (SI)*. 2020.

[88] R. Judd and J. Wade, "Temperature Distribution in the Soil," *Eng. J.*, pp. 22–55, 1969.

[89] Minister of Natural Resources Canada, "RETScreen® Software Online User Manual," 2005.

[90] G. Myhre, D. Shindell, F. M. Bréon, W. Collins, J. Fuglestvedt, J. Huang, D. Koch, J. F. Lamarque, D. Lee, B. Mendoza, T. Nakajima, A. Robock, G. Stephens, T. Takemura, H. Zhang, "Anthropogenic and Natural Radiative Forcing," 2013.

[91] M. J. S. Sánchez, S. Bhattacharya, and K. Mareckova, "Chapter 8: Reporting Guidance and Tables," 2006.

[92] G. Florides and S. Kalogirou, "Annual ground temperature measurements at various depths," in *8th REHVA World Congress CLIMA*, 2005, pp. 1–6.

[93] T. Kusuda and P. R. Achenbach, “Earth Temperature and Thermal Diffusivity at Selected Stations in the United States,” 1965.

[94] M. Ouzzane, P. Eslami-Nejad, M. Badache, and Z. Aidoun, “New correlations for the prediction of the undisturbed ground temperature,” *Geothermics*, vol. 53, pp. 379–384, 2015.

Appendix A

7. Ground Temperature Model Equations

7.1 Ground Temperature Correlation

The ground temperature correlation used was retrieved from [92]. Florides & Kalogirou altered the equation developed by Kusuda & Achenbach in 1965 [93], they equated the phase angle at the earth's surface to the time of the year multiplied by 2π and used the time frame of days opposed to hours. The parameters in [92] are more readily accessible to be able to determine the ground temperature. Therefore, the equation used in the ground temperature model is Equation 7.1.

$$T_{soil} = T_{mean} - T_{amp} e^{-d\sqrt{\frac{\pi}{365\alpha}}} \cos\left(\frac{2\pi}{365}\left(t_{year} - \frac{x}{2}\sqrt{\frac{365}{\pi\alpha}} - t_{shift}\right)\right) \quad (7.1)$$

Table 7.1: Parameters for the Florides & Kalogirou ground temperature equation

Variable	Description
T_{soil}	Soil temperature a depth D and Time of year [°C]
T_{mean}	Mean surface temperature [°C]
T_{amp}	Amplitude of surface temperature [°C]
d	Depth below the surface (surface = 0) [m]
α	Thermal diffusivity of the ground [m^2/s]
t_{year}	Current time [days]
t_{shift}	Day of the year of the minimum surface temperature [days]

7.2 Ground Surface Temperature

A correlation was developed by Ouzzane et al. [94], through experimentally obtained ground temperatures and recorded meteorological data, relating the ground surface temperature to the ambient air temperature. Ouzzane et al. discovered that the ambient air temperature was the

dominant factor in the determination of the ground surface temperature and developed a simplified equation, Equation 7.2, for approximating the earth's surface temperature.

$$T_s = 17.898 + 0.951T_{amb} \tag{7.2}$$

Table 7.2: Parameters for the earth's surface temperature correlation

Parameter	Description
T_s	Undisturbed ground surface temperature [°K]
T_{amb}	Ambient (dry bulb) air temperature [°K]

7.3 Dymola Model of Ground Temperature

In Dymola a model was developed, entitled *GroundTempDepth*, which combines the ground surface and ground temperature equations along with the local ambient air temperatures, in order to obtain a temperature at the depth of the buried pipe for heat transfer to the ground. The model contains the components displayed in Figure 7.1 and built in equations in the text layer.

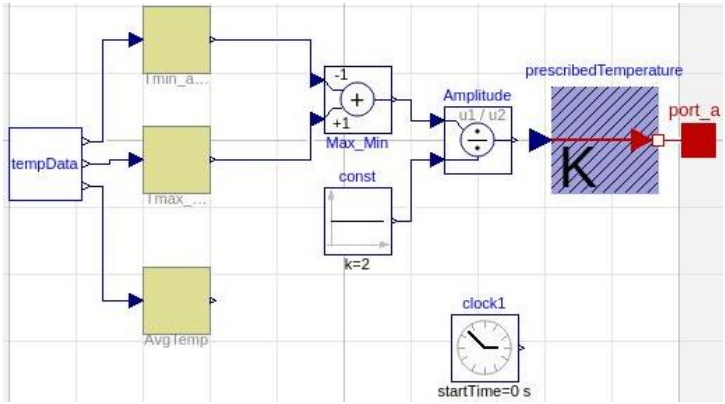

Figure 7.1: Ground temperature model in Dymola

The model contains user input for a temperature data file which needs to contain the minimum, maximum, and average ambient air temperatures. The temperature data maximum time resolution should be daily, however, since the daily average for all temperatures is computed; finer data is

also permitted. Once the daily average and amplitude have been calculated from the temperature data, Equation 7.2 is used to correlate the ambient temperatures into a ground surface temperatures.

In the model, the user will have the choice to specify the thermal conductivity, density, and heat capacity of the soil for the model to calculate the thermal diffusivity or enter the thermal diffusivity of the soil itself. If the *calculate thermal diffusivity* option is chosen, Equation 7.3 is used. The model then uses the ground surface temperatures, thermal diffusivity, and depth of the buried pipe to calculate the temperature of the soil using Equation 7.1. After the soil temperature has been determined, the *prescribedTemperature* block converts the temperature into a heat flowrate for connection to the thermal network piping.

$$\alpha = \frac{k_{soil}}{\rho_{soil} c_{p,soil}} \tag{7.3}$$

Table 7.3: Parameter descriptions and units for the thermal diffusivity equation

Parameter	Description
k_{soil}	Thermal conductivity of the soil [W/mK]
ρ_{soil}	Density of the soil [kg/m^3]
$c_{p,soil}$	Specific heat capacity of the soil [J/kgK]
α	Thermal diffusivity of the soil [m^2/s]

Appendix B

8. Heating HP Analysis

8.1 Heating HP Evaporator Limits

The 50-70°C scenarios will be looked at, as the 50°C temperature is out of bounds for the heating HP. The maximum evaporator outlet is 40°C, therefore, with a 5°C temperature difference, 45°C is the maximum temperature that can enter the evaporator.

For the 50-70°C network, harvesting on-peak, with a 1,500kW_{th} CHP the temperatures entering the evaporator were analyzed. From Figure 8.1, there are only a handful of instances where the network temperature drops below 45°C. Only the temperatures of the network during off-peak periods were displayed in Figure 8.1. The temperatures of 70°C result from preheating of the network during off-peak times and the temperature remaining at 70°C right after the CHP has been turned off, direct heat exchange is used at these times. Access to a HP that has an evaporator inlet temperature of 50°C was not available, therefore, a comparison in electricity consumption cannot be made. The current model, using a maximum evaporator inlet of approximately 45°C, results in an overestimation of the electrical consumption. If the larger evaporator temperatures were used, the COP would increase, and less power would be required to heat the temperature of the buildings. Since the heat pump is used during the off-peak period, the overestimation in electrical consumption does not cause a large increase in the GHG emissions. For example, if the cumulative power of the heating HPs were to decrease by 15 kW, amounting to 131 MWh, the yearly emissions would only decrease by 0.28 tCO_{2e}.

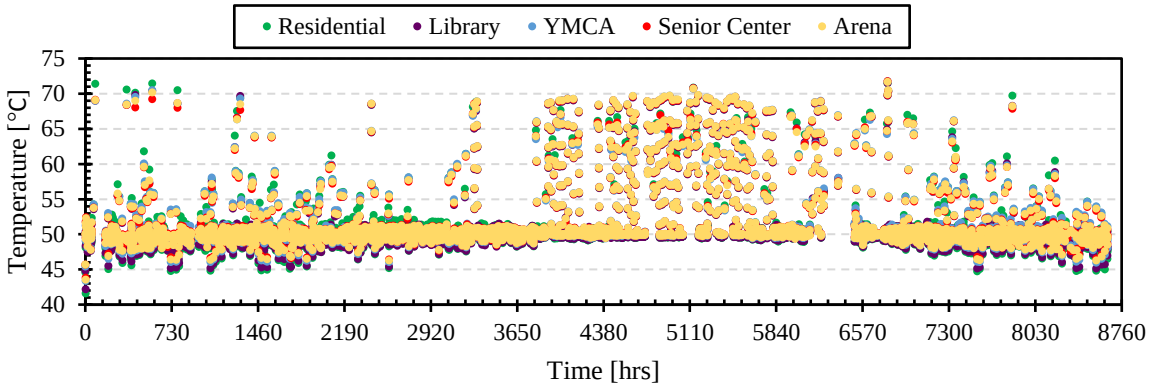

Figure 8.1: Evaporator inlet temperatures for the heating HP with a 50°C cool network set point

8.2 Utilizing a Different HP Model

A low temperature (LT) HP equation was developed to compare the electrical consumption to the existing 30-60°C scenarios with a building set point of 45°C, which is currently out of range of the heating HP. The harvesting electricity consumption is also analyzed as the majority of off-peak harvesting temperatures are out of the existing HP bounds.

8.2.1 Low Temperature HP Model

The LT HP model uses the exact same methodology as described in Section 3.3.4.1 Heating Heat Pump Model. The model described in Section 3.3.4.1 will be the high temperature (HT) HP model as the condenser outlet and evaporator outlet temperatures are higher than the LT model.

The LT HP model is based off of the Daikin WHA420 model. Daikin was used due to its in depth publicly available data sheet [71] and wide range of temperatures. The condenser outlet maximum is 59.3°C and the minimum is 18.2°C. The evaporator outlet maximum is 26.67°C and the minimum is -6.7°C. The COP equation has the form of Equation 8.1.

$$COP = A + B\,T_{eva_{in}} + C\,\dot{m}_{eva} + D\,T_{con_{out}} + E\,T_{eva_{in}}^2 + F\,T_{con_{out}}^2 + G\,T_{eva_{in}} \cdot T_{con_{out}} \quad (8.1)$$

Table 8.1: Parameter description and units for the heating LT HP COP correlation

Parameter	Description
$T_{eva_{in}}$	Evaporator inlet temperature [°C]
$T_{con_{out}}$	Condenser outlet temperature [°C]
$\dot{m}_{eva}$	Mass flowrate through the evaporator [kg/s]

Analysis in MiniTab concluded that the mass flowrate through the condenser had a negligible influence on the HP COP and was not included in the equation. The variable with the largest influence on the COP is the condenser outlet temperature. Two training sets were developed using the data set. Table 8.2 provides the R^2 and RMSE values for the two equations.

Table 8.2: LT heating HP equation performance results

	Training Set #1	Training Set #2
R^2	99.66%	99.62%
RMSE	0.092881	0.097367

To further compare the performance of both equations, the predicted COP is compared with the manufacturer COP in Figure 8.2. Both equations demonstrate the ability to accurately predict the COP.

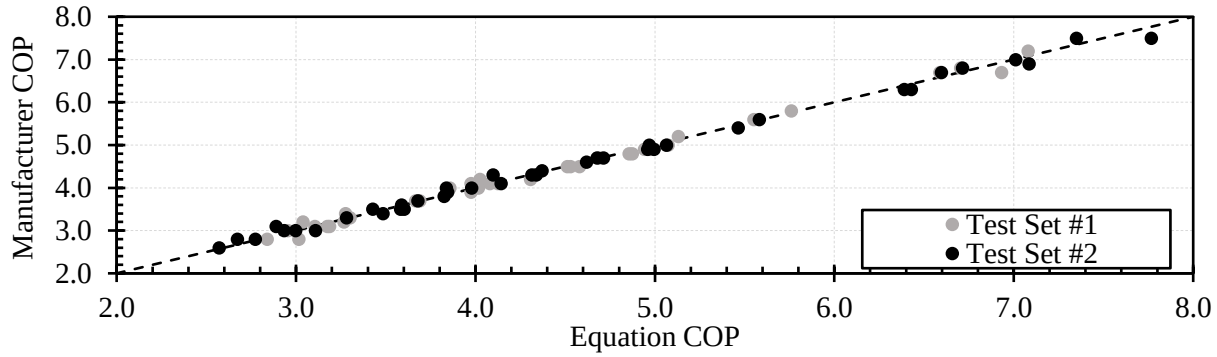

Figure 8.2: LT HP equation performance

Ultimately, training set #1 was chosen due to the greater R^2 value and the lower RMSE. The resulting equation is Equation 8.2.

$$COP = 6.93 + 0.142T_{eva_{in}} + 0.145\dot{m}_{eva} - 0.157T_{con_{out}} + 0.000777T_{eva_{in}}^2 + 0.00112\,T_{con_{out}}^2 - 0.00188T_{eva_{in}} \cdot T_{con_{out}} \quad (8.2)$$

8.2.2 Comparing the LT and HT HP Models

Using the LT HP equation developed, the 30-60°C network with 10,000 m^3 network storage simulation was used to compare the performance of the HT and LT HPs. In the simulation, the LT HP replaced the HT HP in all ETSs for harvesting and for heating. The HT HP remained as the HP interfacing with the network storage, as the temperatures would be out of the bounds for the LT HP.

The COP of the heating HP decreased on average by 0.55 using the LT HP resulting in a 114 MWh increase in electricity consumption. The HT HP demonstrates better performance than the LT HP, even though the HT HP is lifting the temperature of the network 10°C greater than the LT HP, the COP is greater and requires less electrical consumption.

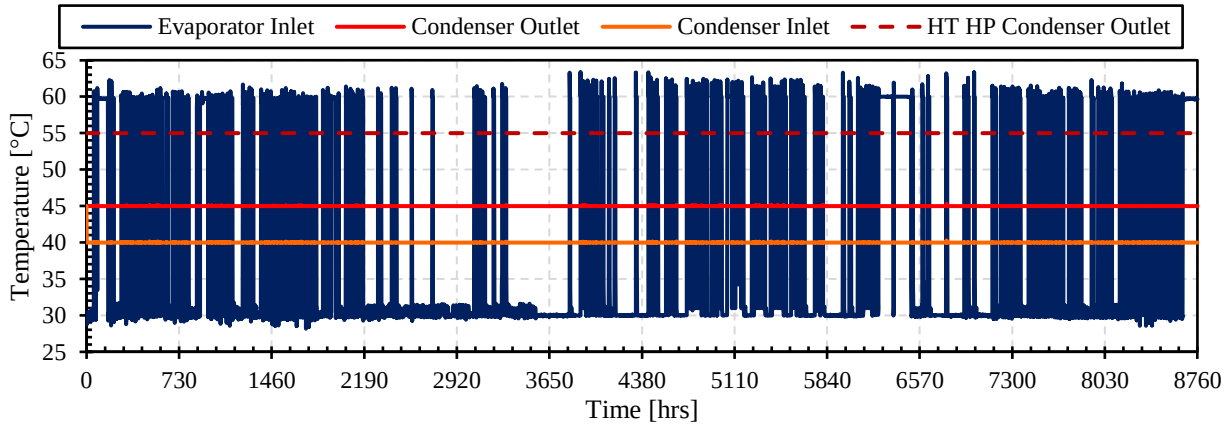

Figure 8.3: LT and HT heating HP temperature profiles

The COP increased on average by 0.66 using the LT HP for harvesting leading to a decrease in electricity consumption of 72 MWh. These is a decrease in electrical consumption with the LT HP due to the large overall decrease in temperature difference across the HP. With the HT HP, the

~20°C heat from the building chiller was being increased to 55°C in the COP equation. Where with the LT HP, the COP equation is using the actual temperature of the thermal network which is ~30°C. The temperature difference across the HP decreases from 35 to 10°C

This would also apply to all other simulations where the network temperature is below the HT HP minimum condenser outlet temperature. This results in an overestimation of the electricity required by the harvesting HP. The overestimation of harvesting HP electricity takes place during off-peak periods where the emission factor associated with electricity consumption is not high. When heat is harvested on-peak, the temperature of the evaporator and condenser are within the operating limitations of the HT HP. An accurate portrayal of electricity consumption on-peak was obtained, when the on-peak emission factor is large. As calculated in Section 8.1, a change in off-peak electricity consumption does not have a large impact on emissions.

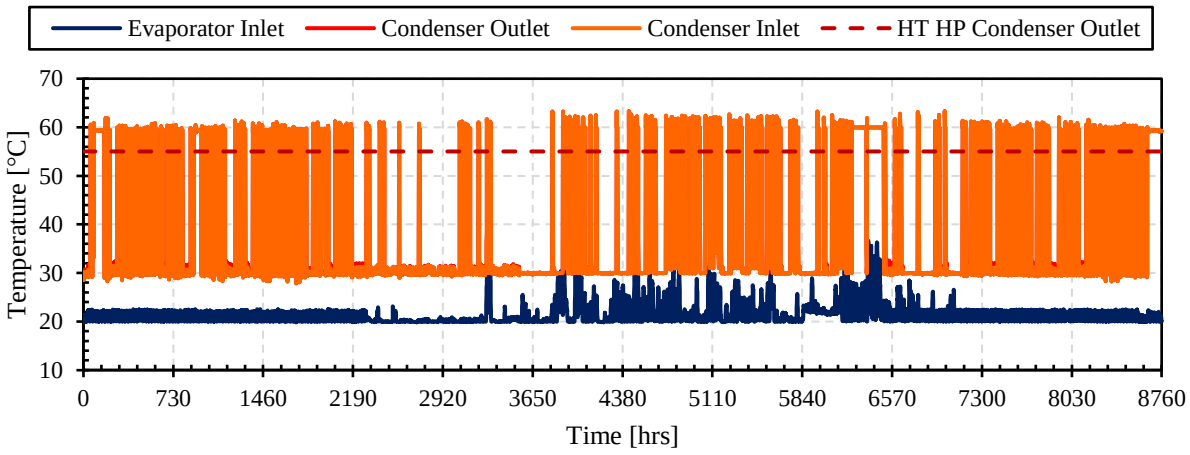

Figure 8.4: LT and HT harvesting HP temperature profiles

Overall, the LT HP lead to a decrease in emissions compared to the use of the HT HP. The LT HP increased electricity consumption of the system by 42.4 MWh. The increase in power by the heating HP resulted in less heat being drawn from the network off-peak, therefore, the boiler was

not resupplying as much heat to the network. The poorer performance of the LT HP for heating resulted in an emissions reduction of the system by 9.2 tCO_{2e}.

In conclusion, the results comparing the HT to the LT HP do not result in drastic performance differences. The results presented throughout this thesis demonstrate accurate comparisons between different micro-thermal network scenarios.

Appendix C

9. Individual Building Load Profiles

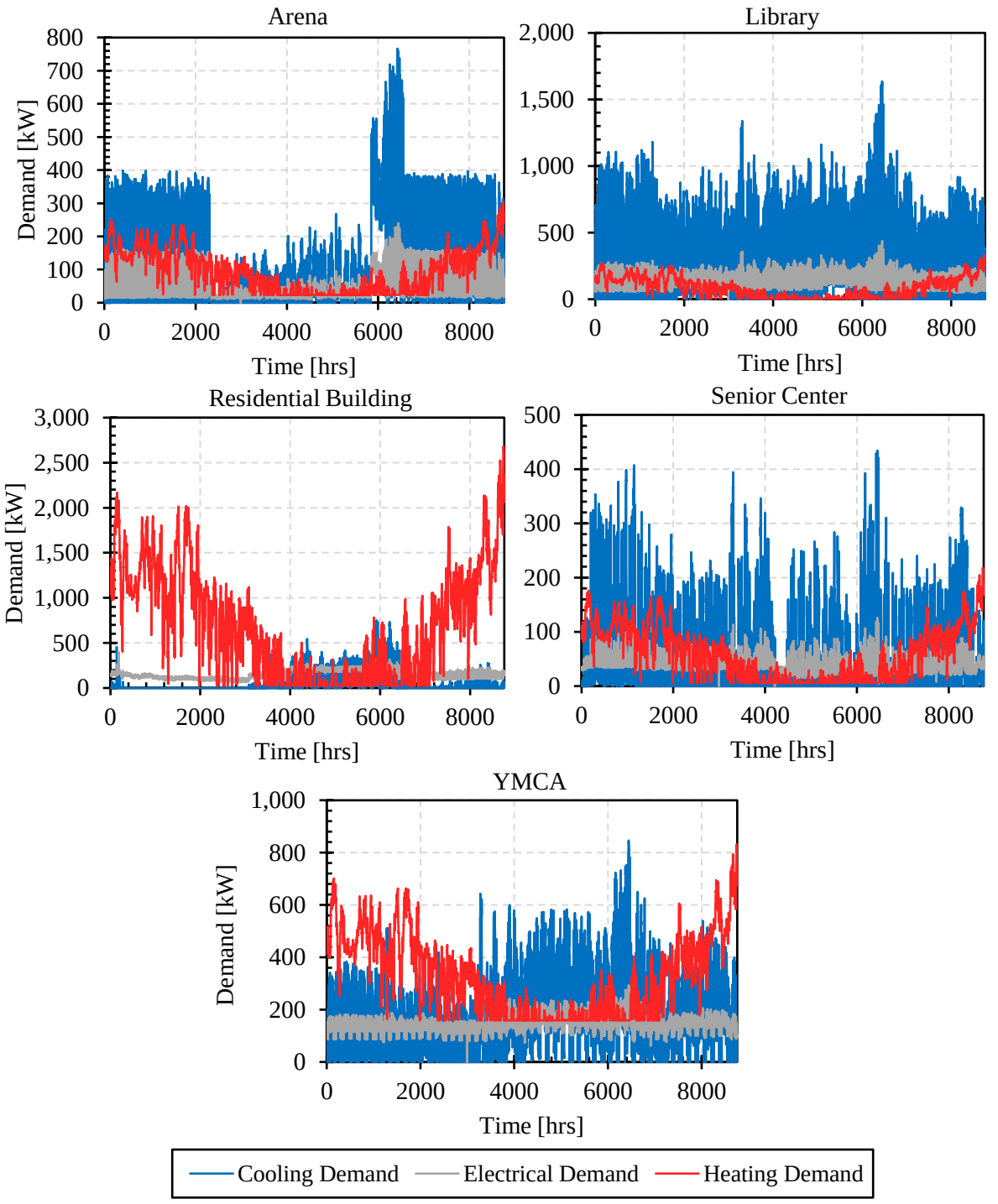

Figure 9.1: Individual building load profiles

Appendix D

10. Simulations with 2015 Data

The ICE-Harvest system was further analyzed for the year 2015 to determine the behaviour of the system when natural gas peaking power plants were operated more frequently. The year 2015 was chosen because the natural gas peaking power plants were operational for 8,529 hours of the year. This is significantly greater than the 3,347 hours previously considered in Chapter 5 for the year 2017.

The reference scenarios were determined for the year 2015 along with a 20°C, 70°C, and 20-70°C MTN. Electricity consumption and boiler utilization for the conventional boiler case remained unchanged in both 2015 and 2017. The on-peak and off-peak electricity consumption for the GSHP scenario was determined with the hours of natural gas peaking power plant generation. The total quantity of electricity consumed by the GSHP also remains unchanged because the ground temperature profile for 2017 was used in the 2015 case. The 20°C constant temperature network, the 70°C constant temperature network, and the 20-70°C changing temperature network case were simulated with the CHP schedule based on 2015 data. The 20-70°C changing temperature case utilizes the boiler to change the temperature of the MTN (outlined in Section 5.4.2). Only the operational schedule of the CHP changed in the simulations to represent the increase in on-peak hours. All other parameters and inputs for the 2015 cases are the same as outlined in Chapter 5 to provide a direct comparison between the two years.

From the thermal distribution in Figure 10.1, the majority of the heating HP and harvesting HP operation took place during the on-peak period. The boiler and EMC storage utilization decreased compared to the year 2017. Since the off-peak period only comprises 3% of the year, there is

limited opportunity to discharge and use the EMC storage. The boiler is rarely required off-peak in the 70°C case. In the 20°C and 20-70°C case, the boiler was not required at all during off-peak periods. The boiler was predominantly used on-peak to help meet the large thermal loads. Energy required from the boiler is 13% of the 2017 value. Instantaneous use of the CHP was able to meet, on average, 47% of the heating demand. In contrast to 2017, wherein the CHP was able to meet 20% of the heating demand.

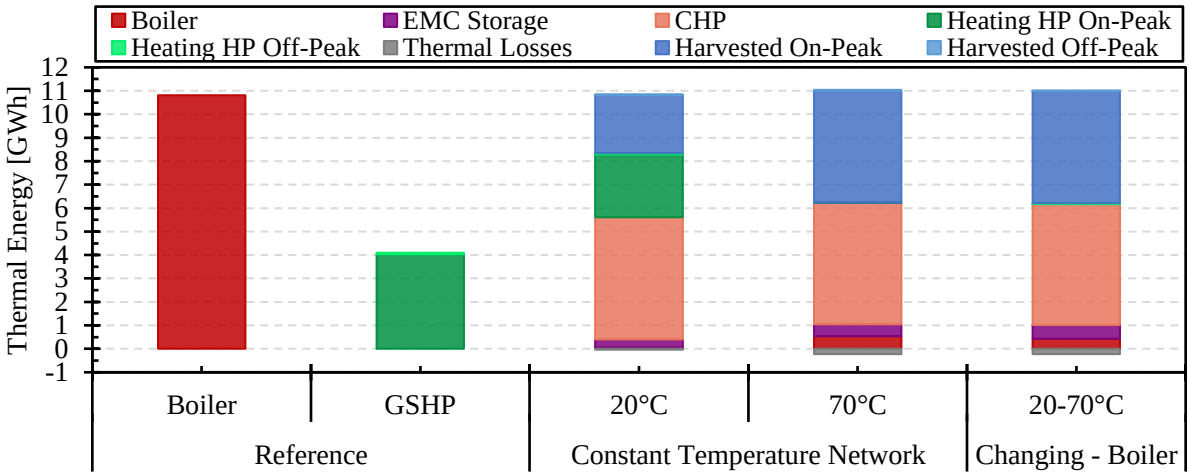

Figure 10.1: Thermal energy distribution for the year 2015

The emissions for all 2015 cases and their reduction from the conventional boiler scenario are displayed in Figure 10.2. With the increase in on-peak hours, the GSHP only provides a 25% reduction in emissions compared to the conventional boiler and doubles its emissions from 2017. Since the majority of electricity is consumed on-peak, the natural gas peaking power plants are required to meet the increased demand, leading to an increase in emissions. In the year 2017, since the majority of the year consisted of an off-peak period, there were greater amounts of carbon free electrical generation available to meet the GSHP demands. Similarly, the same trends are seen in the 20°C network case. Operating the network at a constant temperature of 70°C provided an emissions reduction of 61%. The removal of the electricity requirement for heating in on-peak

periods caused the large reduction in emissions. The 20-70°C case yielded very similar results to the 70°C case. Since the on-peak period is 97% of the year, in the 20-70°C case the MTN operated at its hot temperature of 70°C for 97% of the time. The 20-70°C case exhibits the greatest emissions reductions due to the limited electricity required from the grid on-peak and the electrification of heating in the off-peak periods eliminating the need for the boiler.

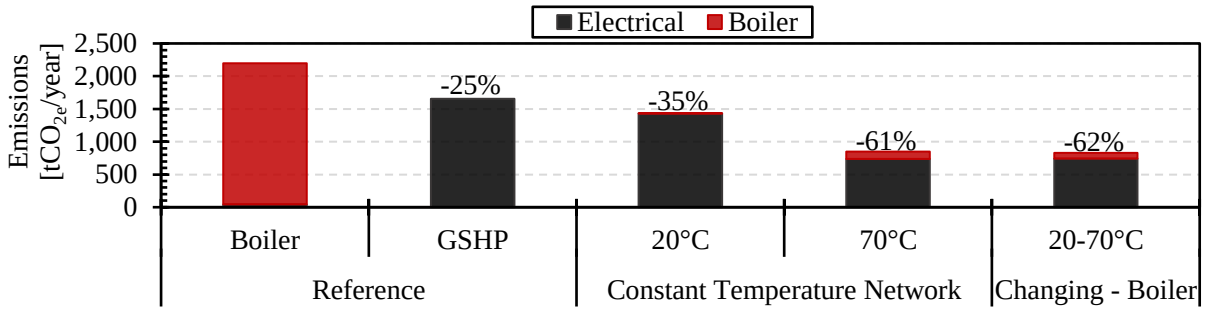

Figure 10.2: GHG emissions for the year 2015

The electrical energy consumption and supply are outlined in Figure 10.3. Electricity consumed on-peak in the conventional boiler and GSHP case require electricity from the grid to meet the full demand. The CHP is able to supply over 90% of the on-peak electricity consumed in the remaining cases. Percentage of on-peak electricity met by the CHP is the same as the year 2017, but the quantity of additional CHP electricity is much greater. Due to the increase in operational hours of the CHP, the additional CHP electricity increased on average by 360%.

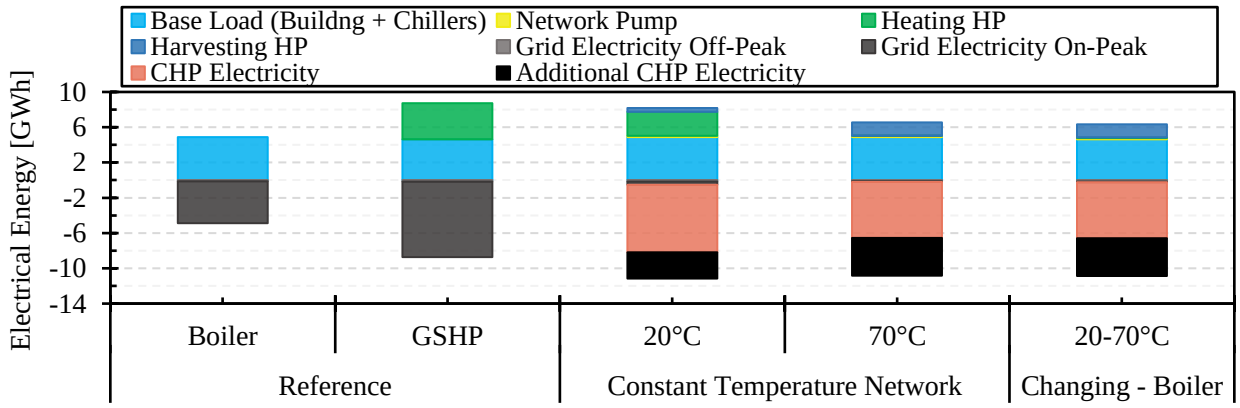

Figure 10.3: Electrical energy consumption and supply for the year 2015

Due to the larger operation time of the CHP there is much more heat unrecovered. All unrecovered energy is presented in Figure 10.4. On average, the amount of unrecovered CHP heat increased by 520%. With greater operational hours of the CHP, it appears that a smaller CHP coupled with long-term storage would be extremely beneficial in reducing the unrecovered heat. The unrecovered heat would be able to be stored in the warm months and used in the cold months to make up for the reduction in CHP capacity. In the year 2017, the 1,500 kW_{th} CHP does not seem oversized due to the fewer operating hours. The fewer operating hours lead to a greater utilization of the EMC storage and larger quantities of boiler energy off-peak. Long-term storage would be beneficial in 2017 to reduce the quantity of boiler use during the off-peak periods.

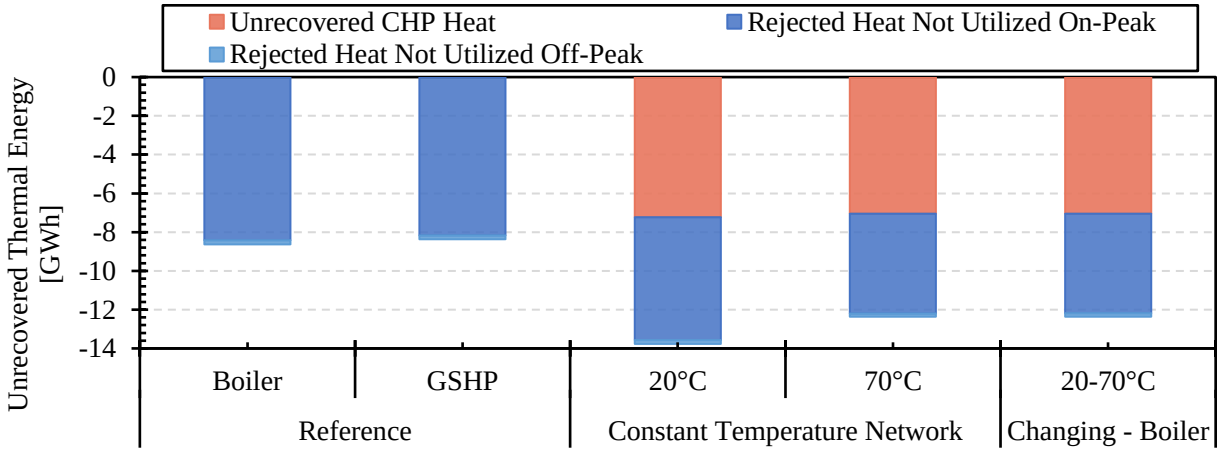

Figure 10.4: Unrecovered thermal energy for the year 2015

Appendix E

11. Micro-Thermal Network Energy Balance

To ensure all areas of heat loss and heat gain on the micro-thermal network are being considered in the energy calculations, the energy balance around the network was performed.

In Dymola, all components were modeled with minimal thermal mass. Within each component, the mass or time delay was set to a value that resulted in the least amount of thermal mass without causing system instabilities. Therefore, the most significant area of thermal mass is the micro-thermal network. Throughout the simulation, the fluid in the MTN can store heat or heat can be removed from the fluid to meet the heating demands.

An energy balance was conducted around the micro-thermal network, as displayed in Equation 11.1.

$$E_{in} + E_{generated} - E_{out} = E_{stored} \quad \begin{cases} E_{in} = Q_{EMC} + Q_{harvested} \\ E_{generated} = 0 \\ E_{out} = Q_{pipe\ losses} + Q_{heating} \\ E_{stored} = M_N c_p \dfrac{dT_N(t)}{dt} \end{cases}$$

$$M_N c_p \frac{dT_N(t)}{dt} = Q_{EMC} + Q_{harvested} - Q_{pipe\ losses} - Q_{heating} \tag{11.1}$$

To determine the energy stored in the MTN pipes, the enthalpy of the pipes at the inlet and outlet was used to determine the energy stored within each pipe segment. For i pipe segments, the enthalpy was obtained at the inlet (H_{inlet_i}) and outlet (H_{outlet_i}) of the plug flow pipe model. The resulting equation for the energy stored in the MTN is presented as Equation 11.2. The Dymola model with all six pipe segments labeled can be seen in Figure 11.1.

$$M_N c_p \frac{dT_N(t)}{dt} = \sum_i^6 \left[\dot{m}_N \left(H_{outlet_i} - H_{inlet_i}\right) - Q_{pipe\ losses_i}\right] \tag{11.2}$$

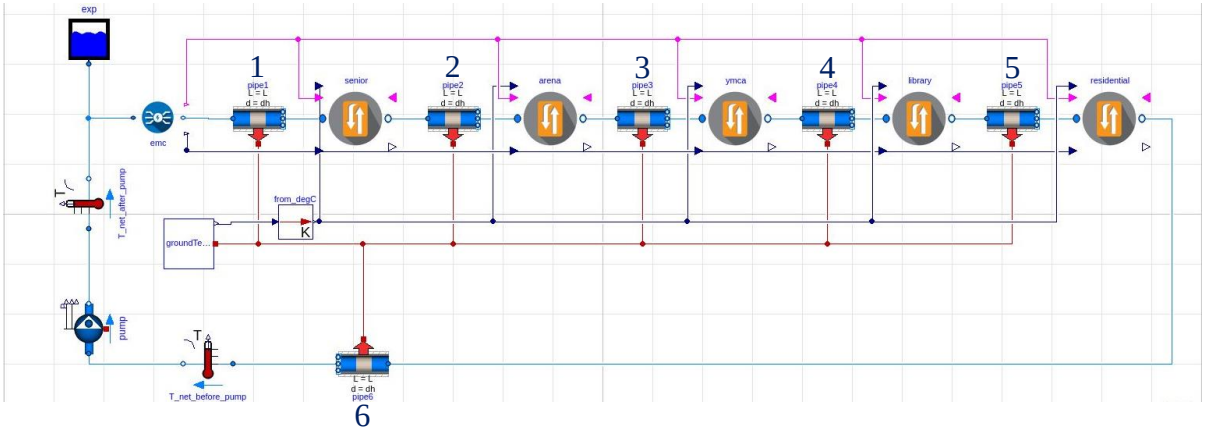

Figure 11.1: System model in Dymola

The resulting energy balance for the thermal network is Equation 11.3. The pipe losses were present on both sides of the equation and have summed to zero.

$$\sum_i^6 \dot{m}_N \left(H_{out_i} - H_{in_i}\right) = Q_{EMC} + Q_{harvested} - Q_{heating} \tag{11.3}$$

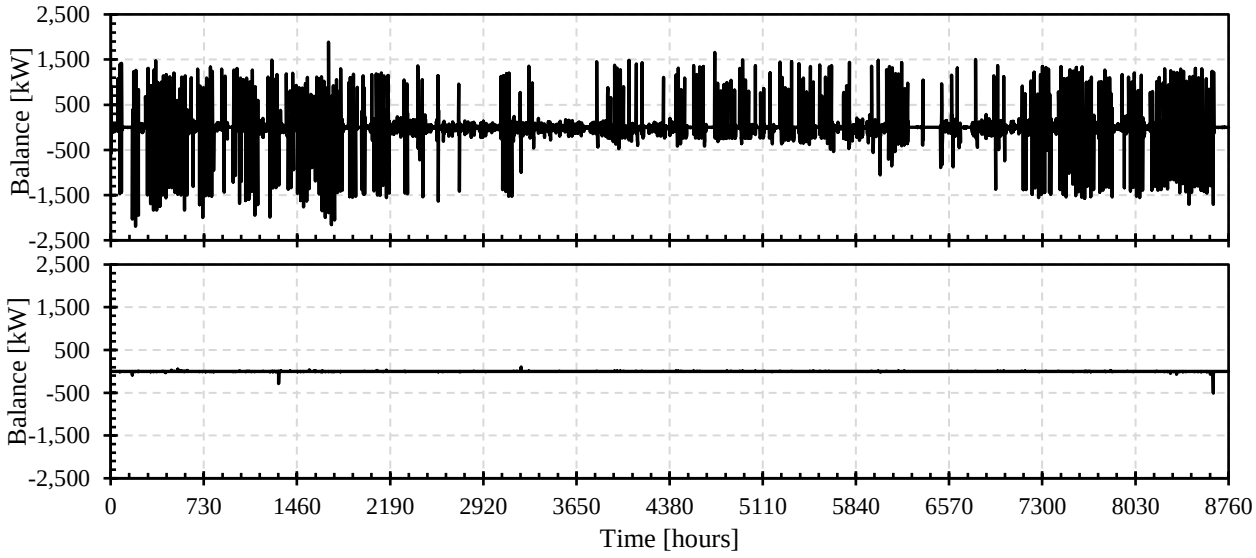

Figure 11.2: Energy balance of the MTN excluding the piping thermal mass (top) and including the piping thermal mass (bottom)

Using the simulation conducted for the 50-70°C no on-peak harvesting case with a 1,500 kW_{th} CHP (from Section 5.4.3), the energy balance around the MTN was calculated. Figure 11.2 displays the energy balance around the thermal network excluding the energy stored in the MTN (the right-hand side of Equation 11.1) and including the energy stored (Equation 11.3). The addition of the network thermal mass reduced the imbalance around the network by 99.5%. Minor fluctuations are still present in the energy balance as it does not equal zero all of the time. The energy balance of the system with a finer grid is displayed in Figure 11.3. Minor areas of thermal mass are not accounted for, such as in the heat exchangers and heat pumps, causing there to be a slight imbalance. It was determined that the imbalance was negligible in the system calculations as the imbalance is only 0.04% of the heating load.

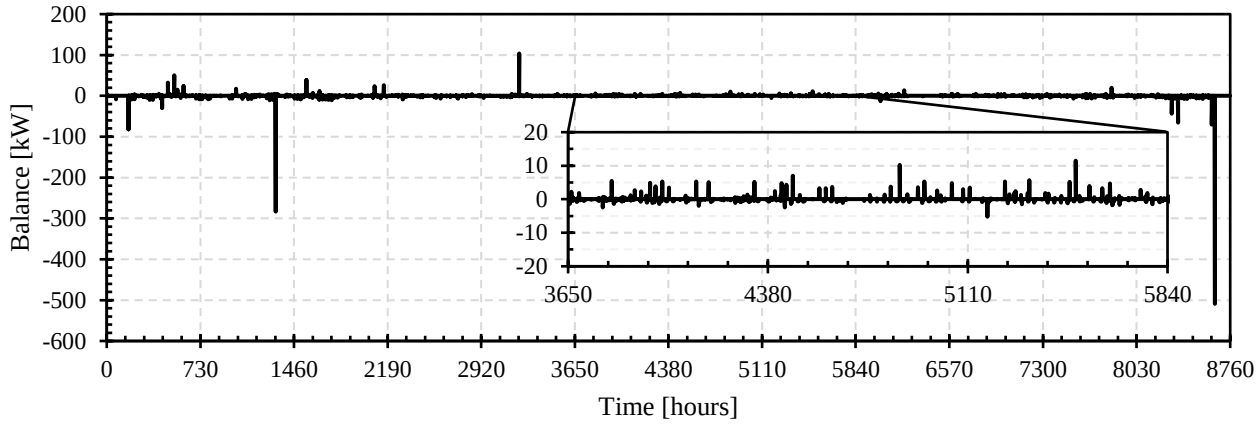

Figure 11.3: Closer look at the MTN energy balance including the piping thermal mass